UNDERSTANDING THE ROLE OF PANCREATIC DUCTAL ADENOCARCINOMA CHEMORESISTANCE AND INTERTUMORAL HETEROGENEITY ON VESICULAR STOMATITIS VIRUS-BASED ONCOLYTIC THERAPY

by

Dakota Wayne Goad

A dissertation submitted to the faculty of
The University of North Carolina at Charlotte
in partial fulfillment of the requirements
for the degree of Doctor of Philosophy in
Biology

Charlotte

2023

Approved by:

_____
Dr. Valery Grdzelishvili

_____
Dr. Andrew Truman

_____
Dr. Didier Dréau

_____
Dr. Christine Richardson

_____
Dr. Yvette Huet

_____
Dr. Jennifer Weller

ABSTRACT

DAKOTA WAYNE GOAD. Understanding The Role of Pancreatic Ductal Adenocarcinoma Chemoresistance and Intertumoral Heterogeneity on Vesicular Stomatitis Virus-based Oncolytic Virotherapy. (Under the direction of DR. VALERY GRDZELISHVILI)

Viruses are obligate intracellular parasites that are now being increasingly harnessed as therapeutics for human diseases. Investigating different cellular factors and processes that affect viral infection allows us to improve the efficacy of virus-based therapeutics. This dissertation examines a member of the order *Mononegavirales*, vesicular stomatitis virus (VSV), and is focused on 1) how chemoresistant pancreatic ductal adenocarcinoma (PDAC) impacts the efficacy of VSV-based oncolytic virotherapy and 2) how intertumoral heterogeneity of mouse PDACs impacts VSV-based oncolytic virotherapy and how intertumoral heterogeneity can be addressed in a PDAC mouse model. Here, for the first time, we examined how experimentally acquired chemoresistance impacts the effectiveness of OV therapy. We demonstrate that long-term exposure of PDAC cells to gemcitabine results in the development of cross-resistance of PDAC cells to gemcitabine and VSV. The increase in resistance to VSV correlated with upregulated levels of a subset of antiviral interferon related genes ISGs in gemcitabine resistant cell lines. First the first time, we also systematically examined the impact of intertumoral heterogeneity on oncolytic virus (OV) virus efficacy. We examined phenotypically and genotypically 3 commonly used allograftable mouse PDAC cell lines. Mouse PDAC cell lines showed high divergence in their permissiveness to VSV, which negatively correlated with their abilities to mount antiviral immune responses. Also, mouse PDAC showed high divergence in their karyotype and exome.

ACKNOWLEDGEMENTS

I would like to thank Dr. Valery Grdzelishvili for his astute guidance and unyielding support. I would like to thank Dr. Andrew Truman, Dr. Didier Dréau, Dr. Christine Richardson, Dr. Yvette Huet, and Dr. Jennifer Weller for serving on my committee and providing valuable feedback and support. I would like to thank current and past members of the Grdzelishvili Lab, Cassandra Catacalos, Sara Seegers, Chris Castagno, and Molly Penton for their friendship and assistance throughout my Ph.D. journey. I would also like to thank the UNCC Graduate School for the Graduate School Summer Fellowship awards for funding my summer research endeavors. Lastly, I would like to thank my incredible family, Wayne and Tonia Goad, Richard and Lisa Burchette, Carol and Ralph Macemore, Houston Goad, and all my family and friends who encouraged, loved, and supported me through so many years of graduate education.

DEDICATION

To my parents
and
Dr. Gary L. Walker.

TABLE OF CONTENTS

LIST OF FIGURES viii

LIST OF TABLES x

LIST OF ABBREVIATIONS xi

CHAPTER 1: INTRODUCTION 1

CHAPTER 2: ACQUIRED CHEMORESISTANCE CAN LEAD TO INCREASED RESISTANCE OF PANCREATIC CANCER CELLS TO ONCOLYTIC VESICULAR STOMATITIS VIRUS 22

2.1 Introduction 22

2.2 Materials and Methods 25

2.3 Results 31

2.4 Conclusions 41

2.5 Figures 43

2.6 Tables 52

CHAPTER 3: INTERTUMORAL HETEROGENEITY IMPACTS ONCOLYTIC VESICULAR STOMATITIS VIRUS EFFICACY IN MOUSE PANCREATIC CANCER CELLS 55

3.1 Introduction 55

3.2 Materials and Methods 58

3.3 Results 65

3.4 Conclusions 83

3.5 Figures 85

3.6 Tables 98

CHAPTER 4: DISSERTATION SUMMARY 99

LIST OF FIGURES

FIGURE 1: How oncolytic viruses work 17

FIGURE 2: VSV virion structure and genome 18

FIGURE 3: Overview of VSV life cycle 19

FIGURE 4: General overview of Oncolytic Virotherapy 20

FIGURE 5: Range of Permissiveness of PDAC to VSV 21

FIGURE 6: Gemcitabine transport, intracellular activation/deactivation, and mechanism of action 43

FIGURE 7: Experimental generation of gemcitabine-resistant (GR) SUIT-2 cells 44

FIGURE 8: Viral replication kinetics 45

FIGURE 9: Relative infectivity and infection foci of VSV in C and GR cells 46

FIGURE 10: Replication kinetics of viruses and cell viability in C and GR cells 47

FIGURE 11: VSV and antiviral protein expression 48

FIGURE 12: Total RNA was isolated from C and GR cells in triplicate and analyzed by RNA-seq 49

FIGURE 13: Time course expression of antiviral proteins in C and GR cells after VSV infection 50

FIGURE 14: Human PDAC cell cross-resistance to gemcitabine and VSV-ΔM51 51

FIGURE 15: Development and characterization of mouse PDAC cell lines 52

FIGURE 16: Relative infectivity to VSV in a panel of different cell lines 85

FIGURE 17: Viral replication kinetics and cell viability 86

FIGURE 18: VSV and antiviral protein expression 87

FIGURE 19: Responsiveness to mouse IFN-α 88

FIGURE 20: Responsiveness to human IFN-α 89

FIGURE 21: Cytokine array 90

FIGURE 22: Combinatorial treatments of PDAC cells using VSV-ΔM51-GFP in combination with different drugs 91

FIGURE 23: Chemoresistance of mouse PDAC cell lines to gemcitabine and 5-FU 92

FIGURE 24: Spectral karyotyping (SKY) of mouse PDAC cell lines 93

FIGURE 25: Exome analysis of all genes in three mouse PDAC cell lines 94

FIGURE 26: Exome analysis of 2079 genes involved in tumor, microenvironment and immune response 95

FIGURE 27: A proposed novel platform to study OV-based therapies against phenotypically different PDACs in immunocompetent mice 96

LIST OF TABLES

TABLE 1: Differentially expressed antiviral genes in GR cells compared to C cells 48

TABLE 2: Expression of other genes with known roles in resistance to gemcitabine in GR cells compared with C cells 49

TABLE 3: Human PDAC cell lines used in this study 50

TABLE 4: Exome mutation in selected Type I IFN pathway genes 91

LIST OF ABREVIATAIONS

dFdC	2',2'-difluoro deoxycytidine
ds	double-stranded
FFU	focus-forming units
G	glycoprotein
GEMM	genetically engineered mouse model
IC50	half maximal inhibitory concentration
IFN	interferon
IRDS	interferon-related DNA damage resistance signature
ISG	interferon-stimulated gene
L	large protein
M	matrix protein
M51	deletion of methionine at position 51
MOI	multiplicity of infection
WST	water soluble tetrazolium
N	nucleocapsid protein
NNS	non-segmented negative-sense
ORF	open reading frame
OV	oncolytic virus
PDAC	pancreatic ductal adenocarcinoma
P	phosphoprotein
PFU	plaque forming unit
RdRp	RNA-dependent RNA polymerase
RNP	ribonucleoprotein

SeV	Sendai virus
ss	single-stranded
TCID50	median tissue culture infectious dose
VSV	vesicular stomatitis virus
WT	wild type

CHAPTER 1: INTRODUCTION

Viruses are submicroscopic obligate intracellular parasites, which replicate only inside living cells. Viruses are comprised of a nucleic acid genome which is surrounded and protected by a protein coat called a capsid. Viruses are found in almost every ecosystem on Earth and infect all known life forms, from animals and plants to microorganisms. Many diseases are caused by viruses such as AIDS, hemorrhagic fevers, COVID-19, and the flu. However, many viruses are beneficial to humans as they 1) have led to important discoveries and have contributed to our understanding of cell and molecular biological processes such as DNA replication, transcription, RNA processing, translation, protein transport, and immunology, and 2) have been harnessed as therapeutic agents, for example in vaccines, gene therapy, and cancer therapy (Russell et al., 2012) (Bulcha et al., 2021; Travieso et al., 2022).

There were interesting observations in the early and mid-20th century where cancer patients who contracted an infectious disease went into brief periods of clinical remission. For leukemia, it was recognized that influenza infection sometimes produced beneficial effects (Dock, 1904; Pelner, 1958). As it turns out, some naturally occurring viruses preferentially infect and replicate in cancer cells, as cancer cells typically have defects in Type I interferon (IFN)-mediated antiviral responses compared to normal cells (Russell et al., 2012) (Fig. 1). Viruses can also be engineered in order to exploit unique features of cancer cells (Tian et al., 2022). These viruses, both naturally occurring and engineered for use as cancer therapies have been called oncolytic viruses (OVs).

There are currently three OVs approved for clinical use: Talimogene laherparvec (T- Vec) (based on herpes simplex virus 1) approved in the United States and European Union for melanoma, (Orloff, 2016) Rigvir (based on enteric cytopathic human orphan virus 7) approved in

Latvia and several other countries for melanoma,(Donina et al., 2015) and Gendicine (based on adenovirus type 5) approved in China for head and neck squamous cell carcinoma (Garber, 2006). Importantly, the ideal OV treatment should allow for not only the preferential infection and lysis of the cancer cells but also to induce the activation of the adaptive immune response to the tumor site, as well as distant metastatic sites (Fig. 4) (Holbrook et al., 2021).

The work in this dissertation is focused on one promising OV, vesicular stomatitis virus (VSV) (Fig. 1). VSV is a nonsegmented negative-strand (NNS) RNA virus (order *Mononegavirales*, family *Rhabdoviridae*, genus *Vesiculovirus*). This means that the viral genome consists of a single genome segment, and not in multiple segments (i.e. multipartite) like influenza, for example. Virus RNA genomes exist in different forms, those that are single-stranded (ss) and those that are double-stranded (ds). Virus ssRNA genomes can either be positive-sense (i.e. +ssRNA) or negative-sense (i.e. -ssRNA). A +ssRNA viral genome has the same polarity as mRNA (5'-3') and can be immediately translated by the host cell. However, -ssRNA viral genomes are complementary (3'-5') to viral mRNA and thus must be first transcribed by a viral RNA-dependent RNA polymerase (RdRp), which must come packaged in each virion(Wolf et al., 2018). VSV is already in stage I clinical trials against various malignancies (Clincaltrials.gov trials NCT01628640, NCT03865212, NCT03120624, NCT02923466, NCT03647163, and NCT03017820). Not only is VSV being investigated as an OV, but also as a vaccine and gene therapy vector (Munis et al., 2020). An exciting and recent VSV success was a replication-competent VSV-based vaccine vector pseudotyped, or engineered with glycoproteins from a different virus, with the glycoprotein of Ebola virus (Suder et al., 2018). This recombinant VSV-based vaccine vector conferred full protection in preclinical non-human primate studies (Jones et al., 2005). This vector (rVSV-ZEBOV) was used during the last

outbreak of Ebola in West Africa in 2013-2016(Agnandji et al., 2016). In a phase III trial, it was demonstrated that this vaccine was safe for use in humans and showed promising efficacy (Henao-Restrepo et al., 2017; Henao-Restrepo et al., 2015). The rVSV-ZEBOV vaccine was approved for use in the US and the EU in 2019 (Piszczatoski & Gums, 2020). Due to the success of this VSV-based vaccine, other studies are ongoing investigating the recombinant VSV vaccine platform to combat other emerging viruses(Fathi et al., 2019).

VSV has a genome of approximately 11-kb that encodes 5 genes (Fig. 2): nucleoprotein (N), phosphoprotein (P), matrix protein (M), glycoprotein (G), and large protein (L). The VSV genome is encapsidated by the N protein, where it forms a nuclease-resistant nucleocapsid. The VSV RNA dependent RNA polymerase complex is comprised of the L and P proteins and is carried in each virion (Lyles DS, 2007). The overview of the VSV life cycle is shown in Fig. 3, which consists of attachment, endocytosis, uncoating, primary transcription, translation, genome replication, secondary transcription, viral assembly and budding. The VSV G protein allows VSV to attach to the host cell, which includes most (if not all) mammalian cell types. Currently, no specific cell-surface receptor has been demonstrated for the VSV G protein, with binding attributed to negatively-charged membrane lipids (Lyles DS, 2007). After attachment, VSV enters the cell via clathrin-mediated endocytosis (Cureton et al., 2010). Once the VSV virion is internalized, endosomal acidification results in G protein conformational changes which facilitate fusion of the viral envelope with the endosomal membrane, thus releasing the VSV ribonucleoprotein (RNP) into the cytoplasm (Stanifer et al., 2011). The N, P and L proteins make up the transcriptionally active unit of the virus (Lyles DS, 2007). The five genes of VSV are arranged in the order of 3'N-P-M-G-L 5', and the relative amount of each transcript is associated with its genomic position. The viral mRNAs are transcribed sequentially in the order they appear

in the genome from 3’ to 5’. The amount of each transcript decreases as the distance increases from the 3’ end due to a single RdRp entry site at the 3’ end (Emerson, 1982). Due to this, the transcription of each gene depends on the prior transcription of upstream genes. This mechanism of sequential transcription is considered a stop-start mechanism, where cis-acting signals in the RNA template dictate the RdRp activity at each gene junction. Each of the gene junctions contain a gene “end” sequence for the upstream gene (3’AUACUUUUUUU5’), a dinucleotide (G/CA), that is not transcribed, and a gene start sequence for the downstream gene (3’UUGUC5’) (Rose, 1980). Following the elongation of viral mRNA, the RdRp complex meets a termination signal (3’AUACUUUUUUU5’) at the end of each gene, which leads the RdRp to “stutter” over the 7 Us, resulting in polyadenylation of the viral mRNA (Barr & Wertz, 2001; Barr et al., 1997). Following polyadenylation (which stops after adding around 200 As, the RdRp complex has two possible fates. Most commonly, the RdRp traverses the two intergenic nucleotides and continues transcription at the initiation signal of the downstream gene. Around 25% of RdRp complexes fail to continue transcription of the downstream gene and dissociate from the template, leading to around 25% reduction of expression of the downstream gene at each gene junction (Iverson & Rose, 1981; Villarreal et al., 1976; Wertz et al., 1998). This discontinuous transcription results in a gradient of mRNA and subsequent protein expression such as N > P > M > G > L. This type of transcription attenuation is a general feature of NNS RNA viruses, and is an important mechanism in regulating abundance of mRNAs. In fact, the importance of gene order in regulating relative levels of viral proteins has been demonstrated experimentally by rearranging VSV genes. The consequent changes in abundance of viral proteins resulted in significant reductions in viral replication and pathogenesis (Ball et al., 1999; Wertz et al., 1998).

An important principle in replication of NNS RNA viruses is that the ability of RdRp to replicate the viral genome is dependent on new virus protein synthesis to encapsidate the newly made RNA genome. This requirement for new viral protein synthesis offers a regulatory mechanism to ensure that templates are used for mRNA synthesis until sufficient levels of viral proteins are available before these templates are used for genome replication. In particular, the VSV N protein is critical for genome replication (Patton et al., 1984). In infected cells, a complex of N protein and P protein is the active complex which promotes genome replication (Peluso & Moyer, 1988). The P protein in this complex maintains the solubility and appropriate folding of the N protein such that the nascent RNA can be encapsidated (Davis et al., 1986; Masters & Banerjee, 1988). Based on analyses in insect cells, the N-P complex contains one N protein and two P proteins (Mavrakis et al., 2003). The encapsidation of nascent RNA constitutes a signal for the viral RdRp to ignore sequences in the genome template at gene junctions (that govern the start-stop mechanism for transcription), and generates full-length, encapsidated RNA that are complementary to the genome (i.e. antigenome). The antigenomes are used then as templates for the synthesis of progeny genomes. After nucleocapsids containing progeny genomes start to accumulate in infected cells, they are used for secondary transcription and are then assembled into progeny virions. In particular for VSV, most of the nucleocapsids that are made in the infectious cycle are not released as progeny virions (Knipe et al., 1977; Soria et al., 1974), suggesting that the use of nucleocapsids as templates for transcription predominates over their use in progeny virions. Interestingly, virus assembly actually begins at about the same time as secondary transcription (2-3 hours) and reaches a maximum rate at around 8-10 hours when viral protein synthesis is at a maximum, and declines correspondingly with a decline in viral protein synthesis towards then end of the infectious cycle (16-20 hours) (Lyles DS, 2007).

In infected cells, VSV mRNAs are preferentially translated. However, it is currently unclear what allows the translation of viral mRNAs but inhibits translation of the host cell mRNA, as both viral and host cell mRNA are structurally similar (5'-cap and 3'-polyadenylation) (Lyles DS, 2007).There are studies which suggest that this effect is independent of viral mRNA cis-acting sequences, but rather a role of the translational machinery in VSV-infected cells, such as dephosphorylation of the cap-binding subunit eIF4E (Connor & Lyles, 2002) might favor newly produced mRNAs(Whitlow et al., 2006). Other studies support the role of VSV M protein in the preferential translation of viral mRNA, with M protein residue D125 being critical (Mire & Whitt, 2011).

In nature, the primary hosts of VSV are cattle, horses, pigs, and other mammals where it can cause symptoms identical to those of the foot and mouth disease virus (Katz et al., 1997), such as fever and blistering stomatitis on the amongst the oral cavity, feet, and teats (Hastie & Grdzelishvili, 2012). There are many advantages for using VSV as a research model, as 1) VSV can be safely studied in the laboratory, 2) it has a small and simple genome, 3) its ability to replicate in a wide range of cell types, and 4) there are reverse genetic systems already established (Lyles DS, 2007). The pantropism exhibited by VSV is largely due to its use of ubiquitously expressed cell surface molecules for attachment and entry to host cells, such as low-density lipoprotein receptor (LDLR) (Finkelshtein et al., 2013), phosphatidylserine (Carneiro et al., 2006; Schlegel et al., 1983), sialoglycolipids (Schloemer & Wagner, 1975), and heparan sulfate (Guibinga et al., 2002). The oncoselectivity of most OVs, including VSV, is mainly due to defective or suppressed type I interferon (IFN) mediated antiviral responses in many cancers (Lichty et al., 2004; Stojdl et al., 2000; Zhang et al., 2010), because most type I IFN responses are antiproliferative, antiangiogenic, and proapoptotic (Wang et al., 2011).

This work primarily focuses on VSV-ΔM51, which is an attenuated VSV with a deletion of the methionine at amino acid position 51 (M51) of the VSV M protein. Wild-type (WT) M protein of VSV plays a major role in viral assembly via binding the viral nucleocapsid to the cytoplasmic surface of the plasma membrane during the budding process (Flood et al., 2000), in addition to inducing budding of virus envelopes (Jayakar et al., 2000). As well, the VSV M protein is responsible for many of the cytopathic effects associated with VSV infection, including cell rounding and inhibition of host gene expression (Lyles, 2000). This inhibition of host gene expression is due to the ability of VSV M protein to block nuclear-cytoplasmic transport of host RNAs and proteins (Ahmed & Lyles, 1998). The ΔM51 mutation ablates VSV M protein in its ability to inhibit host antiviral gene expression (Ahmed et al., 2003; Stojdl et al., 2003), while still allowing VSV to replicate in cancers cells, as cancer cells typically have defective type I IFN antiviral machinery. Of note, the ΔM51 mutation greatly reduces the neurotoxicity found to be associated with WT VSV (Hastie & Grdzelishvili, 2012).

Pancreatic ductal adenocarcinoma (PDAC) is an aggressive malignancy that accounts for approximately 95% of pancreatic cancers, and is the number four cause for cancer-related deaths in the U.S. The 5-year survival rate for PDAC patients has remained around 10%, while survival rates for other cancers have significantly improved (Siegel et al., 2023). The poor survival rate for PDAC is largely attributed to late diagnoses and limited treatment options (Mizrahi et al., 2020, as most PDAC tumors are either intrinsically resistant to chemotherapy or rapidly acquire resistance {Orth, 2019 #154). The mechanisms of chemoresistance are not fully understood and are likely multifactorial (Zeng et al., 2019). The only curative treatment for PDAC is surgical resection, but unfortunately this option is only possible in less than 20% of patients (Lowery & O'Reilly, 2015).

The main drivers of PDAC include mutations in KRAS, CDKN2A, TP53, and SMAD4 (Orth et al., 2019). Mutations in the KRAS, CDKN2A, TP53, and SMAD4 genes are present in around 90%, 95%, 50-75%, and 50% of PDAC tumors, respectively (Siegel et al., 2020). Mutations in the KRAS gene leads to an aberrant, constitutively active Ras protein which results in activation of pathways associated with survival and proliferation (Buscail et al., 2020). Mutation subsequent inactivation of CDKN2A results in the loss of p16, which serves as a regulator of the cell cycle G1-S checkpoint. Mutations on TP53 reduce its ability to act as a tumor suppressor, including its role as a regulator of DNA-damage checkpoints. In addition, many p53 mutants can acquire gain-of-function oncogenic activities, including promoting cell survival, proliferation, migration, invasion, chemoresistance, and inflammation. SMAD4, associated with the TGF-β pathway, can acquire mutations which results in abnormal signaling of TGF-β that can lead to increased growth rate and replication. Germline mutations in BRCA1, BRCA2, and ATM were also frequently identified in PDACs that increase susceptibility to PDAC development (Salo-Mullen et al., 2015). Since 1997, gemcitabine (2'-deoxy-2',2'-difluorocytidine monohydrochloride; dFdC; trade names Gemzar, Infugem) chemotherapy has been the first-line treatment for PDAC patients with unresectable locally advanced or metastatic disease with a median survival rate if 4-6 months, in particular in patients not healthy enough for combination therapeutic approaches (Springfeld et al., 2019).

Our previous studies showed that VSV is effective against most hum an PDAC cell lines, both *in vitro* and *in vivo* (Murphy et al., 2012). However, we also reported that some PDAC cell lines are resistant to VSV-mediated infection, replication, and/or oncolysis due to multiple mechanisms, including an upregulated expression of type I IFNs and/or interferon-stimulated genes (ISGs) (Hastie et al., 2016; Hastie et al., 2015; Moerdyk-Schauwecker et al., 2013),

reduced viral attachment (Felt et al., 2017), and/or resistance to virus-mediated apoptosis (Felt et al., 2015). Our laboratory also demonstrated multiple strategies to overcome these mechanisms of resistance to OV therapy (Felt et al., 2017; Holbrook et al., 2021).

The need for more effective treatment options for PDAC is critical, and thus clinically relevant PDAC models are imperative. Preclinical PDAC models are important for investigating and understanding the biology of PDAC, are platforms for developing new strategies against PDAC, and are a critical part of the drug development pipeline. There are multiple features for an ideal PDAC model system: 1) the ability to test OV against numerous different PDACs, characterized by various responsiveness to different therapies (i.e., intra- and inter-tumoral heterogeneity), 2) the ability to recapitulate the complex tumor microenvironment (TME) of PDAC, 3) tractability of the model system, ideally being able to track both tumor cells and OV, 4) the ability to deliver OV systemically, and 5) the ability to detect and measure innate and adaptive immune responses against both OV and tumor cells.

Many human PDAC cell lines have been established and can be characterized by their distinctive genotypic and phenotypic variations, including their permissiveness or resistance to OV infection (Deer et al., 2010; Moerdyk-Schauwecker et al., 2013). Utilizing cell lines as a model system offers several advantages for studying PDAC, including easy propagation and unlimited growth. These features represent a cost-effective and dependable model that can easily be used to study molecular mechanisms and biomarkers of resistance or permissiveness of PDAC cells to OVs (Deer et al., 2010; Moerdyk-Schauwecker et al., 2013). While cell line-based approaches represent quick and consistent models, several features reduce their clinical translatability. First, the homogeneous nature of cell lines fail to accurately represent the heterogeneous nature of typical in vivo tumors (Moerdyk-Schauwecker et al., 2013), including

PDAC (Gillet et al., 2013). As such, cell lines are under selection for mutations and phenotypes allowing growth advantage in a monolayer, however, the selection mechanisms in vivo are quite different (Froeling et al., 2010). In fact, established PDAC cell lines not only lose the heterogeneity present in the primary tumor, but the adaptation of these cell lines to grow in culture may obscure genetic aberrations present in the primary tumor (Deer et al., 2010). Additionally, many PDAC cell lines are originated from metastasized disease, so the ability to study PDAC progression is severely limited. Secondly, cell lines cultured in a monolayer lack the important three-dimensional structure and function as seen *in vivo* (Froeling et al., 2010). Thirdly, the PDAC cell line model fails to represent the TME, which is understood to be a dynamic player in PDAC tumor progression (Froeling et al., 2010). Lastly, cultured cell lines lack selection pressure from the host adaptive immune system, thus leaving mutations necessary for evading host immunity underrepresented. The outcome of the OV therapy depends on the complex interactions between tumor cells, virus, and innate and adaptive immune systems of the host. One of the desirable outcomes of these interactions is OV-mediated stimulation of immune response against tumor cells. However, normal PDAC stromal cells can induce innate antiviral responses against OV replicating in tumor cells, and adaptive immune response can prematurely clear virus infection instead of targeting tumor cells. Cell culture-based models cannot address these important issues.

While cell line models have clear disadvantages, they nevertheless remain an appropriate proof-of-principle platform that our group has used to investigate mechanisms regarding responsiveness or resistance to OV therapy (Cataldi et al., 2015; Eric Hastie, 2013; Felt et al., 2017; Hastie et al., 2016; Moerdyk-Schauwecker et al., 2013). For example, our group has assessed how and why some PDAC cell lines are more resistant to VSV infection compared to

other PDAC cell lines. In those investigations, cell line models allow for reliable comparative measurements of virus replication, spread, and cell lysis. Additionally, cell line models allow for relatively straightforward screening of both cellular and viral genes and proteins of interest. Cell line models also permit an efficient virus tractability through reporter genes such as GFP (Torres et al., 2013). Additionally, cell culture-based systems enable innovative imaging approaches for single-cell real-time analysis of OV replication and efficacy in pancreatic cancer cells (Quillien et al., 2021).

Depending on the nature of the investigation, either human or murine PDAC cell lines can be used. Human PDAC cells, derived from primary pancreatic tumors or "cell line-derived xenograft (CDX)" models, have been used as early as 1963 to characterize and test anti-cancer drugs (Dobrynin, 1963). The use of human PDAC cells provides the clear benefit of investigation using the genetic makeup of the human disease, including key PDAC mutations in KRAS, CDKN2A, p53, and SMAD4 (Orth et al., 2019). Although human PDAC cell lines as models led to an improved understanding of the disease, the translation to *in vivo* studies remains challenging. Indeed, the use of human PDAC cell lines in vitro has been until recently limited to implantation in immunocompromised T cell-deficient nude athymic (nude), or B and T cell-deficient severe combined immunodeficient (SCID) mice (Walters et al., 2013). However, PDX models with combined immune system transplantation are bridging that gap {Okada, 2019 #1107}{Giri, 2021 #1106}.While such *in vivo* models have many applications, they lack the ability to assess the role of the adaptive immune system against PDAC as well as OV, both important when determining the efficacy of potential OV therapeutics. To avoid this caveat, murine PDAC cell lines may be used. Using murine PDAC cells derived from murine PDAC tumors allows researchers to establish PDAC in immunocompetent mice, enabling the study of

OV therapy in the presence of a functional adaptive immune system. One notable drawback to this model is the potential genetic dissimilarity, and thus the limited clinical translatability between mouse and human PDAC cells.

Generally, murine PDAC cell lines are originated from mice that have PDAC due to either chemical induction or genetic modifications in genetically engineered mouse model (GEMM). One commonly used PDAC cell line that was cultured from a chemically induced PDAC tumor is Panc02, which has been extensively used for PDAC research (Corbett et al., 1984). The PDAC tumor from which it was derived was established by implanting 3-methyl-cholanthrene (3-MCA)-saturated threads of cotton in the pancreas of C57BL/6 mice. Despite its long-term use in evaluating various therapeutic strategies, Panc02 cells lack clinical significance for PDAC due to the absence of some common mutations found in human PDAC. More relevant murine PDAC cell lines are originated from the KPC mouse model of PDAC (LSL- $Kras^{G12D}$; LSL-$Trp53^{R173H}$; *Pdx*1-*Cre*) (Corbett et al., 1984). KPC mice develop spontaneous PDAC which closely resemble the genetics, physiology, tumor progression, and metastatic hallmarks of human PDAC (Lee et al., 2016), and will be discussed here.

Current *in vivo* PDAC mouse model systems fail to recapitulate all key characteristic of human PDAC disease especially tumor microenvironment, metastasis, adaptive immune response (He et al., 2020; Holbrook et al., 2021; Kong et al., 2020). Importantly, many studies, which use mouse models to investigate PDAC biology and therapies fail to address intertumoral heterogeneity. Intertumoral heterogeneity refers to the differences between tumors in different individuals, where intratumoral heterogeneity refers to the differences within a single tumor. While intratumoral heterogeneity is very important, our main focus is in intertumoral heterogeneity. This is a key issue, as our previous studies demonstrated a wide range of

permissiveness of human PDAC cells to OVs, from highly permissive to highly resistant, which is largely determined by the abilities of PDAC cells to mount effective innate antiviral responses (Hastie et al., 2016; Moerdyk-Schauwecker et al., 2013; Murphy et al., 2012). Mouse PDAC cell lines, which are widely used for *in vivo* examination of the adaptive immune responses during OV and other therapies, have never been examined systematically for virus-host interactions and the role of intertumoral heterogeneity in OV therapy.

Overall, our laboratory is interested in understanding the mechanisms of responsiveness and resistance of PDACs to VSV-based OV therapy. Our laboratory has characterized numerous human PDAC cell lines and has discovered a wide range of permissiveness of PDAC cell lines to VSV-based OV therapy (and other OVs) (Fig. 4) (Cataldi et al., 2015; Felt et al., 2017; Hastie et al., 2016; Moerdyk-Schauwecker et al., 2013; Murphy et al., 2012). Phenotypes of PDAC cells to OV therapy range from “super permissive” to “super resistant”, with in between “moderately permissive/resistant” phenotypes.

Our previous studies investigated some of the mechanisms associated with PDAC cell permissiveness. We have shown that there is a high level of diversity regarding the ability of PDAC cells to produce and respond to type I interferon (IFN), where the evaluation of IFN sensitivity and IFN production can be used as a predictor for PDAC cell lines responsiveness to OV therapy (Fig. 4) (Moerdyk-Schauwecker et al., 2013; Murphy et al., 2012). We have also demonstrated biomarkers of PDAC cell resistance to VSV-based OV therapy. In particular, the genes MX1, EPSTI1, XAF1, GBP1, SAMD9, and SAMD9L (Hastie et al., 2016). We have further demonstrated that the cell cycle also plays a role in PDAC cell resistance to VSV. Compounds inducing cell cycle arrest in G1 or S phase strongly inhibited VSV replication, while arrest of G2/M phase led to enhanced VSV replication in cells with functional antiviral signaling

(Christian Bressy, 2018). We found that G2/m arrest inhibited IFN production and expression of interferon related genes (ISGs). Together, these investigations highlighted that the uninterrupted cell cycle in cancer cells may be key to the oncoselectivity for OVs, as it may enable virus replication via inhibition of antiviral responses in dividing cancer cells during G2/M phase.

The inhibition of apoptosis is one of the hallmarks of cancer, including PDAC (Hamacher et al., 2008). PDAC with deceased expression or activation of certain apoptotic proteins have the potential to limit cell death following VSV infection (Cary et al., 2011; Gaddy & Lyles, 2005). Our previous studies have demonstrated that VSV with wild type M protein (VSV-M(wt)) induced caspase 3 cleavage, however, VSV-ΔM51 induced greater caspase 3 cleavage in all PDAC cell lines with active type I IFN, despite comparable replication levels of virus (Felt et al., 2015). Overall, these observations indicated that the resistance of some PDAC cell lines to VSV-mediated apoptosis could not only be due to various levels of type I IFN responses that limit virus replication, but also to cell defects in the apoptotic pathways.

Inefficient attachment to PDAC cells is also a mechanism of resistance to VSV-based OV therapy. VSV tumor tropism is mostly dependent on the permissiveness of cancer cells to virus replication rather than to receptor specificity. However, our previous work highlighted that VSV attachment on HPAF-II cells one of most resistant PDAC cell lines to VSV was significantly weaker (Felt et al., 2017). Interestingly, HPAF-II cells showed the lowest levels of low-density lipoprotein receptor (LDLR) expression and consequent lower levels of low-density lipoprotein (LDL) uptake.

In order to further understand mechanisms of PDAC resistance, this dissertation examined whether acquired chemoresistance in human PDAC cells impacted the efficacy of OV therapy (Chapter 2) and investigated how the role of intertumoral heterogeneity impacts OV therapy and

characterized three promising mouse PDAC cell lines as potential models to test OV-based therapeutics *in vivo* (Chapter 3). Understanding how chemoresistance impacts the efficacy of VSV is important as a patients' treatment regimen should be tailored to their own specific cancer characteristics. For example, if we understand that a patient's PDAC tumor is chemoresistant, is OV therapy still a viable treatment strategy? In addition, clinically relevant PDAC models which recapitulate key characteristics of PDAC, such as the dense stromal microenvironment, metastasis, and the complex role of the adaptive immune system are critical for investigating therapeutic possibilities.

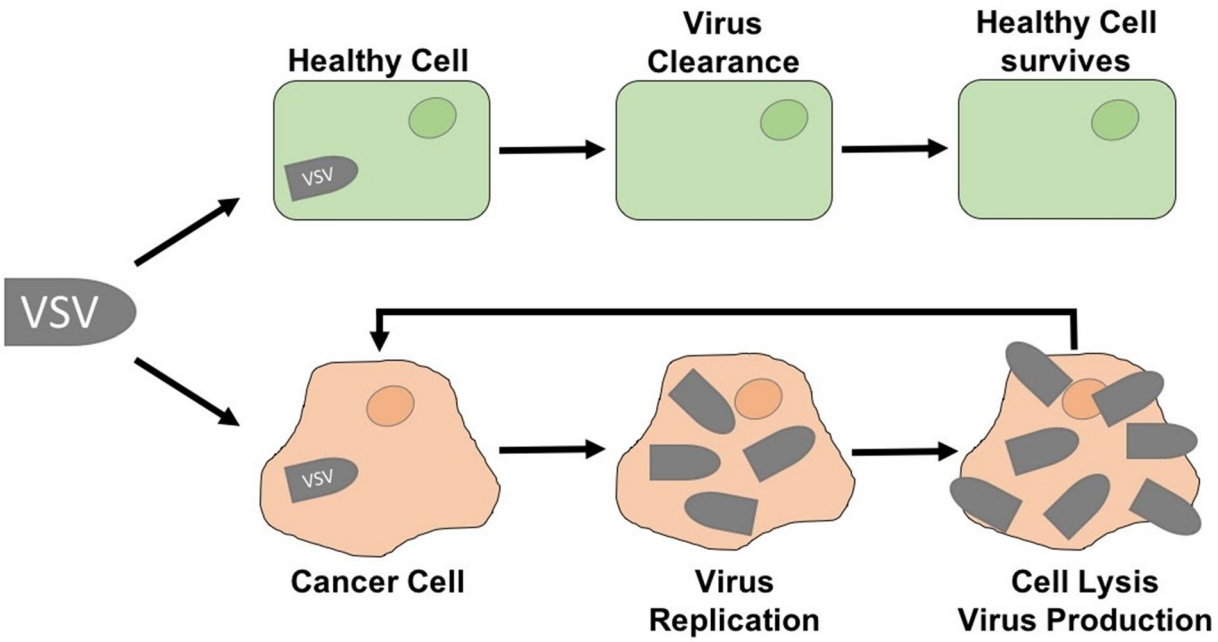

Figure 1**:** How oncolytic viruses work. VSV preferentially replicates in and kills cancer cells, but is cleared in normal healthy cells. This is due to the fundamental biological properties of most cancer cells, where they typically have defective antiviral signaling, as antiviral signaling is pro-apoptotic and anti-proliferative. While defective antiviral signaling confers a growth advantage for the cancer cells, it also allows the cancer cells to preferentially infected with virus compare to normal cells with normal antiviral signaling.

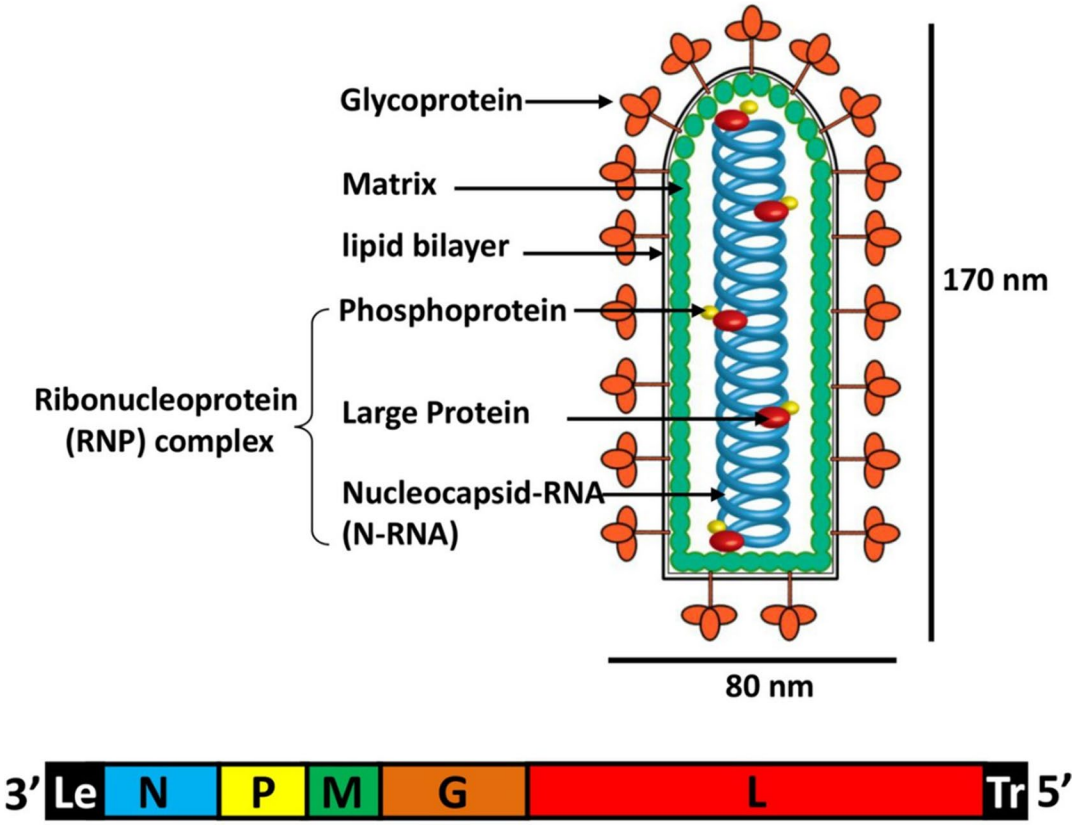

Figure 2: VSV virion structure and genome. The genome is encapsidated with the N protein to form a helical N-RNA complex. The N-RNA complex is tightly associated with the L and P proteins, which make up the RNA-dependent RNA polymerase (RdRp). Altogether, this structure is called the viral ribonucleoprotein (RNP) complex. This RNP complex is surrounded by the M protein and the G protein is anchored in the viral envelop, which is comprised of a lipid bilayer acquired from the host cell the virion budded from. Adapted from Jianrong Li and Yu Zhang (2012).

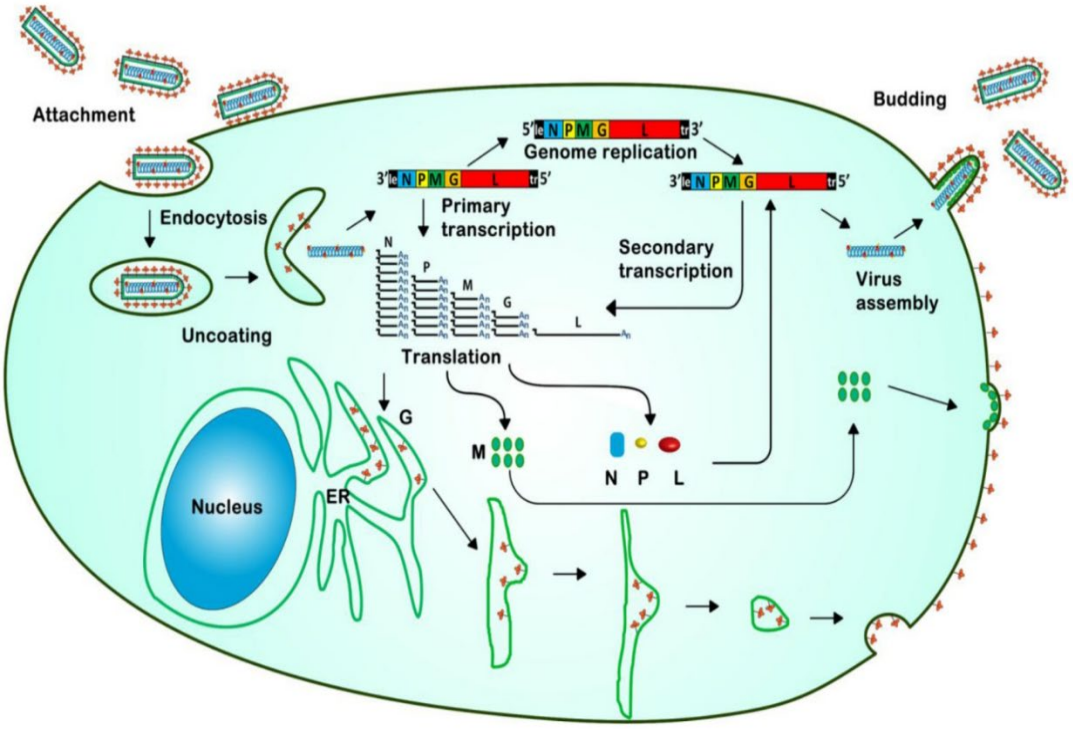

Figure 3: Overview of VSV life cycle. The VSV life cycle starts with attachment and entry via receptor mediated endocytosis. A decrease in pH in the endosome triggers uncoating and the release of the RNP complex into the cytoplasm of the cell. Primary transcription occurs next mediated by RdRp using the N-RNA template. Mature mRNAs are then translated to yield viral proteins that are required for viral genome replication. During viral genome replication, RdRp synthesizes a full length antigenome (+ sense) that is used as a template for progeny genomes (- sense). Progeny genomes are then used as templates for secondary transcription or assembled into new virus particles. Adapted from Jianrong Li and Yu Zhang (2012).

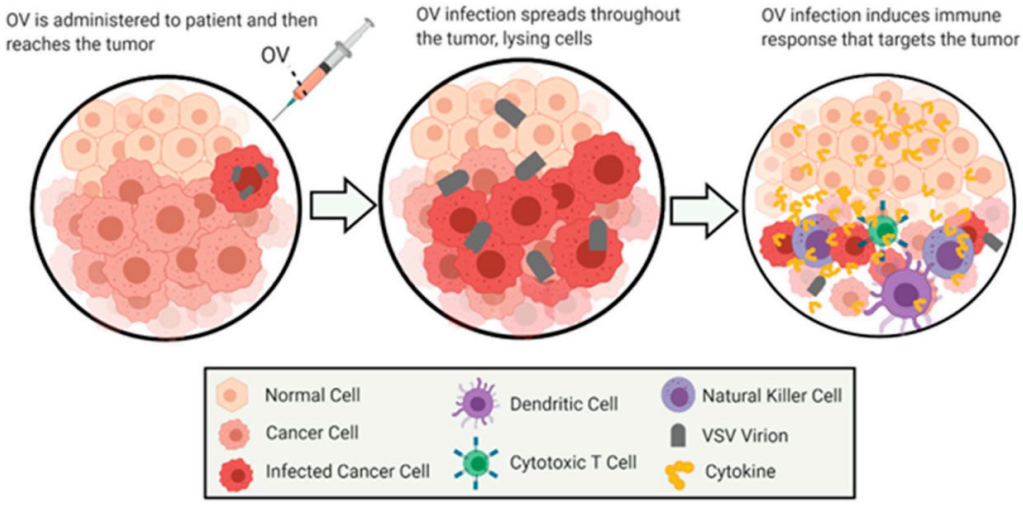

Figure 4: General Overview of Oncolytic Virotherapy. This demonstrates the general method of action for the treatment of cancer by oncolytic virotherapy using VSV as an oncolytic virus. The ideal OV therapy not only results in direct lysis of cancer cells by the virus, but also activates innate and adaptive anticancer immune responses. The images depict the infection and oncolysis of malignant cells over time, followed by immunostimulation of cells invading the cleared area. Adapted by Holbrook et al. (2021).

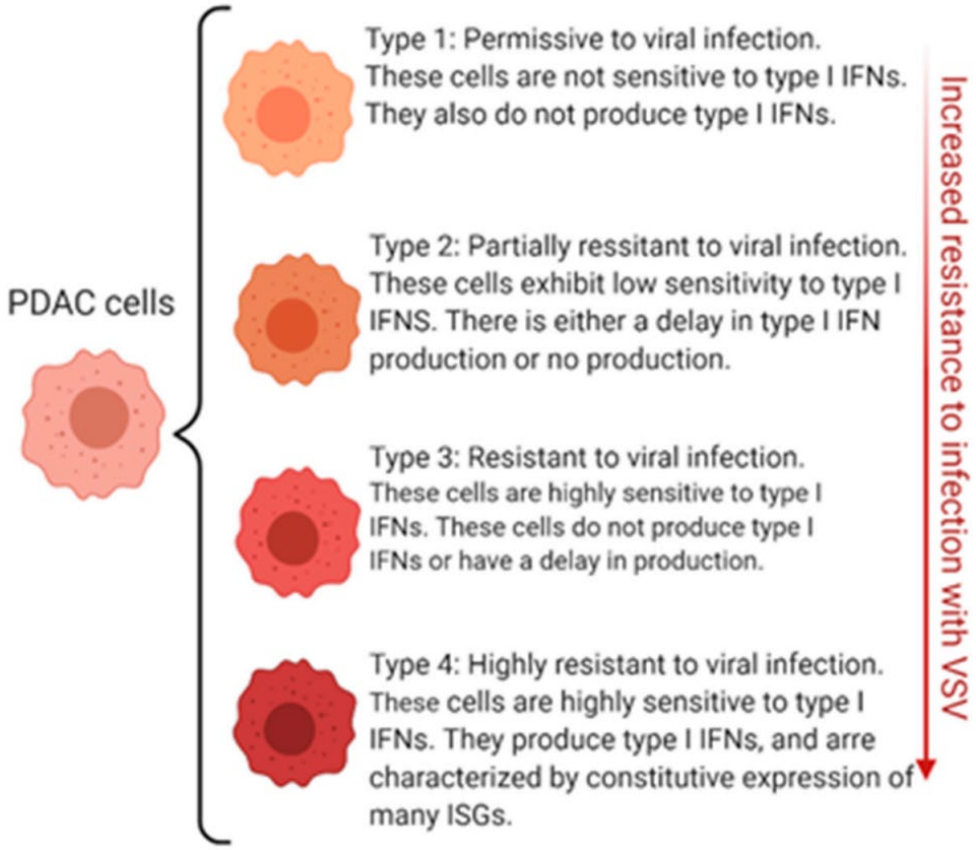

Figure 5: Range of Permissiveness of PDAC to VSV: This figure demonstrates the variability across PDAC cells in regard to permissiveness to infection by VSV. Permissiveness refers to the cells allowance for viral attachment, infection, and replication. Adapted from Holbrook et al. (2021).

CHAPTER 2: ACQUIRED CHEMORESISTANCE CAN LEAD TO INCREASED RESISTANCE OF PANCREATIC CANCER CELLS TO ONCOLYTIC VESICULAR STOMATITIS VIRUS

2.1 Introduction

Since the 1970s, the 5-year survival rate for PDAC patients is about 9%, while many other cancer types have significantly improved (Siegel et al., 2020). The poor survival rate for PDAC is largely attributed to late diagnoses and limited treatment options, as most PDAC tumors are either intrinsically resistant to chemotherapy or rapidly acquire resistance (Orth et al., 2019). The mechanisms of chemoresistance are not fully understood and are likely multifactorial (Zeng et al., 2019).

Chemoresistant PDAC is a major hurdle and a key reason for the poor survival outcomes of PDAC patients. One important question that remains unanswered is how tumor chemoresistance (inherent or acquired) may impact its responsiveness to OV therapy. As tumor chemoresistance may be one of the predictors for the success of OV therapy, understanding this could benefit the way the individualized treatment regimens for PDAC patients are rationally scheduled.

Gemcitabine (2'-deoxy-2',2'-difluorocytidine monohydrochloride; dFdC; trade names Gemzar, Infugem) is a deoxycytidine analogue, and gemcitabine-based chemotherapy regimens are the standard of care for patients with PDAC (Amrutkar & Gladhaug, 2017). Gemcitabine has multiple modes of action once inside the cell (Fig. 4). dFdC must be metabolized to the active triphosphate form. Cell uptake of gemcitabine is mediated by membrane proteins called human nucleoside transporter (hNTS), which allow for nucleoside and nucleoside analog transport (Mackey et al., 1998). Once inside the cell, gemcitabine is phosphorylated by deoxycytidine kinase (dCK) into the monophosphate (dFdCMP) form and phosphorylated again by nucleoside monophosphate

kinase (NMPK) to the diphosphate form (dFdCDP) (Van Rompay et al., 1999). The final phosphorylation step from dFdCDP to dFdCTP is mediated via nucleoside diphosphate kinase (NDPK) (Wong et al., 2009). The rate limiting step of gemcitabine metabolism is considered to be the first phosphorylation event by dCK (Ohhashi et al., 2008). Often, gemcitabine is inactivated via deamination by cytidine deaminase (CDA), and also by deoxycytidylate deaminase (dCTD) when gemcitabine is in monophosphate form (Xu & Plunkett, 1992). The product of deamination via CDA is 2',2'-difluorodeoxyuridine (dFdU), and when this molecule is phosphorylated (dFdUMP), it can act to inhibit thymidylate synthase, directing impacting the deoxynucleotide triphosphate (dNTP) pool (Bergman et al., 2000). As well, gemcitabine can be inactivated by dephosphorylation of the monophosphate form via 5'-nucleosidase (5'NT) (Aksoy et al., 2009). The main mechanism of action of gemcitabine is the inhibition of DNA synthesis. Upon dFdCTP being incorporated into newly synthesized DNA, a single deoxynucleotide is incorporated directly after, preventing further elongation (Gandhi et al., 1996). This non-terminal position of gemcitabine renders DNA polymerases unable to proceed, a process termed "masked chain termination", which also blocks the removal of gemcitabine by DNA repair enzymes(Huang et al., 1991). Additionally, gemcitabine acts to self-potentiate its incorporation into DNA, as the diphosphate form (dFdCDP) inhibits ribonucleotide reductase (RR) visa binding to its active site, thus lowering the deoxycytidine triphosphate (dCTP) pool (Xu et al., 2006) and consequently making dFdCTP more likely to be incorporated into new synthesized DNA.

Here, we experimentally generated human PDAC cells with increased resistance to gemcitabine and examined how the acquired phenotype affected responsiveness of PDAC cells to OV therapy. Our data show that the acquired resistance to gemcitabine can lead to cross-resistance of PDAC cells to three different OVs, including VSV-ΔM51. We also show that the increased resistance of

these cell lines to both gemcitabine and OVs correlated with upregulated levels of a subset of ISGs, resembling the interferon-related DNA damage resistance signature (IRDS), often associated with resistance of cancer cells to chemotherapy and/or radiation therapy (Erdal et al., 2017; Weichselbaum, Ishwaran, Yoon, Nuyten, Baker, Khodarev, Su, Shaikh, Roach, Kreike, Roizman, Bergh, Pawitan, van de Vijver, et al., 2008), (Padariya et al., 2021), (Budhwani et al., 2018). The analysis of ten different PDAC cell lines showed a moderate correlation between chemoresistance and resistance to VSV, and 4 PDAC cell lines most resistant to VSV were also highly resistant to gemcitabine, and they all displayed IRDS-like expression in our previous reports (Hastie et al., 2016), (Cataldi et al., 2015), (Holbrook et al., 2021; Moerdyk-Schauwecker et al., 2013). To the best of our knowledge, this is the first study to examine how experimentally acquired chemoresistance impacts the effectiveness of OV therapy.

2.2 Materials and Methods

Virus and cell lines

The recombinant virus VSV-ΔM51 was previously described (Wollmann et al., 2010), in which the methionine at amino acid position 51 of the matrix protein is deleted and the green fluorescent protein (GFP) open reading frame (ORF) inserted at position 5 of the viral genome (between VSV G and L genes). VSV-M(wt) is similar to VSV-ΔM51 (and contains the GFP ORF inserted at the same position) but has wild type M (Das et al., 2006). The recombinant Sendai virus SeV-GFP (SeV-GFP-F_{mut}), as described previously (Wiegand et al., 2007), has the GFP ORF at position 1 of the viral genome and a mutation in the cleavage site of the fusion (F) protein, allowing F activation and production of infectious particles in cells without acetylated trypsin added to the medium. Baby hamster kidney fibroblast cells BHK-21 (ATCC CCL-10) were used to grow virus and to determine titers. Viral titers were determined by adding serial dilutions of a virus to BHK-

21 cells using an agar overlay followed by calculating either focus forming units per milliliter (FFU/mL) or plaque-forming units per milliliter (PFU/mL). To count PFUs, cells were fixed and stained with crystal violet. To count FFUs, VSV-encoded GFP fluorescent foci were quantified using fluorescent microscopy. The human PDAC cells used in this study were SUIT-2 (Iwamura et al., 1987), HPAF-II (Metzgar et al., 1982), AsPC-1 (Chen et al., 1982), Capan-1 (Kyriazis et al., 1982), Capan-2 (Kyriazis et al., 1986), CFPAC-1 (Schoumacher et al., 1990), MIA PaCa-2 (Yunis et al., 1977), HPAC (Gower et al., 1994), T3M4 (Okabe et al., 1983), and HS766t (Owens et al., 1976). The human origin of all tested PDAC cells lines was confirmed as previously described (Hastie et al., 2016). SUIT-2, MIA PaCa-2, HS766t, HPAC, CFPAC-1, and Capan-1 cells were maintained in Dulbecco's modified Eagle's medium (DMEM [Corning, 10-013-CV]). Capan-2, AsPC-1, and T3M4 cells were maintained in Roswell Park Memorial Institute (RPMI [Corning, 10-040-CV]) 1640 medium. HPAF-II and BHK-21 cells were maintained in Minimum Essential Medium (MEM [Corning 10-010-CV]). All cell growth media were supplemented with 10% fetal bovine serum (FBS [Gibco]), 4 mM L-glutamine, 900 U/mL penicillin, 900 μg/mL streptomycin, and 1% nonessential amino acids. HPAF-II and BHK-21 cells were additionally supplemented with 17.5% glucose. Cells were kept in a 5% CO_2 atmosphere at 37°C. For all experiments, cells were kept no more than 15 passages (except for C and GR cell lines, which were specially passaged as described below).

Generation of gemcitabine-resistant SUIT-2 cells

To select for gemcitabine-resistant SUIT-2 cells, six T75 cell culture flasks were independently passaged in parallel for 20 passages. Three flasks were cultured without the presence of gemcitabine (Selleck, S1714), while three flasks were cultured with increasing concentrations of gemcitabine. The concentration of gemcitabine ranged from 100 nm at passage 1, to 25.6 μM at

passage 20. Each passage of SUIT-2 cells was grown to 100% confluence before the next passage. At each passage, 1/3 cells were used for the next immediate passage, 1/3 cells were frozen for protein/RNA, and 1/3 cells were frozen for future cell culture.

Virus replication kinetics

For all experiments, MOI was calculated by determining the titer of viruses using standard plaque assays on BHK-21 cells in 24 or 12-well plates. For virus replication kinetics experiments, cells were seeded into 96-well plates. Virus dilutions were prepared in DMEM with 0% FBS. Cells were washed once with PBS, followed by the addition of virus for 1 h at 37ºC. Virus-containing medium was aspirated, and fresh DMEM with 5% FBS was added back to cells and then incubated at 37ºC in 5% CO_2 for the duration of the experiment. Virus-encoded GFP fluorescence was measured at different times over a 72-h time course using a fluorescence multiwall plate reader. GFP fluorescence was read at 485/530nm.

Cell viability assay

For cell viability assays in a 96-well plate layout, cells were infected at either MOI 1, 0.1, or 0.01. Each cell line was also mock-treated (negative control). At 70 h post-infection (h p.i.), WST-8 (Dojindo, CK04) was added to each well for 4 h at 37ºC in 5% CO_2, then read using a multi-well plate reader at 450 nm. Results are expressed as fold change compared to mock treatment.

RNA isolation, cDNA generation, PCR amplification, RNA-Seq analysis and gene expression analysis

Three biological repeats were used for each treatment condition for RNA-Seq. SUIT-2-C1, SUIT-2-GR1, SUIT-2-GR2, and SUIT-2-GR3 cell lines were seeded into 12-well plates ($0.4x10^6$ cells per well) in DMEM containing 10% FBS. After 8 h, cellular RNA was isolated with TRIzol

(Life Technologies) according to the manufacturer's protocol. The RNA samples were then subjected to DNAse treatment (Invitrogen TURBO DNA-free™) and sent to GeneWiz for RNA sequencing. Sequence reads were trimmed to remove possible adapter sequences and nucleotides with poor quality using Trimmomatic v.0.36. The trimmed reads were mapped to the Homo sapiens GRCh38 reference genome available on ENSEMBL using the STAR aligner v.2.5.2b. The STAR aligner is a splice aligner that detects splice junctions and incorporates them to help align the entire read sequences. BAM files were generated as a result of this step. Unique gene hit counts were calculated by using feature Counts from the Subread package v.1.5.2. The hit counts were summarized and reported using the gene id feature in the annotation file. Only unique reads that fell within exon regions were counted. Since a strand-specific library preparation was performed, the reads were strand-specifically counted. After extraction of gene hit counts, the gene hit counts table was used for downstream differential expression analysis. Using DESeq2, a comparison of gene expression between the customer-defined groups of samples was performed. The Wald test was used to generate p-values and log2 fold changes. Genes with an adjusted p-value < 0.05 and absolute log2 fold change > 1 were called differentially expressed genes for each comparison. A gene ontology analysis was performed on the statistically significant set of genes by implementing the software GeneSCF v.1.1-p2. The goa_human GO list was used to cluster the set of genes based on their biological processes and determine their statistical significance. A list of genes clustered based on their gene ontologies was generated.

Plaque assay

12-well plates were seeded with SUIT-2 (GR1-GR3) and SUIT-2 (C1-C3) for about 90% confluence. The first column was infected at an MOI of 0.01, and then 2-fold serial dilutions were used to infect the remaining columns (down to MOI 0.000019). Each cell line was also mock-

treated (control). One h after infection, virus was aspirated and wells were overlayed with 2% Bacto agar (Difco™ Lactobacilli MRS Agar – 288210) with 5% FBS DMEM. After 72 h, formalin was added to fix cells for 4 h. After fixation, agar was removed and cells were stained with crystal violet stain solution (2% crystal violet in methanol).

Nexcelom cell counting

Cells were seeded in 24-well plates for 95% confluence. Cells were infected with VSV-ΔM51 at MOIs of 0.01 or 1 or mock-infected for 13 h and 24 h. After infection, cells were washed with PBS and trypsinized. Cells were then put in cell counting chambers (Nexcelom Cellometer SD100) and percent GFP-positive cells were counted using a fluorescent cell-counter (Nexcelom Cellometer Vision). Calibration was performed as per the manufacturer's protocol and the percent of GFP-positive cells was determined.

Western blot analysis

Cells were seeded into 12-well plates at 95% confluence. Medium was removed and cells were washed once with PBS. Virus was then added at MOIs of 0.01, 0.1, or 1 in 0% FBS medium and incubated for 1 h at 37ºC. After 1 h of incubation, the medium was removed, and 5% FBS containing medium was added to the cells. Cells were then lysed and total protein was isolated 1-48 h p.i. using buffer exactly as described previously (Bressy et al., 2019). Total protein was separated by electrophoresis on 10-15% SDS-PAGE gels and electroblotted onto polyvinyl difluoride (PVDF) membranes. Membranes were blocked by using 5% nonfat powdered milk or BSA in TBS-T (0.5 M NaCl, 20 mM Tris [pH 7.5], 0.1% Tween 20) for 1 h at room temperature. Membranes were then incubated in TBS-T with 5% bovine serum albumin (BSA) or milk with 0.02% sodium azide and a 1:5,000 dilution of rabbit polyclonal anti-VSV antibodies (raised against VSV virions), a 1:1000 dilution of rabbit anti-phospho-STAT1 (catalog number 9177S, clone p-

S727; Cell Signaling), a 1:1000 dilution of rabbit anti-STAT1 (catalog number 14994T, clone D1K9Y; Cell Signaling), a 1:1000 dilution of rabbit anti-phospho-STAT2 (catalog number 600-401-A93S, clone p-Y689; Rockland), a 1:1,000 dilution of rabbit anti-STAT2 (catalog number 4594, Cell Signaling), a 1:1000 dilution of rabbit anti-phospho-STAT3 (catalog number 9134P, clone Y705, Cell Signaling), a 1:1000 dilution of mouse anti-STAT3 (catalog number 9139P, clone 124H6, Cell Signaling), a 1:1000 dilution of rabbit anti-MX1 (catalog number 13750-1-AP, Proteintech), a 1:1000 dilution of rabbit anti-MX2 (catalog number 43924S, clone E7Y8H, Cell Signaling), a 1:1000 dilution of rabbit anti-IFI16 (catalog number 14970S, clone D8B5T, Cell Signaling), a 1:1000 dilution of rabbit anti-APOBEC3B (catalog number 41494S, clone E9A2G, Cell Signaling), a 1:1000 dilution of rabbit anti-ISG15 (catalog number 2758S, clone 22D2, Cell Signaling), a 1:1000 dilution of rabbit anti-CDK14-PFTK1 (catalog number 21612-1-AP, Proteintech), a 1:1000 dilution of rabbit anti-LARGE2/GYLTL1B (catalog number PA5-63331, Invitrogen), a 1:1000 dilution of rabbit anti-STING (catalog number 13647S, clone D2P2F, Cell Signaling), a 1:1000 dilution of rabbit anti-phsopho-TBK1/NAK (catalog number 5483P, clone S172, Cell Signaling), a 1:1000 dilution of rabbit anti-cGAS (catalog number 79978, clone E5V3W, Cell Signaling, or a 1:1,000 dilution of rabbit anti-cyclin B1 (catalog number 12231T, clone D5C10; Cell Signaling). Starbright Blue 700 goat anti-rabbit (Bio-Rad, 12004161) or anti-mouse (Bio-Rad, 12004158) IgG fluorescent secondary antibodies at 1:5000 dilutions were used for fluorescent Western blotting detection using the Chemidoc MP imaging system from Bio-Rad. To verify total protein, the membranes were stained with Coomassie Blue stain.

IC50 and TCID50

For gemcitabine IC50 determination, cells were seeded into 96-well plates for approximately 50% confluence in medium supplemented with 10% FBS. On the following day, cells were treated

with serial dilutions of gemcitabine (Selleck, S1714) ranging from 1000µM to 0.008µM. A WST-8 (Dojindo, CK04) cell viability assay was performed 48 h later. For VSV IC50 and TCID50 determination, cells were seeded into 96-well plates for approximately 95% confluence in medium supplemented with 10% FBS. On the following day, cells were infected with serial dilutions of VSV ranging from MOI 0.01 to MOI 0.00006. GFP-based FFU were counted at 24 h p.i. for TCID50 using a fluorescent microscope. A WST-8 cell viability assay was performed at 120 h p.i. IC50 values were calculated using GraphPad Prism 7.04. For TCID50 determination, the Reed and Muench method was used as previously described. (Ramakrishnan, 2016)

Statistical analysis

All statistical analyses were performed using GraphPad Prism 7.04 software. Tests used are indicated in the legends of the figures.

2.3 Results

Experimental generation of gemcitabine-resistant human PDAC cells

The human PDAC cell line SUIT-2 (Iwamura et al., 1987) was used for the experimental generation of gemcitabine-resistant cells (Fig. 7A). This cell line has been extensively studied in our laboratory, and SUIT-2 cells display an intermediate level of permissiveness to VSV compared to other tested PDAC cell lines (Hastie et al., 2015; Moerdyk-Schauwecker et al., 2013; Murphy et al., 2012). Parental SUIT-2 cells were split into six individual flasks and passaged twenty times in parallel without gemcitabine treatment to generate three “control” (“C”) cell lines, and in the presence of gemcitabine to generate three “gemcitabine-resistant” (“GR”) cell lines (Fig. 7A). Cells were allowed to reach approximately 100% confluence before being passaged again, and with each passage, the gemcitabine concentration was gradually increased, as conducted in

previous studies (Quint et al., 2012; Samulitis et al., 2015). The C cells were passaged in parallel, but without gemcitabine.

To compare the responsiveness to gemcitabine for SUIT-2 cells passaged 20 times in the presence or absence of the drug, the C cell lines (C1, C2, and C3) and the GR cell lines (GR1, GR2, and GR3) were treated with serial dilutions of gemcitabine for 24 hours (h), 48 h, or 72 h, followed by a WST-8 cell viability assay (Fig. 7B). As expected, GR cells became more resistant to gemcitabine compared to C cells (Fig. 7B). Together, our data show that the long-term exposure of SUIT-2 cells to increased concentrations of gemcitabine resulted in the increased resistance of all three SUIT-2-originated GR cell lines to the drug.

Gemcitabine-resistant PDAC cells developed increased resistance to VSV-ΔM51 infection

To compare C and GR cells in their responsiveness to VSV, we compared the ability of the oncolytic VSV recombinant VSV-ΔM51 to replicate in C and GR cells (Fig. 8). VSV-ΔM51 has a deletion of the methionine residue at position 51 (ΔM51) in the VSV-encoded matrix (M) protein. This mutation prevents VSV-M from binding to the Rae1-Nup98 mRNA export complex required for cellular mRNA transport and subsequent translation. Therefore, VSV-ΔM51 is not able to inhibit antiviral responses in initially infected cells (normal or cancer) by disrupting transport and translation of cellular mRNAs for antiviral genes, which limits its replication in the neighboring normal cells but not in cancer cells as they are typically defective in antiviral responses (Black et al., 1993; Hastie & Grdzelishvili, 2012; Stojdl et al., 2003). In addition, the particular recombinant virus VSV-ΔM51 used in this study contains the green fluorescent protein (GFP) reporter gene inserted at position 5 of the viral genome between the VSV G and L genes which allows for monitoring of virus replication and spread based on VSV replication-driven GFP expression (Wollmann et al., 2010). GFP expression has been shown to correlate well with virus replication

in VSV-ΔM51 infected cells (Wollmann et al., 2010). The C and GR cells were mock-infected or infected with VSV-ΔM51 at a multiplicity of infection (MOI) of 1, 0.1, or 0.01 (herein and after the MOI was calculated based on viral titer on BHK-21, a reference cell line highly permissive to VSV), and GFP expression was examined over time by measuring GFP fluorescence. As shown in Fig. 6A, GR cells showed markedly lower levels of VSV-driven GFP expression compared to C cells at each tested MOI. To examine whether the different levels of GFP expression correlated with cell viability, the C and GR cell lines were infected with VSV-ΔM51 for 70 h, followed by a WST-8 cell viability assay. We found that the decrease in VSV replication-dependent GFP expression in GR cells correlated with higher cell viability of GR cells, compared to C cells (Fig. 8B).

While Figure 6A demonstrates higher overall GFP levels in VSV-infected C cells compared to GR cells, we also wanted to compare the percent of GFP-positive cells over time in C and GR cell lines infected with the same amounts of VSV. Cells were infected with VSV-ΔM51 at an MOI of 1, 0.1, or 0.01 and the percent of GFP-positive cells was measured at 13 h p.i. (Fig. 6C) and 24 h p.i. (Fig. 8D) using a fluorescent cell counter. We found that at 13 h p.i., there were fewer GR cells infected at an MOI 1, and at 24 h p.i., there were markedly fewer GR cells infected at each MOI, compared to C cells.

To compare virus yield in C and GR cell lines, *de novo* VSV virion production was measured in C and GR cells after a low MOI infection condition (for multi-step virus growth kinetics) and a high MOI infection condition (for single-step virus growth kinetics). C and GR cells were infected with VSV-ΔM51 at an MOI of 0.01 (Fig. 8E) or 10 (Fig. 8F). After initial infection, wells were thoroughly washed and fresh media was added. Media was collected at 1, 12, 24, 48, 72, and 96 h p.i., and virus titers were determined for each time point by counting GFP-based fluorescent focus

forming units (FFU) on BHK-21 cells. We found that at 24 h p.i. for both multi-step (Fig. 8E) and single-step kinetics (Fig. 8F), GR cell lines produced significantly fewer virus particles compared to C cell lines. Interestingly, VSV virion production did not differ between C and GR cells at 12 h p.i., suggesting that virus replication and spread were restricted at later stages. There were low or non-detectable levels of virus particles after 48 h p.i., likely due to cell death and expired virus particles, which were detectable at earlier times.

To compare the abilities of VSV-ΔM51 to initiate infections and spread to neighboring cells in C and GR cell lines, we infected cells with the same serial dilutions of VSV-ΔM51, overlaid them with agar, and then microscopically analyzed cell monolayers at 48 or 72 h p.i. to count FFUs and compare sizes of virus-induced fluorescent foci. In addition, we performed a standard plaque assay to count and compare the sizes of virus-induced plaques. In agreement with higher replication levels of VSV-ΔM51 in C cells (Fig.8), we observed markedly larger plaques (Fig. 9A) and fluorescent foci (Fig. 9B) in C cells, compared to GR cells. However, there was no statistically significant difference in the numbers of FFU/ml (Fig. 9C) or PFU/ml (Fig. 9A and data not shown) between C and GR cells. Our data are also in agreement with our analysis of virus yield in C and GR cells at early and later time points (Fig. 8E-F), suggesting that VSV-ΔM51 has similar abilities to initiate infection in C and GR cells, but that virus replication and spread was restricted at later stages in GR cells.

To examine how stable is the observed difference in the permissiveness to VSV-ΔM51 between GR and C cell lines, C and GR cell lines were passaged 20 additional times in the absence of gemcitabine to generate passage 40 (“P.40”) C (C1, C2 and C3) cell lines and P.40 GR (GR1, GR 2 and GR 3) cell lines, and then cells were either mock treated or infected with VSV-ΔM51 at MOIs of 1.0, 0.1, or 0.01 and GFP fluorescence was measured over time from 1 h p.i. to 72 h p.i.

(Fig. 9A). In addition, P.40 C and P.40 GR cells were examined for cell viability at 70 h p.i. (Fig. 10B). Our data demonstrate that that GR cell lines stably maintain higher resistance to VSV compared to C cells (Fig. 10A-B).

GR cells exhibit increased resistance to other OVs

To examine if the increased resistance of GR cells is specific to VSV-ΔM51 only, we infected C and GR cell lines with either VSV-ΔM51 or VSV-M(wt) (VSV containing a wild-type matrix (M) protein and GFP reporter gene) or a recombinant Sendai virus (SeV, a paramyxovirus) SeV-F_{mut} at MOIs 1, 0.1, and 0.01, and measured virus replication driven GFP fluorescence over time. Similar to VSV-ΔM51, VSV-M(wt) and SeV-F_{mut} replicated at lower levels in GR cells compared to C cells at most tested MOIs (Fig. 10C). These data suggest that the acquired chemoresistance in GR cells produced resistance not only to VSV-ΔM51, but also other OVs.

GR cell lines exhibit increased STAT1/STAT2 antiviral signaling compared to C cell lines

Our previous studies demonstrated the major role of constitutive or virus-induced type I IFN antiviral responses in resistance of some PDAC cell lines to VSV and other tested OVs (Hastie et al., 2016; Holbrook et al., 2021; Moerdyk-Schauwecker et al., 2013; Murphy et al., 2012). The observed resistance of GR cells to both VSV and SeV could suggest the same mechanism in GR cells. In the canonical type I IFN-induced signaling pathway (Mazewski et al., 2020), the interaction of type I IFNs (IFN-□ or IFN-□) with IFN-α receptor (IFNAR) activates the IFNAR-associated protein tyrosine kinases Janus kinase 1 (JAK1) and tyrosine kinase 2 (TYK2), which phosphorylate the cytoplasmic transcription factors signal transducer and activator of transcription 1 (STAT1) and 2 (STAT2). Phosphorylated STAT1-STAT2 heterodimer then dissociates from the

receptors and recruits IFN-regulatory factor 9 (IRF9) in the cytoplasm to form a trimolecular complex called IFN-stimulated gene factor 3 (ISGF3). ISGF3 then translocates to the nucleus, where it binds to DNA sequences with so-called IFN-stimulated response elements (ISREs), directly activating the transcription of a large number of antiviral ISGs.

To examine the role of type I IFN responses in resistance of GR cells to viruses, we infected C and GR cells with VSV-ΔM51 at MOIs 1, 0.1, and 0.01, total protein was isolated at 24 (Fig. 11A) and 48 h p.i. (Fig. 11B), and analyzed by Western blotting for major modulators of type I IFN signaling: total STAT1, phosphorylated STAT1 (p-STAT1-Ser727), total STAT2, and phosphorylated STAT2 (p-STAT2-Tyr689). VSV protein accumulation was also analyzed. In agreement with our hypothesis, at both 24 and 48 h p.i., and at all tested MOIs, protein accumulation of total STAT1, p-STAT1, total STAT2, and p-STAT2 were greater in GR cells compared to C cells, which also negatively correlated with overall VSV protein accumulation. In mock-treated cells, we were unable to detect clear differences in STAT1, p-STAT1, STAT2, or p-STAT2 protein expression, in part due to the low levels of some of these proteins in uninfected cells.

To further study the role of antiviral signaling in the resistance of GR cells to VSV, we examined the effect of ruxolitinib on VSV-ΔM51 replication in GR cells (Fig. 11C) and C cells (Fig. 11D). Ruxolitinib ("Ruxo" in Fig. 10C-D) is an FDA-approved drug (brand names Jakafi and Jakavi) and a selective JAK1/JAK2 kinase inhibitor that shuts down the JAK/STAT signaling axis. We hypothesized that if GR cells are more resistant to VSV due to increased antiviral signaling, then the treatment with ruxolitinib would enhance VSV replication in GR cells compared to C cells. C and GR cells were infected with VSV-ΔM51 at a MOI of 0.01, then either mock-treated or treated with 10 □M or 0.02 □M ruxolitinib, and VSV replication-directed GFP expression was

measured until 80 h p.i. Our data show that at both higher and lower concentrations, ruxolitinib increased VSV-ΔM51 replication in GR cells, but not in C cells (Fig. 11C and 11D).

To further investigate the role of antiviral signaling in the resistance of GR cells to virus infection, we conducted a global transcriptome analysis comparing mRNA levels in uninfected C and GR cells. Our goal was to identify genes and pathways that could potentially play a role in increased resistance of gemcitabine-resistant GR cells to VSV. Total RNA was isolated from untreated C and GR cells, analyzed by RNA sequencing (RNA-Seq) to get a global, transcript-level snapshot of gene expression, and a Gene Ontology (GO) analysis was performed to identify significantly enriched biological processes in GR cells compared to C cells (Fig. 10A). Importantly, among the top 40 biological processes positively or negatively modified in GR cells, there were six processes associated with antiviral signaling, and they were all significantly upregulated in GR cells compared to C cells (Fig. 12A, red text boxes). These data agree with the reduced levels of VSV-ΔM51 replication in GR cells compared to C cells (Fig. 8, 9) and with the increased expression of major antiviral signaling proteins (Fig. 11). To further investigate the specific genes associated with cellular antiviral responses, we utilized the QIAGEN Ingenuity Pathway Analysis (IPA) software. Figure 8B shows some of the most enriched genes that are associated with the IPA-defined processes “Antiviral response” and ‘Replication of viral replicon” between uninfected C and GR cells. The list of the most significantly upregulated genes (indicated by red shapes) includes such well-known antiviral ISGs as MX1, MX2, IRF3, IFITM1, ISG15, RSAD2 (viperin), DHX58 (LGP2), IFIT1, IFITM3, IFI16, IFI44, and APOBEC3B. These data demonstrate that even in the absence of virus infection, GR cells have upregulated levels of antiviral ISGs compared to C cells. Table 1 (“Antiviral” group) shows a more comprehensive list of differentially expressed antiviral genes in GR cells compared to C cells. This analysis revealed

a significant upregulation of well-known ISGs in GR cells in the absence of virus infection, such as IFITM2, which log2 fold change of 1.88 corresponds to a 188% upregulation in GR cells compared to C cells. The canonical IFN-induced ISG expression depends on interaction of IFNs with IFN receptors. Interestingly, however, our RNA-Seq data reveal that despite the upregulation of ISGs in GR cells compared to C cells, we did not observe any upregulation for Type I IFN-α, Type I IFN-β (Fig. 12C), Type II IFN-γ (Fig. 12C), or Type III IFN- (data not shown). Table 2 shows genes in the gene families "cytidine deaminase", "nucleotide transporters", and deoxycytidine kinase", as genes in these groups are known to have roles in resistance to gemcitabine (Amrutkar & Gladhaug, 2017).

Our RNA-Seq data revealed a subset of ISGs, which were significantly upregulated in GR cells compared to C cells at the mRNA level. To examine the protein levels of these ISGs at different times after infection, C and GR cells were infected with VSV-ΔM51 at MOI 0.01, total protein was collected at 1, 12, 24, and 32 h. p.i., and analyzed by Western blotting (Fig. 10A). Most antiviral proteins were expressed greater at later times post-infection, and in most cases, greater levels were observed in GR cell lines compared to Control cell lines, which is consistent with our earlier experiments (Fig. 11). This list includes total STAT1, p-STAT1, total STAT2, p-STAT2, MX1, MX2, IFI16, ISG15, STING, and some other ISGs. Together, our data show that GR cells have upregulated constitutive (Fig. 12) and virus-inducible (Fig. 11,12) expression of antiviral ISGs, which correlates well with the resistance of GR cells to VSV.

It is still unclear if the upregulation of these well-known antiviral ISGs plays any role in the resistance of GR cells to gemcitabine. Previous studies have shown that resistance of some cancers to chemotherapy and/or radiation therapy could be associated with so-called interferon-related DNA damage resistance signature (IRDS) (Budhwani et al., 2018; Erdal et al., 2017; Padariya et

al., 2021; Weichselbaum, Ishwaran, Yoon, Nuyten, Baker, Khodarev, Su, Shaikh, Roach, Kreike, Roizman, Bergh, Pawitan, de Vijver, et al., 2008). Although the exact mechanism of increased resistance of GR cell lines to gemcitabine is beyond the scope of this study, and the exact role of IRDS in resistance of some cancers to chemotherapy and/or radiation therapy is still unclear, we examined whether the ISGs overexpressed in response to VSV are also upregulated in GR cells after treatment with gemcitabine. Cells were either mock-treated, infected with VSV-ΔM51 at MOI 0.01, or treated with gemcitabine at a concentration of either 5 μM or 0.1 μM. Total protein was then isolated after 32 h. As expected, STAT1, MX1, MX2, IFI16, and ISG15 were induced in all VSV-infected cell lines and each gene upregulated greater in VSV-infected GR cells, compared to VSV-infected C cells (Fig. 13B). Interestingly, however, these proteins were also upregulated (although to a lower level, compared to VSV-infected cells) after gemcitabine treatment, and primarily in GR cells. Our future studies will examine whether these and/or other ISGs may play a causative role in the cross-resistance of GR cells to both gemcitabine and VSV.

Analysis of correlation between resistance of different human PDAC cell lines to gemcitabine and VSV

Our data show that when we experimentally generate human PDAC cells to be more resistant to gemcitabine, the cells also become more resistant to VSV, likely via upregulation of ISG expression (constitutive as well as virus-inducible). Our lab has previously published work demonstrating that human PDACs are heterogeneous in their resistance to VSV. To examine whether there is a correlation between gemcitabine resistance and resistance to VSV across ten human PDAC cell lines (Table 2, Fig. 14), C and GR cells were either infected with serial dilutions of VSV-ΔM51 or treated with serial dilutions of gemcitabine for 48 h. In one approach, we examined the correlation between permissiveness of PDAC cells to VSV and the effect of

gemcitabine on PDAC cell viability (Fig. 14A). VSV FFU were counted to obtain TCID50 (Tissue Culture Infectious Dose), which indicates the amount of virus required to infect 50% of cultured cells, and cell viability was determined for gemcitabine treated cells to obtain gemcitabine IC50 (Fig. 14A). In another approach, we examined the correlation between the effect of VSV on PDAC cell viability and the effect of gemcitabine on PDAC cell viability (Fig. 14B shows resistance to VSV indicated as IC50, which was obtained by measuring cell viability after 48 h instead of FFU). In general, the analyses of these ten different human PDAC cell lines show no statistically significant correlation between resistances to gemcitabine and VSV. Thus, AsPC-1 cells are highly permissive to VSV, but they were, together with HPAF-II, the most resistant to gemcitabine among all tested PDAC cell lines. However, 4 PDAC cell lines most resistant to VSV (Hs766t, HPAF-II, CFPAC-1, and HPAC) were also among 5 PDAC cell lines most resistant to gemcitabine. Importantly, the same 4 PDAC cell lines displayed IRDS-like constitutive expression of ISGs in our previous reports (Hastie et al., 2016)·(Cataldi et al., 2015)·(Holbrook et al., 2021; Moerdyk-Schauwecker et al., 2013).

2.4 Conclusions

Here, we investigated how acquired chemoresistance impacts the efficacy of VSV-based OV therapy. Using an experimental evolution approach, we generated gemcitabine-resistant PDAC cell lines with increased resistance to gemcitabine and examined their responsiveness to oncolytic virotherapy. We found that gemcitabine-resistant PDAC cells become more resistant to VSV-ΔM51 and other OVs. The increased resistance to OVs correlated with upregulated levels of a subset of interferon-stimulated genes (ISGs), resembling the interferon-related DNA damage resistance signature (IRDS), often associated with resistance of cancer cells to chemotherapy

and/or radiation therapy. Although analysis of 10 different PDAC cell lines showed no statistically significant correlation between chemoresistance and resistance to VSV, 4 PDAC cell lines most resistant to VSV were also highly resistant to gemcitabine, and they all displayed IRDS-like expression in our previous reports. These results will be further discussed in the dissertation summary (Chapter 4).

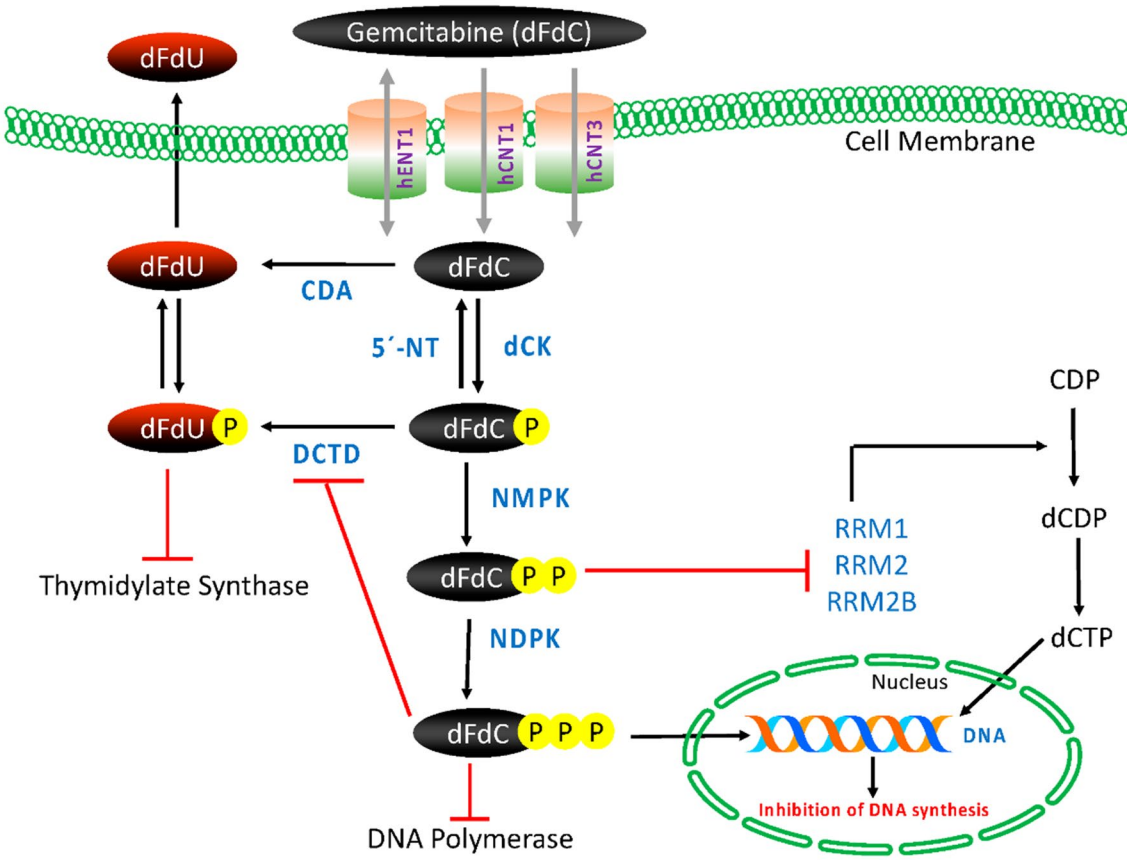

Figure 6: Gemcitabine transport, intracellular activation/deactivation and mechanism of action. CDA cytidine deaminase, dCK: deoxycytidine kinase, dCTD: deoxycytidylate deaminase, dFdC: 2',2'-difluorodeoxycytidine, dFdU: 2',2'-difluorodeoxyuridine, hENTs and hCNTs: human nucleoside equilibrative transporters and human nucleoside concentrative transporters (respectively), NDPK: nucleoside diphosphate kinase, NMPK: nucleoside monophosphate kinase, RR (M1/M2): ribonucleotide reductase, 5'NT: 5'-nucleotidase. Adapted from Manoj Amrutkar and Ivar Gladhaug (2017).

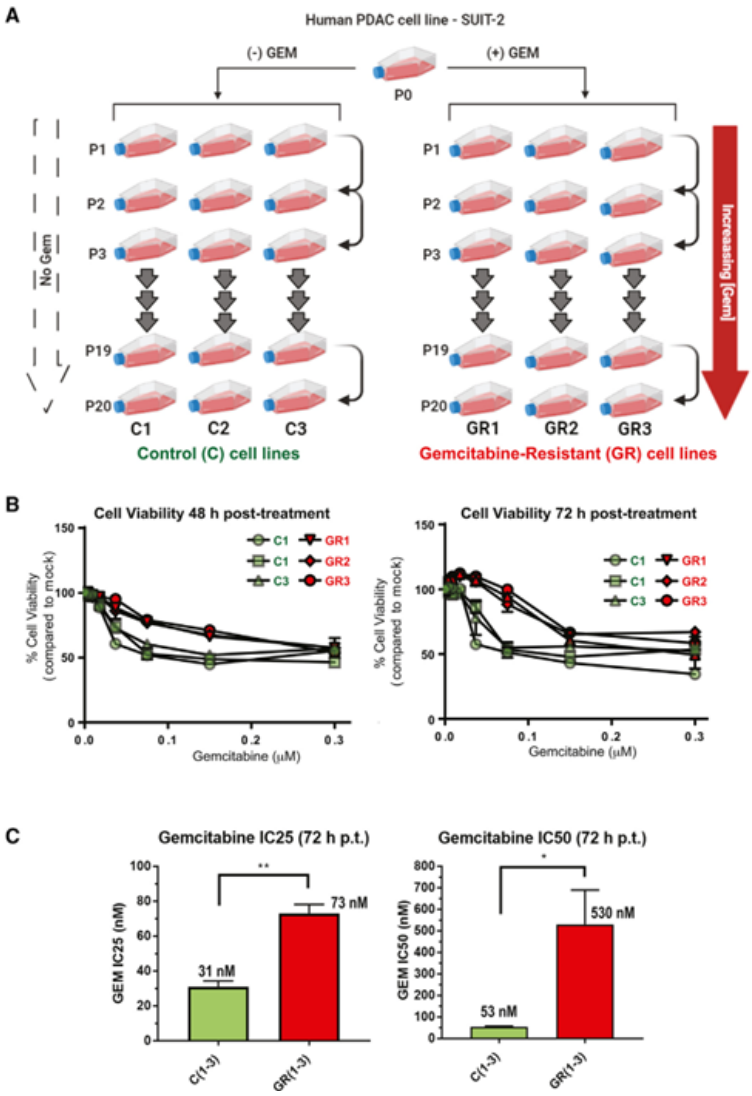

Figure 7: Experimental generation of gemcitabine-resistant (GR) SUIT-2 cells. (A) SUIT-2 cells were passaged in parallel for 20 generations in triplicate in the presence of gemcitabine (GR cells), or without gemcitabine-cultured media (C cells). Cells were exposed to an increasing concentration of gemcitabine from 100 nM (P1) to 25.6 μM (P20). (B) Cell viability of C and GR cells at different concentrations of gemcitabine. Cells were mock treated or treated with gemcitabine at concentrations ranging from 250 to 0.001 μM, and cell viability was measured at 48 and 72 h post-treatment (p.t.) by WST-8. (C) Comparing resistance of C and GR cells to gemcitabine. IC25 and IC50 values were calculated using GraphPad Prism 7.04. (B) and (C) represent results from at least three independent experiments. The data points and error bars shown represent the means and SEM of the means, respectively. Results were analyzed to determine significance using a Student's t test. $*p < 0.05$, $**p < 0.01$.

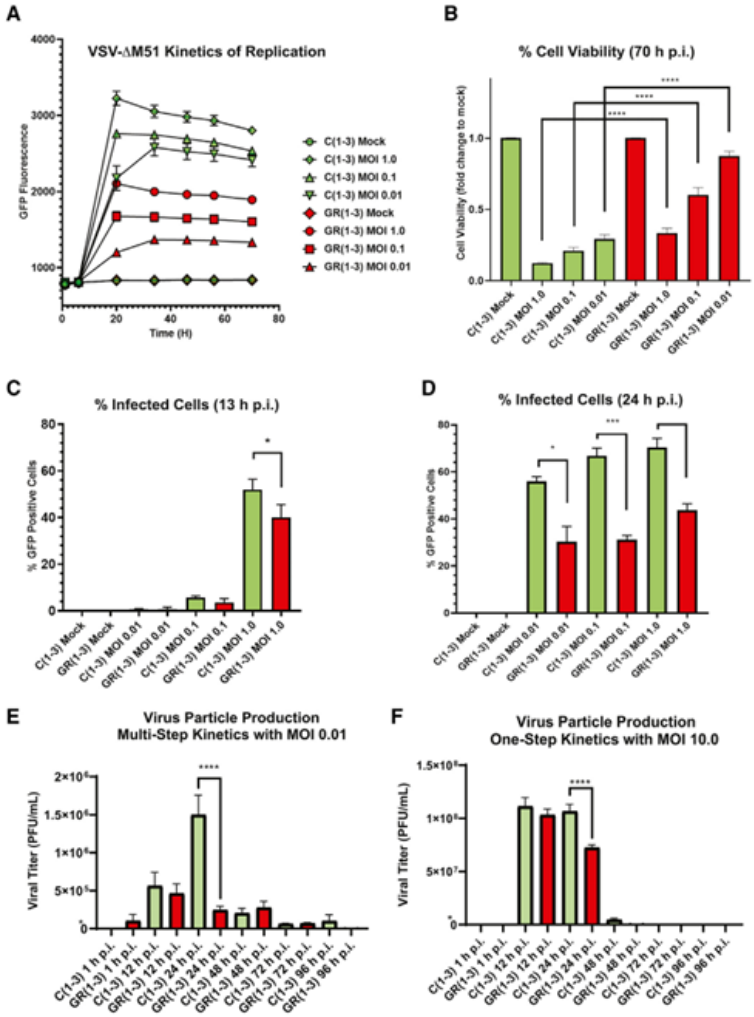

Figure 8: Viral replication kinetics. (A) C and GR cell lines were either mock treated or infected with VSV-ΔM51 at MOIs of 1.0, 0.1, or 0.01. GFP fluorescence was measured over time from 1 to 72 h p.i. Control and GR cell lines 1–3 are combined for each MOI. (B) Control and GR cell lines were either mock treated or infected with VSV-ΔM51 at MOIs of 1.0, 0.1, or 0.01. Cell viability was measure 70 h p.i. The figure represents data from three independent experiments. (C and D) Control and GR cells were infected with VSV-ΔM51 at MOIs of 1.0, 0.1, and 0.01. Samples were collected at 13 and 24 h p.i., trypsinized, and percent of GFP-positive cells was determined via a Nexcelom Cellometer Vision cell counting system. (E and F) Virus particle production: Control and GR cells were infected with VSV-ΔM51 at an MOI of 0.01 (E) or MOI 10 (F). Wells were washed after initial 1-h infection and fresh media was added to all wells. Supernatant was collected at 1, 12, 24, 48, 72, and 96 h p.i. Virus titers were determined using standard plaque assay on BHK-21 cells. The data points and error bars shown represent the means and SEM of the means, respectively (some error bars are too small to be seen in the figures). Results were analyzed to determine significance using a Student's t test or one-way analysis of variance with a Sidak's multiple comparison test at a 95% confidence interval for comparison between each condition. $*p < 0.05$, $**p < 0.01$, $***p < 0.001$, $****p < 0.0001$. Control and GR cell lines 1–3 are combined for each MOI.

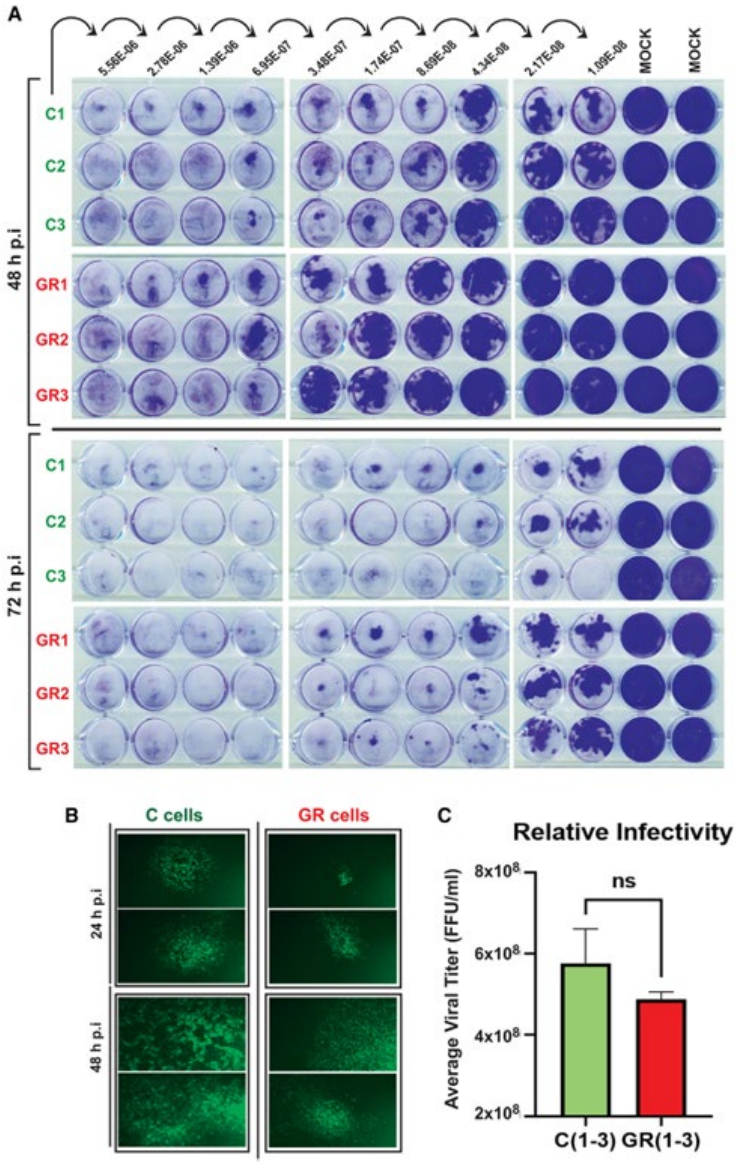

Figure 9: Relative infectivity and infection foci of VSV in C and GR cells. (A) C and GR cells were either mock treated or infected with serial dilutions of VSV-ΔM51 from 5.56 × 10−6 to 2.17 × 10−8. Cells were fixed and stained at 48 and 72 h p.i. (B) Comparing VSV-mediated fluorescent foci in C and GR cells at 24 and 48 h p.i. Two representative foci are shown for each cell line and time point. (C) Comparing VSV titers on C and GR cells. The data points and error bars shown represent the means and SEM of the means, respectively. Results were analyzed to determine significance using the Student's t test. C and GR cell lines 1–3 are combined. ns, not significant.

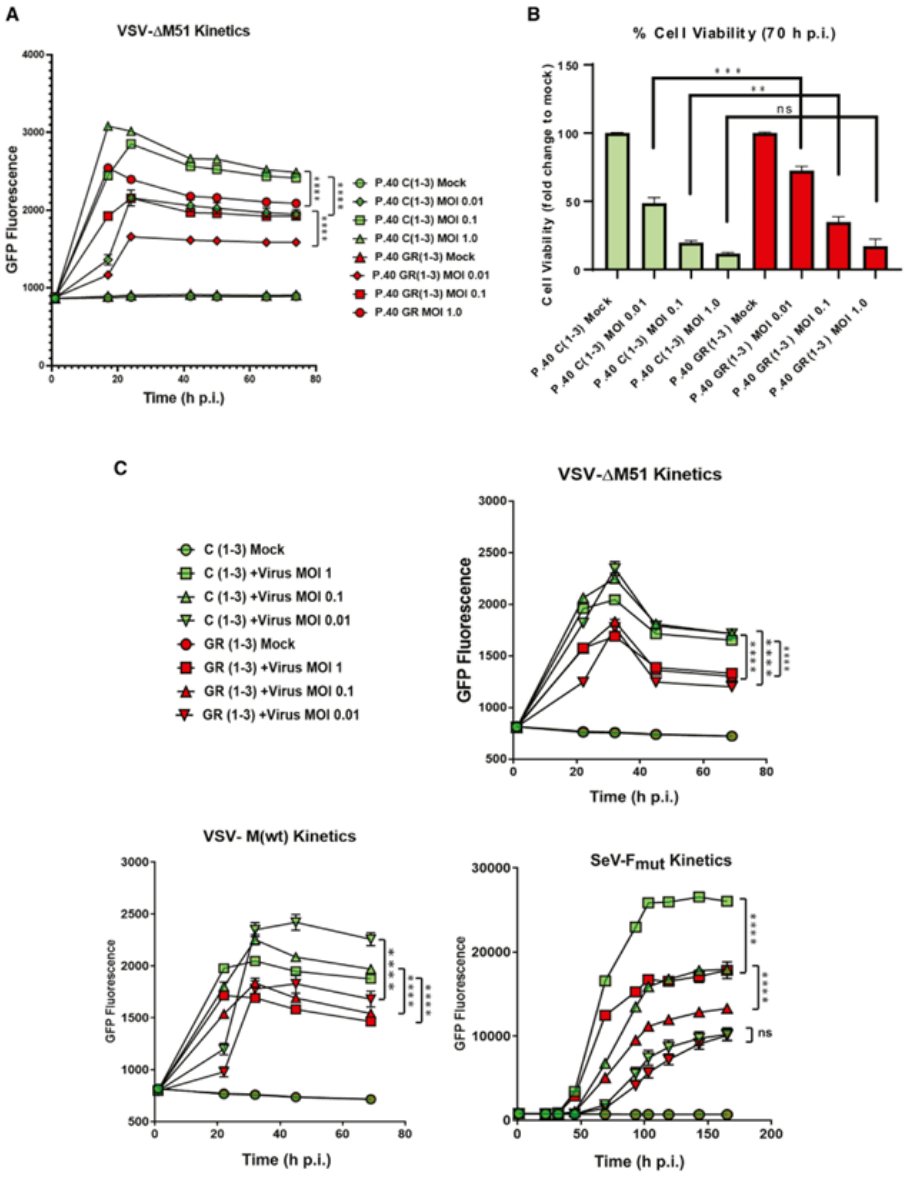

Figure 10: Replication kinetics of viruses and cell viability in C and GR cells. (A) C and GR cell lines were passaged 20 additional times in the absence of gemcitabine to generate passage 40 (P.40) C and P.40 GR cell lines, and viral replication kinetics. Cells were mock treated or infected with VSV-ΔM51 at MOIs of 1.0, 0.1, or 0.01. GFP fluorescence was measured from 1 to 72 h p.i. Control and GR cell lines 1–3 are combined for each MOI. (B) P.40 C and P.40 GR cell lines were either mock treated or infected with VSV-ΔM51 at MOIs of 1.0, 0.1, or 0.01. Cell viability was measured 70 h p.i. The figure shows data from three independent experiments. (C) C and GR cells were either mock treated or infected with VSV-ΔM51 (A), VSV-M(wt) (B), or SeV (C) at MOIs of 1.0, 0.1, and 0.01. GFP fluorescence was measured over times ranging from 1 to 165 h p.i. The data points and error bars shown represent the means and SEM of the means, respectively (some error bars are too small to be seen in the figures). C and GR cell lines 1–3 are combined for each MOI. Results were analyzed to determine significance using the Student's t test. $**p < 0.01$, $***p < 0.001$, $****p < 0.0001$. ns, not significant.

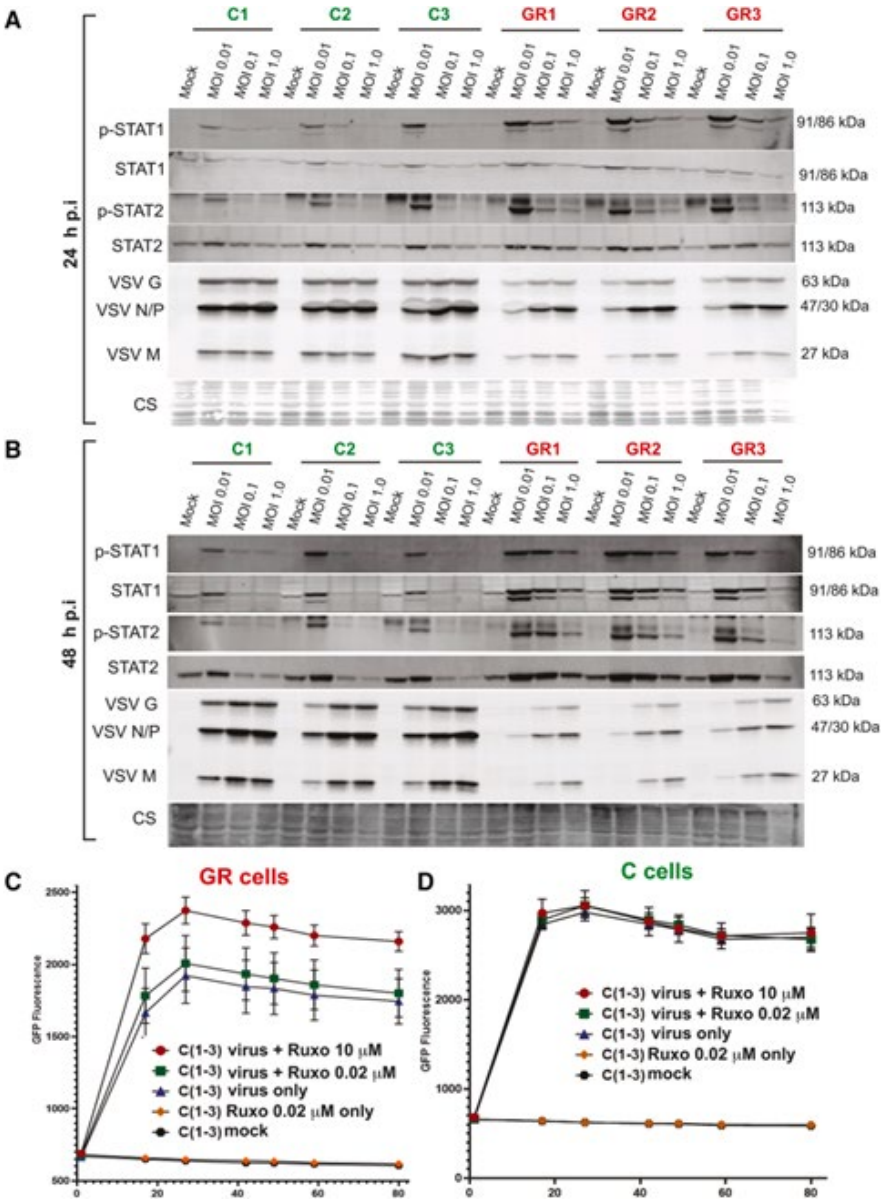

Figure 11: VSV and antiviral protein expression. (A and B) C and GR cells were either mock treated or infected with VSV-ΔM51 at MOIs of 1.0, 0.1, and 0.01. Protein sample were analyzed at 24 h p.i. (A) and 48 h p.i. (B) by western blotting for expression of phospho-STAT1 (p-STAT1), phospho-STAT2 (p-STAT2), STAT1, STAT2, and VSV proteins (G, N/P, and M). Cell line and treatment conditions are indicated above blots. Equal protein loading is indicated by Coomassie blue. (C and D) The effect of ruxolitinib on VSV-ΔM51 replication kinetics based on GFP fluorescence. C and GR cells were either mock treated, treated only with ruxolitinib, treated only with VSV-ΔM51, or treated with both VSV-ΔM51 and ruxolitinib. Cells were infected at MOI of 0.01. Ruxolitinib was added to cells after 1 h VSV incubation period. GFP fluorescence was measured from 1 to 80 h p.i. The data points and error bars shown represent the means and SEM of the means, respectively. Control and GR cell lines 1–3 are combined for each treatment.

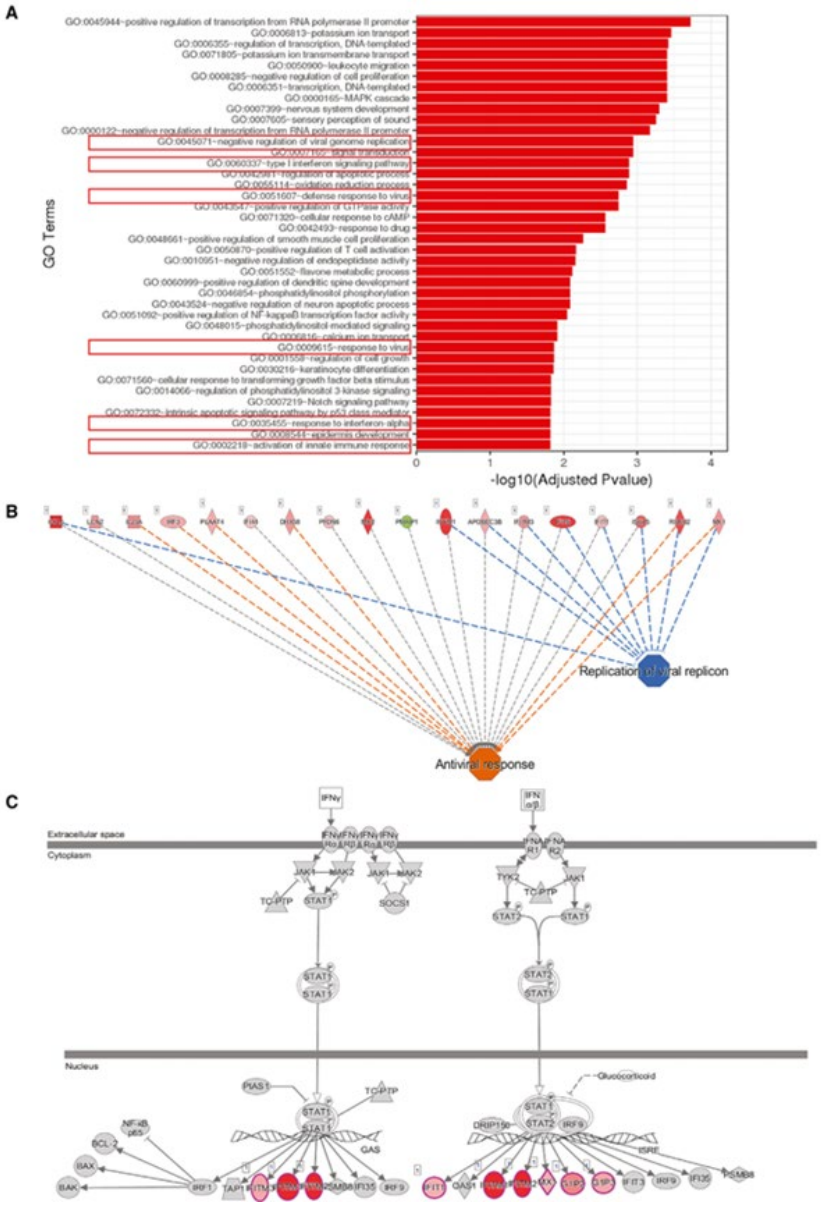

Figure 12: Total RNA was isolated from C and GR cells in triplicate and analyzed by RNA-seq. Significant differentially expressed genes were clustered by their gene ontology, and the enrichment of gene ontology terms was tested using Fisher exact test (GeneSCF v1.1-p2). (A) Gene ontology terms that are significantly enriched with an adjusted p value less than 0.05 in the differentially expressed gene sets in GR cells compared with C cells in the absence of virus infection. Processes relating to antiviral signaling are boxed in red. (B) Ingenuity Pathway Analysis (IPA) illustrating gene products enriched in GR cells compared with control cells in the absence of virus infection. (C) IPA conical IFNα/β and IFNγ pathways and gene products involved. Enriched genes are colored red (darker red indicates greater enrichment).

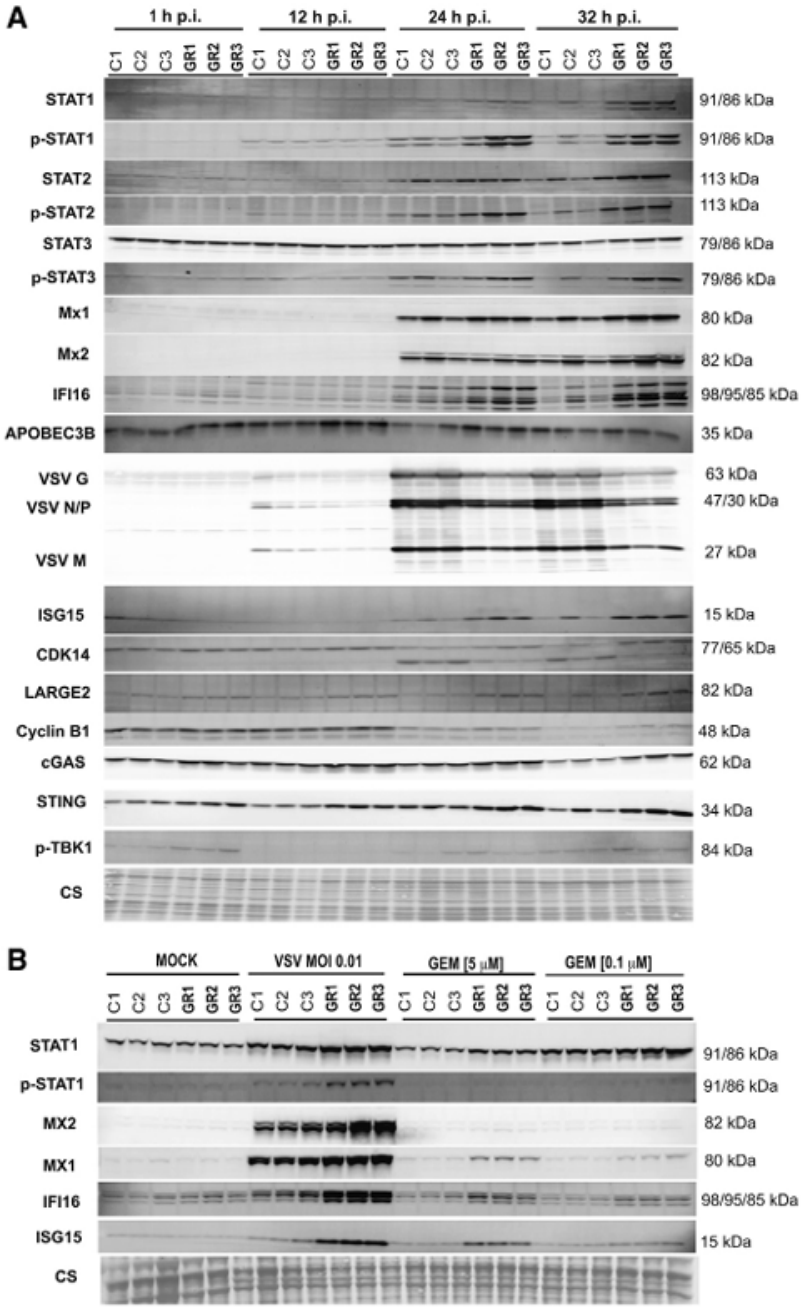

Figure 13: Time course expression of antiviral proteins in C and GR cells after VSV infection. (A) C and GR cells were infected with VSV-ΔM51 at MOI 0.01. Protein samples were collected at 1, 12, 24, and 32 h p.i. and analyzed by western blotting. Cell lines and time points are indicted above the blots. Equal protein loading is indicated by Coomassie blue. (B) C and GR cells were either mock treated, infected with VSV-ΔM51, or treated with 5 μM gemcitabine or 0.1 μM gemcitabine. Protein samples were collected after 32 h and analyzed by western blotting for expression of ISGs. Cell lines and time points are indicted above the blots. Equal protein loading is indicated by Coomassie blue.

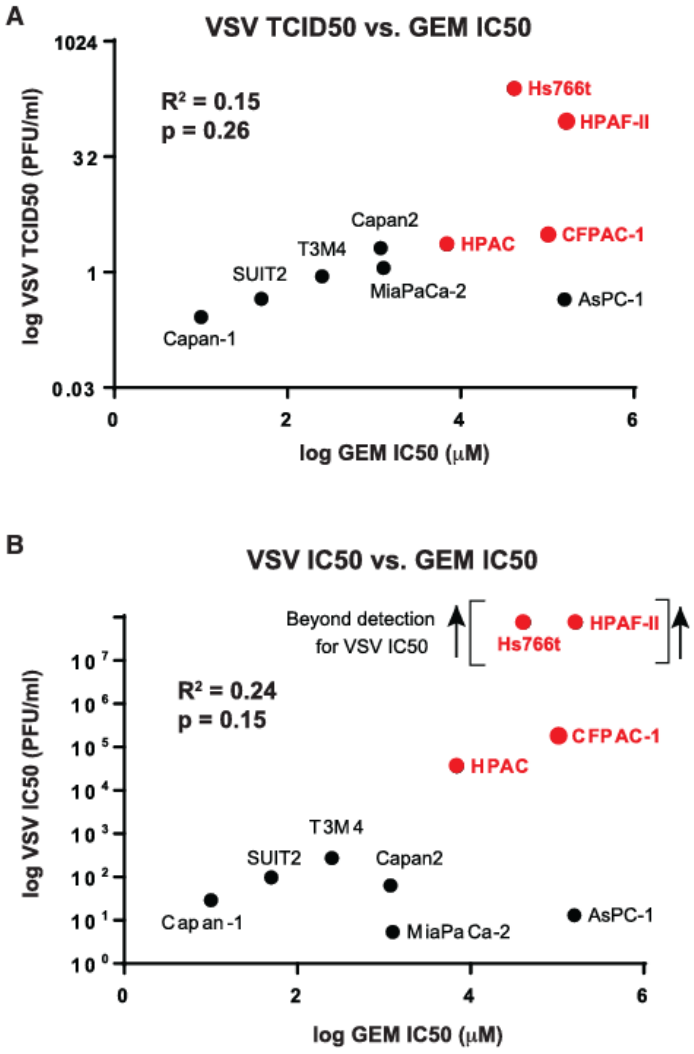

Figure 14: Human PDAC cell cross-resistance to gemcitabine and VSV-ΔM51. (A and B) Cell lines were either infected with serial dilutions of VSV-ΔM51 from 0.01 to 0.00006 PFU/mL. GFP-based FFU were counted at 24 h p.i. to calculate TCID50 values. A cell viability assay was performed at 120 h p.i. to calculate IC50 values. Separately, cell lines were treated with serial dilutions of gemcitabine at concentrations of 1,000–0.008 μM. At 120 h p.i., a cell viability assay was performed to calculate IC50 values.

2.6 Tables

Table 1. Differentially expressed antiviral genes in GR cells compared to C cells

Gene id	Gene name	GR1 vs. C1 (log2 fold change)	GR2 vs. C1 (log2 fold change)	GR3 vs. C1 (log2 fold change)
ENSG00000130303	*BST2*	0.99*	0.79*	0.54*
ENSG00000163739	*CXCL1*	1.41*	1.44*	1.27
ENSG00000161921	*CXCL16*	0.73*	0.78*	0.87*
ENSG00000107485	*GATA3*	0.89*	0.71*	0.49*
ENSG00000204257	*HLA-DMA*	1.03*	0.94*	0.76*
ENSG00000242574	*HLA-DMB*	1.75*	1.89*	1.57*
ENSG00000179344	*HLA-DQB1*	1.27*	0.78*	0.88*
ENSG00000196126	*HLA-DRB1*	0.82*	0.76*	0.76*
ENSG00000204632	*HLA-G*	0.63	0.27	0.28
ENSG00000230795	*HLA-K*	0.76*	0.68*	0.57
ENSG00000132196	*HSD17B7*	0.46*	0.58*	0.39
ENSG00000163565	*IFI16*	1.35*	1.25*	1.14*
ENSG00000119632	*IFI27L2*	0.74*	0.61*	0.11
ENSG00000068079	*IFI35*	0.47*	0.21	−0.03
ENSG00000137965	*IFI44*	0.51*	0.47*	0.22
ENSG00000185745	*IFIT1*	0.57*	0.59*	0.48*
ENSG00000119917	*IFIT3*	0.35*	0.28	0.07
ENSG00000185885	*IFITM1*	1.39*	1.61*	1.11*
ENSG00000185201	*IFITM2*	1.88*	1.72*	1.55*
ENSG00000142089	*IFITM3*	0.82*	0.65*	0.41*
ENSG00000126456	*IRF3*	0.67*	0.58*	0.38*
ENSG00000117595	*IRF6*	0.56*	0.48*	0.39*
ENSG00000187608	*ISG15*	1.12*	0.87*	0.61*
ENSG00000078081	*LAMP3*	0.84*	0.97*	0.78*
ENSG00000168961	*LGALS9*	1.58*	1.39*	0.81*
ENSG00000167656	*LY6D*	0.86*	0.63*	0.39
ENSG00000160932	*LY6E*	0.93*	0.81*	0.53*
ENSG00000157601	*MX1*	0.80*	0.62*	0.12
ENSG00000183486	*MX2*	1.38*	1.62*	1.51*
ENSG00000183486	*MX2*	1.38*	1.62*	1.51*
ENSG00000135114	*OASL*	0.48*	0.4	0.08
ENSG00000178685	*PARP10*	0.77*	0.61*	0.44*
ENSG00000134321	*RSAD2*	1.24*	1.04	0.77
ENSG00000196154	*S100A4*	1.00*	0.84*	0.64*
ENSG00000197249	*SERPINA1*	2.42*	2.06*	2.15*
ENSG00000188488	*SERPINA5*	0.65*	0.58*	0.60*
ENSG00000170099	*SERPINA6*	2.57*	2.54*	2.35*
ENSG00000167711	*SERPINF2*	1.15*	0.94*	0.84*
ENSG00000115415	*STAT1*	0.08	0.22	0.29
ENSG00000126561	*STAT5A*	0.86*	0.62*	0.43
ENSG00000166888	*STAT6*	0.64*	0.65*	0.68*
ENSG00000204610	*TRIM15*	0.68*	0.79*	0.56*
ENSG00000112343	*TRIM38*	0.51*	0.47*	0.44*
ENSG00000132481	*TRIM47*	0.44*	0.41*	0.23
ENSG00000169871	*TRIM56*	0.38*	0.30*	0.18
ENSG00000141569	*TRIM65*	0.38*	0.34*	0.32*
ENSG00000146054	*TRIM7*	0.38*	0.40*	0.28
ENSG00000027697	*IFNGR1*	−0.01	0.06	0.1
ENSG00000142166	*IFNAR1*	0.01	0.07	0.11
ENSG00000159110	*IFNAR2*	0.2	0.36*	0.3
ENSG00000159128	*IFNGR2*	0.32*	0.37*	0.21
ENSG00000182393	*IFNL1*	ND	ND	ND
ENSG00000183709	*IFNL2*	ND	ND	ND
ENSG00000184995	*IFNE*	−0.54	−0.27	−0.92
ENSG00000185436	*IFNLR1*	0.08	0.11	0.17
ENSG00000197110	*IFNL3*	ND	ND	ND
ENSG00000238271	*IFNWP19*	−0.89	−0.67	−0.13

Gene log2 fold change values compared with C cells. Values denoted with an asterisk indicate a p value of less than 0.05.

Table 2. Expression of other genes with known roles in resistance to gemcitabine in GR cells compared with C cells

Group	Gene id	Gene name	GR1 vs. C1 (log2 fold change)	GR2 vs. C1 (log2 fold change)	GR3 vs. C1 (log2 fold change)
Cytidine deaminases	ENSG00000179750	*APOBEC3B*	0.66*	0.59*	0.68*
	ENSG00000128394	*APOBEC3F*	−0.09	0.01	−0.18
	ENSG00000243811	*APOBEC3D*	0.73*	0.68*	0.56*
	ENSG00000244509	*APOBEC3C*	0.42*	0.45*	0.27
	ENSG00000158825	*CDA*	0.05	−0.06	−0.16
	ENSG00000102543	*CDADC1*	−0.05	−0.22	−0.01
Nucleoside transporters	ENSG00000076685	*NT5C2*	−0.38	−0.16	0.09
	ENSG00000111696	*NT5DC3*	−0.39*	−0.34	−0.15
	ENSG00000122643	*NT5C3A*	0.13	0.13	0.16
	ENSG00000125458	*NT5C*	0.74*	0.45	0.27
	ENSG00000135318	*NT5E*	−0.58*	−0.45*	−0.38*
	ENSG00000141698	*NT5C3B*	0.54*	0.38*	0.25
	ENSG00000168268	*NT5DC2*	0.32*	0.23	0.15
	ENSG00000178425	*NT5DC1*	−0.01	0.09	0.07
	ENSG00000205309	*NT5M*	0.57	−0.13	−0.27
Deoxycytidine kinase	ENSG00000156136	*DCK*	−1.01*	−0.91*	−0.66*
Thymidylate synthase	ENSG00000176890	*TYMS*	−0.19	−0.11	−0.13

Gene log2 fold change values compared with C cells. Values denoted with an asterisk indicate a p value of less than 0.05

Table 3. Human PDAC cell lines used in this study

Cell line	Origin	Chemo or radiation therapy
HPAF-II (ATCC: CRL-1997)	1982, metastasis (ascites), male, 44 years	NA
AsPC-1 (ATCC: CRL-1682)	1982, metastasis (ascites), female, 62 years	chemo and radiation
Capan-2 (ATCC: HTB-80)	1986, primary, male, 56 years	chemo
CFPAC-1 (ATCC: CRL-1918)	1990, metastasis (liver), male, 26 years	NA
MIA PaCa-2	1977, primary, male, 65 years	NA
SUIT-2	1987, primary and metastasis (lymph node), male, 73 years	NA
Capan-1 (ATCC: HTB-79)	1974, metastasis (liver), male, 40 years	chemo, 5-FU (resistant)
HPAC (ATCC: CRL-2119)	1985, primary, female, 64 years	NA
T3M4	1978, metastasis (lymph node), male, 64 years	NA
HS766t	1973, metastasis (lymph node), male, 64 years	NA

The catalog number of cell lines sold by ATCC are indicated beside the cell line nam
Cell lines with "chemo" and/or "radiation" indicate treatments administered to the pa
tient. The specific treatments are listed if information is available.

CHAPTER 3: INTERTUMORAL HETEROGENEITY IMPACTS ONCOLYTIC VESICULAR STOMATITIS VIRUS EFFICACY IN MOUSE PANCREATIC CANCER CELLS

3.1 Introduction

Pancreatic ductal adenocarcinoma (PDAC) is an aggressive malignancy that accounts for approximately 95% of pancreatic cancers, and is the number four cause for cancer-related deaths in the U.S. The 5-year survival rate for PDAC patients has remained around 10%, while survival rates for other cancers have significantly improved (Siegel et al., 2023). The poor survival rate for PDAC is largely attributed to late diagnoses and limited treatment options (Mizrahi et al., 2020).

Oncolytic virus (OV) therapy is a promising anticancer approach that utilizes replication-competent viruses that preferentially infect, replicate in, and kill cancer cells (Engeland & Bell, 2020; Shalhout et al., 2023). Vesicular stomatitis virus (VSV) is a nonsegmented negative-strand (NNS) RNA virus (order *Mononegavirales*, family *Rhabdoviridae*, genus *Vesiculovirus*) and a promising OV (Felt & Grdzelishvili, 2017; Hastie & Grdzelishvili, 2012; Liu et al., 2021). VSV-based OVs are already in phase I clinical trials (Clinicaltrials.gov trials NCT01628640, NCT03120624, NCT04046445, NCT03865212, NCT03017820, NCT03647163). VSV is able to infect and replicate in a wide variety of cell types (Hastie et al., 2013). The pantropism exhibited by VSV is largely due to its use of ubiquitously expressed cell surface molecules for attachment and entry to host cells, such as low-density lipoprotein receptor (Finkelshtein et al., 2013). The oncoselectivity of most OVs, including VSV, is mainly due to defective or suppressed type I interferon (IFN) mediated antiviral responses in many cancers (Lichty et al., 2004; Stojdl et al., 2000; Zhang et al., 2010), because most type I IFN responses are antiproliferative, antiangiogenic, and proapoptotic (Shi et al., 2022).

Current *in vivo* PDAC mouse model systems fail to recapitulate all key characteristic of human PDAC disease including tumor microenvironment, metastasis, adaptive immune response (He et al., 2020; Holbrook et al., 2021; Kong et al., 2020). Importantly, many studies, which use mouse models to investigate PDAC biology and therapies fail to address intertumoral heterogeneity (the differences between tumors in different individuals). This is an important issue, as our previous studies demonstrated a wide range of permissiveness of human PDAC cells to OVs, from highly permissive to highly resistant, which is largely determined by the abilities of PDAC cells to mount effective innate antiviral responses (Hastie et al., 2016; Moerdyk-Schauwecker et al., 2013; Murphy et al., 2012). Mouse PDAC cell lines, which are widely used for *in vivo* examination of the adaptive immune responses during OV and other therapies, have never been examined systematically for virus-host interactions and the role of intertumoral heterogeneity in OV therapy.

In this study, we examined 3 different allograftable mouse PDAC cell lines. Two of these cell lines originated form genetically engineered mouse models (GEMM) of PDAC. GEMMs are generated by introducing specific gene mutations in oncogenes and/or tumor suppressor genes that are central in human PDAC, effectively recapitulating PDAC in the mouse. The most robust and well-described PDAC GEMM is the KPC mouse, which is characterized by mutations in the Kras and Trp53, both of which are driven by a pancreas-specific Cre recombinase (via the Pdx1 promoter) which is expressed in all cells of the pancreas from early stages in development (Hingorani et al., 2005). Importantly, the KPC GEMM recapitulates many of the PDAC disease features of the human disease, as well as commonly associated disease symptoms such as pain and cachexia (Gilabert et al., 2014; Stopczynski et al., 2014). Although the resulting PDAC in the KPC GEMM model is highly similar to the human disease, the use of KPC mice is labor intensive and costly as tumor initiation and formation can take one year or more. Alternatively, syngeneic mouse

models are developed by introducing mouse tumor cells or tissues into immunocompetent mice of the same or similar genetic background by implanting PDAC cells (e.g., KPC cell lines originated from the KPC mouse (Torres et al., 2013)) or tissue from a C57BL6 background mouse into a "wild-type" (WT) C57BL6 mouse. Syngeneic mouse models can be established in immunocompetent mice either subcutaneously (SC) or orthotopically, and in addition, PDAC cell lines can be engineered to constitutively express luciferase allowing for tumor monitoring through bioluminescence intensity measurements.

In this study, we examined phenotypically and genotypically 3 mouse PDAC cell lines (2 KPCs and one non-KPC). Our study (i) characterized the ability of oncolytic vesicular stomatitis virus (VSV) to infect, replicate in, and kill these mouse PDAC cells; (ii) examined their innate antiviral responses; (iii) compared their permissiveness to VSV and chemotherapeutic drugs; (iv) analyzed their karyotype and exome. Our studies demonstrate that, similarly to human PDACs, mouse PDAC cell lines show high divergence in their permissiveness to VSV. Importantly, their permissiveness negatively correlated with the ability of cells to mount innate antiviral responses. Mouse PDAC cell lines also show high divergence in their karyotype and exome. Our study provides essential data about 3 allograftable model mouse PDAC cell lines and propose a novel platform to study OV-based therapies against phenotypically different PDACs in immunocompetent mice.

3.2 Materials and Methods

Virus and cell lines

The recombinant virus VSV-ΔM51-GFP was previously described (Wollmann et al., 2010), in which the methionine at amino acid position 51 of the matrix protein is deleted and the GFP open reading frame (ORF) is inserted at position 5 of the viral genome (between VSV G and L genes).

Baby hamster kidney fibroblast cells BHK-21 (ATCC CCL-10) were used to grow virus and to determine viral titers. Titers were determined by adding serial dilutions of virus to BHK-21 cells using an agar overlay followed by calculating either FFU/mL or PFU/mL. To count PFUs cells were fixed and stained with crystal violet. To count FFUs, VSV-encoded GFP fluorescent foci were quantified using fluorescent microscopy. The mouse PDAC cell lines used in this study were KPC-Luc-4580 (Erstad et al., 2018), KPC-Luc-A (Manuel et al., 2015), and PANC02-Luc (Corbett et al., 1984). The human PDAC cell lines used in this study were SUIT-2(Iwamura et al., 1987), HPAF-II (Metzgar et al., 1982) and MIA PaCa-2 (Yunis et al., 1977). The human and mouse origin of all tested PDAC cell lines was confirmed (Hastie et al., 2016) (IDEXX BioAnalytics Case# 18142-2019). KPC-Luc-4580, KPC-Luc-A, MIA PaCa-2, and SUIT-2 cell lines were maintained in Dulbecco's modified Eagle's medium (DMEM [Corning, 10-013-CV]). HPAF-II and BHK cells were maintained in Minimum essential medium Eagle (MEM [Corning, 10-010-CV]). PANC02-Luc cells were maintained in RPMI 1640 medium (Corning, 10-040-CV). All cell growth media were supplemented with 10% fetal bovine serum (FBS [Gibco]), 4mM L-glutamine, 900U/mL penicillin, 900 μg/mL streptomycin, and 1% nonessential amino acids (PANC02-Luc cells were maintained in media without the 1% nonessential amino acids). HPAF-II and BHK cells were additionally supplemented with 17.5% glucose. Cells were kept in a 5% CO_2 atmosphere at 37ºC. For all experiments, cells were kept no more than 15 passages. All described experiments were approved by the University of North Carolina at Charlotte Institutional Biosafety Committee (IBC).

Virus replication kinetics

Virus titers were calculated using standard plaque assays on BHK-21 cells in 12 or 24-wells plates. For virus replication kinetics experiments, cells were seeded into 96-well plates and were

given 24 h to adhere. Virus dilutions were prepared in DMEM with 0% FBS. Cells were washed with PBS, followed by the addition of virus for 1 h at 37ºC. Virus-containing medium was then aspirated and fresh DMEM with 5% FBS was added back to cells and incubated at 37ºC in 5% CO_2 for the duration of the experiment. Virus-encoded GFP fluorescence was measured periodically over a 72-h time course using a fluorescence multiwell plate reader. GFP fluorescence was measured at 485/535 nm.

Cell viability assay

In a 96-well plate layout, cells were seeded at 90% confluence and were given 24 h to adhere. Cells were then washed once with PBS and mock infected, or infected at either MOI 1, 0.1, 0.01, 0.001, or 0.0001. After 1 h incubation at 37ºC, virus was removed and fresh medium containing 5% FBS was added to each well. At 70 h p.i., WST-8 (Dojindo, CK04) was added to each well for 4 h at 37°C in 5% CO_2, then read using a multi-well plate reader at 450 nm. Results are expressed as fold change compared with mock treatment.

Plaque assay

12-well plates were seeded at 90% confluence and were given 24 hours to adhere. Cells were infected with VSV-ΔM51-GFP from dilutions 10^{-3} to 10^{-13} or mock infected (control) for 24, 72 and 120 hours. One hour after infection, virus was aspirated and wells were overlaid with 2% Bacto agar (Difco Lactobacilli MRS Agar- 288210) in DMEM with 5% FBS. After 24, 72, or 120 h, formalin was added to fix cells for 4 h. After fixation, agar was removed and cells were stained with crystal violet (2% crystal violet in methanol). For the plaque assay figures, each row represents one 12-well plate that was cut and stitched in order to view highest amount of virus to the least amount of virus from left to right.

Western blot analysis

Cells were seeded into 12-well plates at 90% confluence and were given 24 h to adhere. Medium was removed and cells were washed once with PBS. Cell lines were either mock treated or infected with VSV-ΔM51-GFP at MOIs of 0.1 and 0.001 either based on virus titer on BHK-21 cells or based on virus titer on each cell line. in medium with 0% FBS and incubated for 1 h at 37ºC. After 1 h incubation, the medium was removed and fresh medium with 0% FBS was added to each well. Cells were lysed and total protein was collected 24 h after infection using buffer as described previously (Bressy et al., 2019). Total protein was separated by electrophoresis on 10% SDS-PAGE gels and electroblotted onto polyvinyl difluoride (PVDF [Millipore IPFL00010]) membranes. Membranes were blocked by using 5% nonfat powdered milk or BSA in TBS-T (0.5 M NaCl, 20 mM Tris [pH 7.5], 0.1% Tween 20) for at least 1 h at room temperature. Membranes were then incubated in TBS-T with 5% BSA or milk with 0.02% sodium azide and a 1:5,000 dilution of rabbit polyclonal anti-VSV antibodies (raised against VSV virions), a 1:1,000 dilution of rabbit anti-phospho-STAT1 (catalog number 9177S, P-STAT1 [S727] Cell Signaling), a 1:1,000 dilution of rabbit anti-STAT1 (catalog number 14994T, D1K9Y, Cell Signaling), a 1:1,000 dilution of rabbit anti-phospho-STAT2 (catalog number PA5-97361, P-STAT2 [Y690], Invitrogen). Starbright Blue 700 goat anti-rabbit (Bio-Rad, 12004161) or anti-mouse (Bio-Rad, 12004158) IgG fluorescent secondary antibodies at 1:5,000 dilutions were used for fluorescent western blotting detection using the Chemidoc MP imaging system from Bio-Rad. To verify total protein in each sample (loading control), membranes were stained with Coomassie brilliant blue.

Cytokine array

Cells were seeded into 12-well plates at 90% confluence and were given 24 h to adhere. Medium was removed and washed once with PBS. VSV-ΔM51-GFP was added at MOI 1 and 0.1 (based on each individual cell line) in medium with 0% FBS and incubated for 1 h at 37ºC. After 1 h incubation, fresh medium was added to each well containing 0% FBS. After 24 h, cell supernatants (for cytokine array) and lysates (for western blot) were collected and stored at -80ºC. Supernatants were then sent to EVE Technologies Corp for Mouse Cytokine/Chemokine 44-Plex Discovery Assay® Array (MD44).

IFN sensitivity assay and IFN IC50

Cells were seeded into 96-well plates at 90% confluence and were given 24 h to adhere. Medium was removed and cells were washed once with PBS. Virus was then added at MOI 0.01 in medium with 0% FBS and incubated for 1 h at 37ºC. After 1 h incubation, the medium was removed and fresh medium (0% FBS) containing mouse IFN alpha (Invitrogen, 14-8312-80) was added at 2500, 500, 100, 20, 4 or 0 units/ml. Virus-encoded GFP fluorescence was measured at 485/535 nm periodically over a 73-h time course using a fluorescence multiwell plate reader. IC50 values were calculated using GraphPad Prism 9.3.1.

Gemcitabine and 5-FU IC50

For gemcitabine and 5-FU determination, cells were seeded into 96-well plates for approximately 50% confluency in medium supplemented with 10% FBS. The next day, cells were treated with serial dilutions of either gemcitabine (Selleckchem, S1714) or 5-FU (Selleckchem, S1209). The serial dilution ranges for gemcitabine and 5-FU was 1000 - 0.008μM and 300 -

0.006μM, respectively. A WST-8 (Dojindo, CK04) cell viability assay was performed 72 h later. IC50 values were calculated using GraphPad Prism 9.3.1.

VSV-ΔM51-GFP combination treatment with Ruxolitinib, TPCA-1, Paclitaxel, and Colchicine

Cells were seeded into 96-well plates at 90% confluence and were given 24 h to adhere. Cells were washed with PBS, followed by the addition of VSV-ΔM51-GFP at MOI 0.01 for 1 h at 37ºC. Virus-containing medium was then aspirated and fresh DMEM (with 5%FBS) containing either 5uM, 0.5uM, or 0.05uM of Ruxolitinib (Selleckchem– S1378), TPCA-1 (Selleckchem- S2824), Paclitaxel (Selleckchem- S1150), or Colchicine (Selleckchem- S2284) was added back to cells and incubated at 37ºC in 5% CO_2 for the duration of the experiment. Virus-encoded GFP fluorescence was measured periodically over a 67 h time course using a fluorescence multiwell plate reader. GFP fluorescence was measured at 485/535 nm.

Spectral karyotyping (SKY) and multicolor fluorescence-in-situ-hybridization (mFISH)

Each cell line was grown to 70% confluence in a T-75 flask (Greiner #658170) and sent to the Cytogenomics Core Laboratory at the University of Minnesota. Adherent cells were harvested with colcemid arrest, treated with 0.75 M KCl hypotonic solution, and fixation with 3:1 methanol: acetic acid. The resulting cells were spread onto glass slides according to standard cytogenetic protocols. A Spectral Karyotyping (SKY) slide was processed according to the manufacturer's protocol (Applied Spectral Imaging). SKY uses a unique combination of five fluorescent dyes to paint all 24 chromosomes. Seven metaphase cells per sample were examined by SKY using the Olympus BX61 microscope with DAPI and SKY fluorescence filter sets. G-band and SKY metaphase cells were imaged and karyotyped using Applied Spectral Imaging (ASI) software. The cytogenetic analyses were performed in the Cytogenomics Shared Resource at the University of

Minnesota with support from the comprehensive Masonic Cancer Center NIH Grant #P30 CA077598.

Exome sequencing and sequence analysis

Each cell line was grown to 90% confluence (about 10^6 cells), trypsinized, pelleted, frozen, and sent to Azenta US (South Plainfield, NJ, USA) for DNA extraction, library preparations, sequencing reactions and bioinformatic analysis. DNA was extracted using the PureLink™ Genomic DNA Mini Kit (ThermoFisher Scientific) following manufacturer's instructions. Genomic DNA sample were quantified using Qubit 2.0 Fluorometer (ThermoFisher Scientific). Enrichment probes were designed against the region of interest and synthesized through Twist Biosciences – Twist Mouse Comprehensive Panel (South San Francisco, CA, USA). Library preparation was performed according to the manufacturer's guidelines. Briefly, the genomic DNA was fragmented by acoustic shearing with a Covaris S220 instrument. Fragmented DNA was cleaned up, end repaired, and adenylated at the 3'ends. Adapters were ligated to the DNA fragments, and adapter-ligated DNA fragments were enriched with limited cycle PCR. Adapter-ligated DNA fragments were validated using Agilent TapeStation (Agilent Technologies), and quantified using Qubit 2.0 Fluorometer. Adapter-ligated DNA fragments were hybridized with biotinylated baits. The hybrid DNAs were captured by streptavidin-coated binding beads. After washing, the captured DNAs were amplified and indexed with Illumina indexing primers. Post-captured DNA libraries were validated using Agilent TapeStation (Agilent) and quantified using Qubit 2.0 Fluorometer and Real-Time PCR (KAPA Biosystems). Libraries were sequenced 2x150 on an Illumina HiSeq instrument. For data analysis, sequencing adapters and low-quality bases in raw reads were trimmed using Trimmomatic 0.39. The reads were then aligned to the GRCm37 reference genome using Sentieon 202112.01. Aligned sequences were then sorted and

PCR/Optical duplicates were marked, producing BAM files. Somatic SNVs and small INDELs were called by using Sentieon 202112 (TNSeq algorithm). The VCF files generated by the pipeline were then normalized (left alignment of INDELs and splitting multiallelic sites into multiple sites) using bcftools 1.13. Overlapped transcripts were identified for each variant and the effects of the variants on the transcripts were predicted by Ensembl Variant Effect Predictor (VEP) v104. The most severe impact was selected for each variant and they are used for downstream cohort analysis. Impact of the variants were also classified based on MAF document specifications. The exome data were deposited to the GenBank Sequence Read Archive (SRA) database under BioProject PRJNA944630. Exome analysis of three murine pancreatic cancer cell lines under the following BioSample and SRA accessions: PANC02-Luc, KPC-Luc-A, and KPC-Luc-4580.

3.3 Results

High variability in permissiveness of model mouse pancreatic cancer cells to oncolytic vesicular stomatitis virus

In this study, we examined and compared three clinically-relevant allograftable mouse PDAC cell lines: PANC02-Luc, KPC-Luc-A, and KPC-Luc-4580. These cell lines originated from C57BL6 mice that had 3 different genetic backgrounds in the pancreas. The PANC02 cell line (alternatively called Pan02 in some publications) is one of the most widely used mouse PDAC cell lines, and it was generated by chemically inducing PDAC in mice via the implantation of 3-methyl-cholantrene (a carcinogen) into the pancreas of genetically unaltered C57BL6 mice (Corbett et al., 1984) (Fig. 15A). The luciferase reporter expressing PANC02-Luc cell line was later generated using lentiviral transduction (Wennier et al., 2012). The KPC-Luc-A cell line was derived from a tumor that developed in an LSL-KrasG12D/+; LSL-Trp53R172H/+; PDX-Cre/+ mouse (Hingorani et al., 2005), and then the luciferase reporter was inserted using lentiviral transduction

(Manuel et al., 2015) (Fig. 15A). The KPC-Luc-4580 cell line (also known as KPC-4580P) was derived from a tumor that developed in an LSL-KrasG12D/+; LSL-Trp53R172H/+; PDX-Cre/+, LSL-ROSA26Luc/+ mouse (Naqvi et al., 2018) (Fig.15A). Importantly, the expression of LSL-KrasG12D/+; LSL-Trp53R172H/+ alleles are specific to the pancreas only, as Cre recombinase is driven by the pancreas-specific PDX1 promotor. All three cell lines, PANC02-Luc (Little et al., 2012) (Jazowiecka-Rakus et al., 2022; Wennier et al., 2012) KPC-Luc-A (Bian et al., 2021; Das et al., 2019; Manuel et al., 2015) and KPC-Luc-4580 (Naqvi et al., 2018; Narayanan et al., 2019), have been widely used as models to study PDAC biology and treatments for PDAC *in vivo*.

In this study, we used the oncolytic recombinant VSV-ΔM51-GFP (Wollmann et al., 2010). VSV-ΔM51-GFP has a deletion of the methionine residue at position 51 (ΔM51) in the VSV-encoded matrix (M) protein and green fluorescent protein (GFP) reporter gene inserted into viral genome (Fig. 15B). The ΔM51 mutation prevents VSV-M from binding to the Rae1-Nup98 mRNA export complex required for cellular mRNA transport and subsequent translation (Her et al., 1997). Therefore, VSV-ΔM51-GFP is not able to inhibit antiviral responses in initially infected cells (normal or cancer) by disrupting transport and translation of cellular mRNAs for antiviral genes, which attenuates its replication in normal cells but not in cancer cells as the latter are typically defective in antiviral responses (Black et al., 1993; Hastie et al., 2013; Hastie & Grdzelishvili, 2012; Stojdl et al., 2003). The GFP reporter gene, inserted at position 5 of the viral genome between the VSV G and L genes, allows for monitoring of virus replication and spread based on VSV replication-driven GFP expression (Wollmann et al., 2010).

To initially examine the ability of VSV to infect and cause oncolysis of PANC02-Luc, KPC-Luc-A, and KPC-Luc-4580, cells were seeded into 12-well plates and infected with 10-fold dilutions of VSV-ΔM51-GFP and then overlaid with agar (to prevent indiscriminate virus

spreading via the flow of the liquid medium during viral propagation). In addition, BHK-21, a baby hamster kidney cell line, was used as a reference cell line for comparison as it is highly permissive to VSV and widely used for VSV amplification and plaque assays. At 72 hours (h) post infection (p.i.) cells were stained with crystal violet. This assay allowed us to compare the ability of VSV to kill PDAC cells by observing oncolysis associated with virus infection (which depends on the ability of VSV to infect, replicate in, spread, and kill infected cells). Not surprisingly, BHK-21 cells were the most permissive among 4 tested cell lines. Among 3 mouse cell lines, we observed the lowest degree of cell lysis in PANC02-Luc cells, as most virus dilutions had no cytopathic effect (CPE) (Fig. 15B). Better cell lysis was observed in KPC-Luc-A and KPC-Luc-4580 cells, with the greatest level of cell lysis in KPC-Luc-4580 cells. These results suggest that the PANC02-Luc cell line is the most resistant to VSV-ΔM51-GFP, while KPC-Luc-4580 is the most permissive among mouse PDAC cell lines tested. Surprisingly, there was a marked difference in the responsiveness of KPC-Luc-A and KPC-Luc-4580 cell lines to VSV, although both KPC cell lines originated from similar genetically engineered mouse models (GEMM) with KrasG12D/+; LSL-Trp53R172H/+; PDX-Cre/+ genotype (notably KPC-Luc-4580 originated from a mouse that also had another genetic alternation, LSL-ROSALuc/+).

Our previous studies demonstrated that there is a wide range of permissiveness of human PDAC cells to OV therapy, from highly permissive to highly resistant, and the success of OV therapy greatly depends on the permissiveness of human PDAC cell lines to OVs (Bressy et al., 2019; Hastie et al., 2016; Moerdyk-Schauwecker et al., 2013; Murphy et al., 2012). Therefore, we compared the permissiveness of the mouse PDAC cell lines to VSV to that of a panel of well-characterized human PDAC cell lines. In addition to three human PDAC cell lines (highly resistant HPAF-II, intermediately resistant SUIT-2, and highly permissive MIA PaCa-2), we included in

this assessment BHK-21 as a positive control. To compare the ability of VSV-ΔM51-GFP to initiate infections, spread to adjacent cells, and induce oncolysis, we infected cells with serial dilutions of our VSV-ΔM51-GFP stock and then used an agar overlay. Following infection, we performed a standard plaque assay at 48 h p.i. to compare the sizes of virus-induced plaques in the cell monolayers (Fig. 16A). In a separate experiment, cell monolayers were examined using fluorescent microscopy to count the virus-directed GFP focus forming units (FFUs) at 24 h p.i. to calculate cell line specific FFU/ml for our VSV-ΔM51-GFP stock (Fig 16B). In agreement with Figure 13B, we found that, among mouse PDACs, PANC02-Luc cells demonstrated the greatest degree of resistance to VSV infection (lowest FFU/ml) (Fig. 16B), VSV spread (smallest size of plaques) and VSV-mediated cell lysis (limited cell clearing), compared to KPC-Luc-A and KPC-Luc-4580 (Fig. 15A). VSV infection, spread and cell lysis was greater in all three model mouse cell lines compared to HPAF-II cells, one of the most resistant PDAC cell lines to VSV as we have demonstrated earlier (Hastie et al., 2016; Moerdyk-Schauwecker et al., 2013; Murphy et al., 2012). The KPC-Luc-4580 cell line demonstrated a greater number of FFU/ml, size of plaques, and cell lysis compared to PANC02-Luc and SUIT2 cells, showing significantly higher number of FFUs and cell lysis compared to KPC-Luc-A (Fig. 16B). The KPC-Luc-A cell line led to a greater size of plaques compared to PANC02-Luc (Fig. 16A), however the differences in FFU/ml were not statistically significant (Fig. 16B). Each of the mouse PDAC cell lines displayed a smaller number of FFUs, size or plaques, and less overall cell lysis compared to MIA PaCa-2 and BHK-21 cells, but larger than HPAF-II and SUIT2 cells. The cell lines in Figure 14A (top to bottom) and 13B (left to right) are arranged from most to least resistant to VSV infection.

To further examine the ability of VSV to replicate in these mouse PDAC cell lines, we analyzed VSV-driven GFP fluorescence using a panel of human and mouse PDAC cell lines and

BHK-21 cells. Cell were seeded in 96-well plates and either mock infected or infected with VSV-ΔM51-GFP at a multiplicity of infection (MOI) of 10, 1, 0.1, 0.01, 0.001, 0.0001, or 0.00001 (based virus titer on BHK-21 cells). As shown in Figure 15A, very high levels of VSV-driven GFP fluorescence was observed in BHK-21 cells at each tested MOI, which exemplifies that in highly permissive cell lines, VSV replication is good even at extremely low MOIs. In contrast, we observed only small levels of VSV-driven GFP fluorescence in HPAF-II cells even at the highest MOI tested, which is expected for cells highly resistant to VSV infection. The levels of VSV-driven GFP in each of the mouse PDAC cell lines were lower than those observed in BHK-21 cells, but higher than those in HPAF-II. Consistent with Figure 15 and 16, amongst the three mouse cell lines, the highest levels of VSV-driven GFP fluorescence were observed in KPC-Luc-A and KPC-Luc-4580 cells and the lowest in PANC02-Luc. Interestingly, despite being more resistant to VSV-mediated oncolysis (Fig. 15 and 16), KPC-Luc-A showed higher GFP expression levels than KPC-Luc-4580. It should be noted, though, that GFP fluorescence depends not only on VSV replication levels, but also on cell viability of virus-infected cells and virus-independent cellular characteristics, such as GFP stability in a given cell line. Therefore, relative GFP fluorescence numbers shown in Figure 17A should not be used alone to compare permissiveness of KPC-Luc-A and KPC-Luc-4580 cells to VSV. In our previous studies, some highly permissive cell lines, in which VSV was able to replicate to very high levels, displayed only moderately high GFP fluorescence (Moerdyk-Schauwecker et al., 2013; Murphy et al., 2012).

To examine the effect of VSV infection on cell viability, cells were infected with VSV-ΔM51-GFP at different MOIs (10, 1, 0.1, 0.01, 0.001, 0.0001, or 0.00001) for 70 h, followed by a cell viability assay (Fig 17B). In general, cell viability negatively correlated with the level of GFP fluorescence at each MOI (Fig 17A). Of note, some cell lines (such as BHK-21) exhibited low

viability even at very low MOI infection. This is likely attributed to the ability of VSV to infect, kill, and spread to neighboring cells even at low MOI due to defective innate antiviral responses and absence of virus restriction factors. In sharp contrast, we found that in highly resistant HPAF-II cells, cell viability was not affected even at the highest MOIs, which is likely due to the presence of previously demonstrated high levels of VSV restriction factors (such as MX1 and OAS2) in this cell line (Cataldi et al., 2015; Hastie et al., 2016; Moerdyk-Schauwecker et al., 2013). In most cell lines, we found that cell viability was only affected at several highest MOIs, which is likely due to the limited presence of VSV restriction factors. Amongst the three mouse PDAC cell lines, PANC02-Luc demonstrated the highest resistance to VSV-mediated reduction in cell viability, followed by KPC-Luc-A and then KPC-Luc-4580. Interestingly, KPC-Luc-A exhibited greater VSV-driven GFP fluorescence compared to KPC-Luc-4580 (Fig. 17A), but this did not correlate with lower cell viability (Fig. 17B).

In general, our data indicate that VSV-ΔM51 differs in its ability to replicate in, spread, and kill each of the three mouse PDAC cell lines. Our data show that PANC02-Luc cells are the overall most resistant to VSV-ΔM51-GFP, followed by KPC-Luc-A and then KPC-Luc-4580.

Resistance of mouse pancreatic cancer cell lines to oncolytic vesicular stomatitis virus is associated with higher level of antiviral JAK/STAT signaling

The differences in VSV-ΔM51-GFP replication, spread and cell lysis observed between the mouse PDAC cell lines suggests potentially varied levels of antiviral signaling. Our previous studies have established that the capacities for type I IFN antiviral signaling between human PDAC cell lines vary dramatically, and strongly correlate to resistance to VSV and other OVs (Hastie et al., 2016; Holbrook et al., 2021; Moerdyk-Schauwecker et al., 2013; Murphy et al., 2012). In the canonical type I IFN-induced signaling pathway (Mazewski et al., 2020), the interaction of type I

IFNs (IFN-α or IFN-β) with IFN-α receptor (IFNAR) activates the IFNAR-associated protein tyrosine kinases Janus kinase 1 (JAK1) and tyrosine kinase 2 (TYK2), which phosphorylate the cytoplasmic transcription factors signal transducer and activator of transcription 1 (STAT1) and 2 (STAT2). Phosphorylated STAT1-STAT2 heterodimers then dissociate from the receptors and recruit IFN-regulatory factor 9 (IRF9) in the cytoplasm to form a trimolecular complex called IFN-stimulated gene factor 3 (ISGF3). ISGF3 then translocates to the nucleus, where it binds to DNA sequences with so-called IFN-stimulated response elements (ISRE), directly activating the transcription of a large number of antiviral interferon (IFN) stimulated genes (ISG). In general, a successful IFN antiviral response, which determines so called antiviral state of a cell, is defined by three major features: cells must be able to 1) sense viral components via cytosolic sensors such as RIG-I and/or MDA-5, 2) produce and secrete IFNs, and 3) respond to IFNs (paracrine and autocrine) via expression of antiviral ISGs.

Here, we hypothesized that more resistant mouse PDAC cell lines have more active type I IFN signaling. To test this hypothesis and examine the role of type I IFN responses of the three mouse PDAC cell lines to virus, cells were either mock infected or infected with VSV-ΔM51-GFP at MOIs 0.1 and 0.001 (based on virus titer on each individual cell line). Total protein was then collected and separated using an SDS-PAGE gel, followed by western blot analysis to determine the expression level of major modulators of type I IFN signaling, total STAT1 and phosphorylated STAT1 (p-STAT1) (Fig. 18). VSV protein expression was also analyzed to assess VSV replication in each cell line. Firstly, we found the greatest level of VSV protein expression in KPC-Luc-4580 cells, an intermediate in KPC-Luc-A, and the least amount of VSV protein expression in PANC02-Luc cells. Our lab has previously shown that highly resistant human PDAC cell lines exhibit constitutive expression of p-STAT1 with corresponding upregulation of ISGs, even in the absence

of VSV infection (Hastie et al., 2016; Moerdyk-Schauwecker et al., 2013). Here, we found that in the absence of VSV infection, there was no detectable p-STAT1 expression in all cell lines. However, in VSV infected samples, PANC02-Luc cells show robust p-STAT1 and total STAT1 expression compared to KPC-Luc-A and KPC-Luc-4580 at both MOI 0.001 and MOI 0.1. There was little to no p-STAT1 or total STAT1 expression in KPC-Luc-4580 cells, and there were intermediate expression levels of p-STAT1 and total STAT1 in KPC-Luc-A cells (Fig. 18). In agreement with our hypothesis that more resistant mouse PDAC cell lines would have greater type I IFN signaling, these data show an inverse correlation between total STAT1 and p-STAT1 expression and levels of VSV protein expression. These data suggest that the differences in the ability of VSV-ΔM51-GFP to infect, spread, and kill our mouse PDAC cell lines may be due to varied levels of antiviral signaling.

To further study the role of antiviral signaling in mouse PDAC cell lines, we examined the antiviral effect of mouse IFNα (mIFNα) on VSV-ΔM51-GFP replication in each cell line. We also used the reference human PDAC cell line, SUIT-2, as this cell line is extensively used in our lab and exhibits an intermediate level of type I IFN antiviral signaling. Importantly, human cells are known to be also sensitive to mIFNα (van Pesch et al., 2004; Weber et al., 1987). Our previous studies have demonstrated that, unlike highly-permissive PDAC cell lines, most human PDAC cell lines are able to respond to type I IFNs (Murphy et al., 2012). Therefore, we hypothesized that the more resistant a cell line is to virus infection, the less mIFNα would be needed to inhibit virus replication. Cells were mock-infected or infected with VSV-ΔM51-GFP at MOI 0.01 (calculated based on VSV titer on BHK-21 cells). Immediately after virus was added, cells were supplemented with 2500, 500, 20, or 4 U/ml of mIFNα. VSV-driven GFP expression was measured over the course of 78 h (Fig 19A). For each cell line, mIFNα inhibited virus replication in a dose-dependent

manner, indicating that each cell line has at least some level of intact type I IFN antiviral signaling capability. However, the overall sensitivity of each line to mIFNα was different. To measure it, we calculated the half maximal inhibitory concentration (IC50) for mIFNα, the amount of mIFNα needed to result in 50% inhibition of virus replication (inversely correlates to the antiviral signaling capability of the cells) (Fig 19B). The analysis shows that SUIT-2 cells exhibit the greatest level of antiviral capability (IC50 = 5.37 U/mL), followed by PANC02-Luc (IC50 = 33.1 U/mL), KPC-Luc-A (IC50 = 61.6 U/mL), and KPC 4580 (IC50 = 354.8 U/mL). These data support our hypothesis that the resistance of mouse KPC cells to VSV at least in part due to their abilities to mount antiviral responses. In agreement with this hypothesis, our data show that PANC02-Luc cells have both the greatest sensitivity to mIFNα and greatest overall resistance to VSV-ΔM51 among tested mouse PDAC cell lines.

Previous studies indicate that mouse cell lines are generally less responsive to human IFN (hIFN) compared to mIFN (van Pesch et al., 2004; Weber et al., 1987). Therefore, we hypothesized that mouse cell lines which are able to respond to hIFN would indicate a higher degree of type I IFN antiviral signaling capacity. To address this hypothesis, mouse cell lines (and SUIT-2 as a reference human PDAC cell line) were mock infected or infected with VSV-ΔM51-GFP at MOI 0.01. Immediately after virus was added, cells were supplemented with 2500, 500, 20, or 4 U/ml of hIFNα. VSV-driven GFP expression was measured over the course of 78 h (Fig. 20). We found that in SUIT-2 cells, hIFNα had the greatest effect at inhibiting VSV-driven GFP fluorescence, while mouse PDAC cell lines responded less efficiently than to mIFNα (compare Fig. 20 and Fig. 19). Importantly, of the mouse cell lines, PANC02-Luc were most responsive to hIFNα inhibition of VSV-driven GFP fluorescence. These data show that PANC02-Luc cells have both the greatest type I IFN antiviral signaling potential and overall resistance to VSV-ΔM51-GFP.

As mentioned above, the functional innate immune responses require not only the ability of cells to respond to IFN, but to produce and secrete IFNs and other antiviral cytokines. We hypothesized that cell lines would differ in their ability to produce and secrete such cytokines. To test this hypothesis, cells were either mock treated or infected with VSV-ΔM51-GFP at MOI 1 and 0.1 (based on virus titer on each individual cell line). At 24 h p.i. cell supernatants were collected and analyzed using the Mouse Cytokine/Chemokine 44-Plex Discovery Assay® Array (MD44) (Fig. 21), which includes critical antiviral and proinflammatory cytokines known to control viral infections. In the absence of VSV infection, we found no detectable levels of MIG (C-X-C motif ligand 9), MIP-1 (macrophage inflammatory protein 1β), IFN-β, or IL-6 (interleukin 6) in any of the three mouse cell lines. For all other cytokines, there were detectable levels in at least one of the three cell lines. The levels of basal production of some cytokines in the absence of VSV infection were strikingly different between cell lines, e.g. LIX (C-X-C motif chemokine 5), IL-1α (interleukin 1α), IL-6 (interleukin 6), TARC (C-C motif chemokine ligand 17), and VEGF (vascular endothelial growth factor). PANC02-Luc cells produced the highest levels of IL-1α, IL-6 and VEGF, while producing the least amount of TARC. KPC-Luc-A cells produced the highest amount of LIX and the lowest amount of VEGF. KPC-Luc-4580 cells produced the highest amount of TARC, while producing the lowest amount of LIX, IL-1α, and IL-6. In the presence of VSV infection, the levels of IFN-β and IFN-γ (type II IFN) were greatest in PANC02-Luc cells, which is consistent with our previous data indicating higher "antiviral status" of this cell line (Fig. 18 and 19). Also, consistent with our previous data, we found that KPC-Luc-A exhibited higher levels of IFN-β and IFN-γ compared to KPC-Luc-4580 (Fig. 18 and 19). In general, the cytokine analysis data show a positive correlation between levels of produced IFN-β and IFN-γ in each cell line and the observed degree of resistance to VSV infection. Interestingly, the levels of other cytokines

between the three cell lines vary dramatically, even between KPC-Luc-A and KPC-Luc-4580, which have the same tumor driver mutations. For example, the levels of TARC produced in KPC-Luc-4580 cells is highest between cell lines, versus the levels of MCP-1 (monocyte chemoattractant protein -1) that was highest in KPC-Luc-A cells. The levels of produced cytokines in MOI 0.1 versus MOI 1 were relatively similar with only some exceptions, such as GM-CSF (granulocyte-macrophage colony-stimulating factor) and MIG (CXCL9). In general, in agreement with our hypothesis, the cytokine analysis data show a positive correlation between levels of produced antiviral and proinflammatory cytokines and the observed degree of resistance of cells to VSV infection.

Combinatorial treatments improve permissiveness of mouse pancreatic cancer cell lines to oncolytic vesicular stomatitis virus

Our previous studies have demonstrated that it is possible to overcome otherwise resistant human PDAC cells to VSV (Bressy et al., 2019; Cataldi et al., 2015; Felt et al., 2017; Moerdyk-Schauwecker et al., 2013). One such approach utilizes combining VSV with drugs such as ruxolitinib and TPCA-1, both of which our lab has shown to enhance VSV replication in human PDAC cells. Ruxolitinib (trade name Jakalfi) is a Janus Kinase 1 (JAK1) and Janus Kinase 2 (JAK2) inhibitor (Mesa, 2010) which greatly enhances VSV replication in cells with functional type I IFN signaling (Cataldi et al., 2015). TPCA-1 is an inhibitor of Inhibitor of Kappa B Kinase (IKK-2), which we previously showed also directly inhibits JAK1, subsequently inhibiting STAT1 and STAT2 phosphorylation and decreasing the expression of antiviral genes (Cataldi et al., 2015). Paclitaxel is a common chemotherapeutic drug that stabilizes the microtubule polymer and protects it from disassembly, ultimately blocking mitosis and triggering apoptosis (Jordan & Wilson, 2004). Colchicine inhibits microtubule polymerization, via binding to tubulin (Dalbeth et al., 2014). Our

previous studies showed that paclitaxel and colchicine enhance VSV replication by arresting cells in the G_2/M phase, resulting in global repression of cellular transcription and thus indirectly inhibiting type I and III IFN production and expression of ISGs (Bressy et al., 2019). While these combinatorial treatments in human PDAC show promising results, we wanted to determine if similar results would be observed in our mouse PDAC cell lines. Importantly, we hypothesized that, as these molecules stimulate VSV replication via inhibition of antiviral cellular responses, they will be more effective in mouse cell lines exhibiting higher levels of antiviral signaling. For example, ruxolitinib would have little effect on VSV replication in a cell line with defective antiviral signaling, because there are no robust antiviral responses for ruxolitinib to inhibit.

To determine if our mouse cell lines would be responsive to virus combination treatments, cells were infected with VSV-ΔM51-GFP at MOI 0.01 plus either 5, 0.5, or 0.05 μM of either ruxolitinib, TPCA-1, paclitaxel, or colchicine over the course of 67 hours. The human PDAC cell line, SUIT-2 (Iwamura et al., 1987), was also tested here for comparison, as this cell line has been extensively studied in our lab and it exhibit an intermediate level of permissiveness to VSV compared to other human PDAC cell lines, and also was shown to be responsive to all those combinatory treatments (Bressy et al., 2019; Cataldi et al., 2015; Hastie et al., 2015; Moerdyk-Schauwecker et al., 2013). As shown in Figure 22, we found that each drug enhanced VSV-ΔM51 replication. In agreement with our hypothesis, ruxolitinib had the greatest effect in PANC02-Luc (and human SUIT-2 cells), and a much lower effect in KPC-Luc-A and KPC-Luc-4580 cells. This finding is consistent with cell lines that are more defective in antiviral signaling, as ruxolitinib is a direct potent inhibitor of JAK1 and JAK2, both of which are major upstream regulators type I and II IFN signaling and subsequent ISG expression. In agreement with that observation, we also found that TPCA-1, which also directly inhibits JAK1 (Cataldi et al., 2015), had the greatest

positive effect in PANC02-Luc cells. Although colchicine and paclitaxel stimulated VSV replication in all tested cell lines, surprisingly, colchicine had the greater positive effect on VSV-ΔM51 replication in KPC-Luc-A and KPC-Luc-4580 cell lines, compared to PANC02-Luc cells, and paclitaxel had the greatest positive effect in KPC-Luc-4580, compared KPC-Luc-A and PANC02-Luc cells. As both colchicine and paclitaxel affect type I IFN signaling indirectly, via arresting cells in the G_2/M phase (Bressy et al., 2019), this unexpected result could be explained by differences of cell lines in their cell cycle regulation.

Interestingly, these data show that the mouse PDAC cell lines respond to VSV-based combination treatments in a similar fashion to human PDAC cell lines. Importantly, these data support the use for these mouse PDAC cell lines for future studies testing OV combination-based treatments *in vivo.*

No correlation between resistance of mouse pancreatic cancer cell lines to oncolytic vesicular stomatitis virus and chemotherapy

We have recently shown that some human PDAC cell lines, which acquire resistance to chemotherapeutical drugs, can also simultaneously develop resistance to OV therapy (Goad et al., 2022) In addition, although the analyses of 10 different human PDAC cell lines showed no statistically significant correlation between their resistance to gemcitabine and VSV, 4 PDAC cell lines most resistant to VSV were also among 5 PDAC cell lines most resistant to gemcitabine (Goad et al., 2022). Chemoresistance of PDACs is one of the major reasons for the poor survival outcomes of PDAC patients. We therefore sought to investigate the inherent resistance of our mouse PDAC cells against commonly used chemotherapeutic drugs, gemcitabine (2'-deoxy-2',2'-difliorocytidine monohydrochloride; dFdC; trade name Gemzar) and 5-FU (fluorouracil; trade

name Adrucil). Gemcitabine is a deoxycytidine analogue that is commonly used in chemotherapeutical regimens for PDAC patients (Amrutkar & Gladhaug, 2017). Fluorouracil acts principally as a thymidylate synthase (TS) inhibitor and is used as a chemotherapeutic for a variety of cancers, including PDAC (Longley et al., 2003). To examine a possible correlation between VSV resistance and resistance to both gemcitabine and/or 5-FU, cells were treated with serial dilutions of either gemcitabine or 5-FU, followed my measuring cell viability 72 hours later (Fig. 23) and calculation of the IC50 for each drug on each cell line as a measure of drug resistance. We found no significant correlation between the level of resistance to VSV and resistance to either gemcitabine or 5-FU. In sharp contrast, PANC02-Luc cells, which are the most resistant VSV-resistant mouse PDAC cell line among the cells tested, were the most drug sensitive with the lowest IC50 for both gemcitabine and 5-FU, 28.8 nM and 2,880 nM, respectively. The IC50 values for gemcitabine and 5-FU in KPC-Luc-A cells were 131.8 nM and 12,020 nM. Interestingly, the mouse PDAC cell line most permissive to VSV among the cells tested, KPC-Luc-4580, demonstrated the greatest resistance to gemcitabine and 5-FU with IC50 values of 199.5 nM and 48,900 nM, respectively. These data suggest that the level of chemoresistance in mouse PDAC cell lines does not correlate with the efficacy of VSV-based OV-therapy, and, promisingly, suggest that chemoresistant tumors can be good targets for OV therapy.

Karyotype and exome analyses of mouse pancreatic cancer cell lines

Although all three tested mouse PDAC cell lines are widely used as models to study PDAC biology and treatments for PDAC *in vivo*, to our knowledge, they have never been tested in detail for overall chromosomal abnormalities or for all genomic mutations in protein coding sequences. To examine the karyotype of these cells, each cell line was grown to 70% confluence and sent to

the Cytogenomics Core Laboratory at the University of Minnesota for Spectral Karyotyping (SKY). We found that each cell line contained numerous chromosomal aberrations (Fig. 24), the "consensus karyotype" is shown in green box). KPC-Luc-4580, KPC-Luc-A, and PANC02-Luc cells exhibited overall chromosome count ranges of 48-51, 65-72, and 97-90, respectively. Interestingly, PANC02-Luc and then KPC-Luc-A cell lines displayed the greatest degree of chromosomal aberration, with karyotypes more closely resembling hypertetraploid and hypertriploid genomes, respectively. Of note, for each cell line the level of chromosomal aberration seems to corelate with the level of resistance to VSV. However, while this potential correlation is interesting, we do not have any data suggesting that it is causative, and investigating specific chromosomal aberrations and how they might affect resistance to VSV is beyond the scope of this study. Rather, these data are important for future studies in understanding major genetic differences between model mouse PDAC cell lines.

Our data highlight that each of the 3 mouse PDAC cell lines are different in their permissiveness to VSV and their antiviral expression profiles. We next hypothesized that more VSV-permissive and more IFN-deficient cell lines will harbor more mutations in genes associated with innate immunity/antiviral response. To examine genomic mutations in protein coding sequences of these 3 mouse PDAC cell lines, cell pellets were sent to Azenta US for DNA extraction, exome sequencing, and exome analysis (Fig. 25). The entire exome data were deposited to the GenBank Sequence Read Archive (SRA) database under BioProject PRJNA944630). Interestingly, we found that both KPC cell lines exhibited a far greater number of mutations compared to PANC02-Luc cells (Fig. 24A). The mutations were further classified based on genome impact (Fig. 25B) as "high" (mutations affecting splice sites, start and stop codons), "moderate" (non-synonymous variations), "low" (synonymous variations), and "modifier"

(variations in non-coding regions e.g. upstream, downstream, intergenic and UTR regions). In both KPC cell lines, the majority of mutations are classified as low impact, followed by moderate, modifier, and high, respectively. In PANC02-Luc cells the majority of mutations were classified as moderate impact, followed by low, modifier, and high, respectively. The mutations were then further broken down by variant type (Fig. 25C). In all cell lines, the majority of mutations were single nucleotide polymorphisms (SNP). Consistent with Fig. 25B, the majority of SNPs in PANC02-Luc cells appear to be of moderate impact, in contrast to both KPC cell lines where the majority of SNPs are low impact. After SNPs, the greatest number of mutations in each cell line were deletions (DEL), followed by insertions (INS), double nucleotide polymorphisms (DNP), and triple nucleotide polymorphism (TNP), respectively. Most of the high impact mutations in each cell line were INSs and DELs.

Focusing on the genes associated with cancer and innate immunity, we utilized the nanoString PanCancer IO 360 Panel, PanCancer Pathways Panel, and the PanCancer Immune Profiling Panel to generate a list of cancer and immune genes of interest. Overall, we found over 2000 mutations in genes associated with cancer and innate immunity (Fig. 26). Interestingly, both KPC cell lines exhibited a significantly greater number of mutations (KPC-Luc-4580: 12,065, KPC-Luc-A: 28,131) compared to PANC02-Luc cells (2,609) (Poisson regression: intercept: mean: 9.4 (standard error: 0.1; slope (KP-Luc-A: 0.84 (0.01); slope (PANC-2-Luc: -1.53; 0.02) (Fig. 26A). In both KPC cell lines, the majority of mutations are classified as low impact, followed by moderate, modifier, and high, respectively. In PANC02-Luc cells the majority of mutations were classified as moderate impact, followed by low, modifier, and high, respectively (Fig. 25B). The majority of mutations were SNPs, with the least mutation type being TNPs (Fig 26C). Importantly, both KPC cell lines contain the classical PDAC Trp53R172H and KrasG12D driver mutations. As

previously reported, we found no mutations in Trp53 and Kras in PANC02-Luc cells (Wang et al., 2012). However, our data indicate that only PANC02-Luc cells contain a nonsense mutation in another important PDAC gene, Smad4 (Smad4 mutation absent in both KPC cell lines).

Consistent with our hypothesis, in both KPC cell lines we found mutations in many key antiviral genes (Table 4). Notably, we found multiple identical missense mutations in the tyrosine kinase 2 (TYK2) gene, a critical upstream modulator of type I IFN signaling. We also found in both KPC cell lines identical missense mutations in JAK2 and JAK3 genes, which are critical upstream modulators of innate and adaptive immunity, respectively. Such identical mutations suggest that these mutations are important for the overall fitness of these cells. Additionally, these mutations in innate immunity associated genes may be responsible in part to the higher permissiveness of KPC cells to VSV infection compared to PANC02-Luc (Table 4). While specific analysis of the role of each mutation in these cell lines is beyond the scope of this study, the exome sequencing data provides valuable information for future studies using these mouse PDAC cell lines.

3.4 Conclusions

Preclinical models of PDAC are vital for understanding the biology of PDAC, and are platforms for developing novel strategies against PDAC, one of the deadliest forms of cancer and a major cause of cancer related deaths in the U.S. since the 1970s (Mizrahi et al., 2020; Siegel et al., 2023). Optimal PDAC model systems should address several key features of PDAC, including the ability to test OV-based therapy against different PDACs, characterized by various responses to different therapies (intertumoral heterogeneity), and the ability of test new therapies in immunocompetent mice.

In this study, we examined phenotypically and genotypically 3 commonly-used allograftable mouse PDAC cell lines: Panc02 (derived from chemically-induced PDAC; also known as Pan02),

and two cell lines originated from PDACs developed in two different KPC ($Kras^{G12D}$, $Trp53^{R172H}$ and Cre) mouse models. Our study (i) characterized the ability of oncolytic vesicular stomatitis virus (VSV) to infect, replicate in, and kill these mouse PDAC cells; (ii) examined their innate antiviral responses; (iii) compared their permissiveness to VSV and chemotherapeutic drugs; (iv) analyzed their karyotype and exome. Similar to human PDACs, mouse PDAC cell lines showed high divergence in their permissiveness to VSV, which negatively correlated with the ability of cells to mount innate antiviral responses. Ruxolitinib (JAK1/2 inhibitor), TPCA-1 (IKK-β inhibitor), paclitaxel, and colchicine enhanced VSV replication and oncolysis in all three mouse PDAC cell lines. Also, mouse PDAC cell lines showed high divergence in their karyotype and exome. Our data provide essential data about 3 allograftable model mouse PDAC cell lines and propose a novel platform to study OV-based therapies against different PDACs in immunocompetent mice. These results are further discussed in the dissertation summary (Chapter 4).

.

3.5 Figures

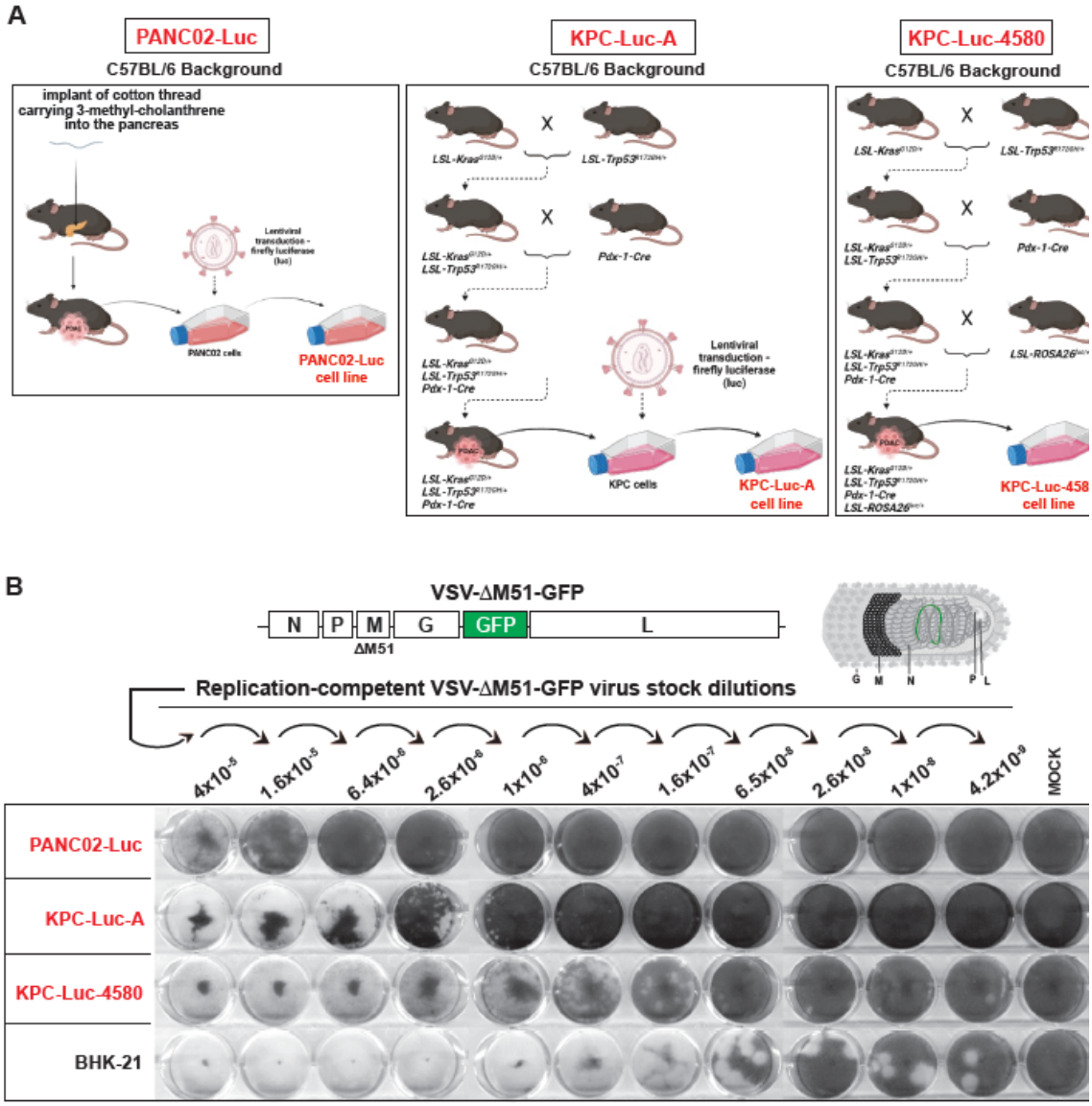

Figure 15. Development and characterization of mouse PDAC cell lines. (A) Three mouse PDAC cell lines, PANC02-Luc, KPC-Luc-A, and KPC-Luc-4580, were isolated from PDAC tumors formed in C57BL/6 mice. The PANC02 cell line was generated by chemically inducing PDAC in mice via the implantation of 3-methyl-cholantrene into the pancreas of genetically unaltered C57BL6, and then the luciferase reporter expressing PANC02-Luc cell line was later generated using lentiviral transduction. The KPC-Luc-A cell line was derived from a tumor that developed in an LSL-KrasG12D/+; LSL-Trp53R172H/+; PDX-Cre/+ mouse, and then the luciferase reporter was inserted using lentiviral transduction. The KPC-Luc-4580 cell line (also known as KPC-4580P) was derived from a tumor that developed in an LSL-KrasG12D/+; LSL-Trp53R172H/+; PDX-Cre/+, LSL-ROSA26Luc/+ mouse. (B) Cell lines were mocked treated or infected with serial dilutions of VSV-ΔM51 under agar. Cells were fixed and stained at 72 h p.i. Results shown are representative of more than five independent experiments.

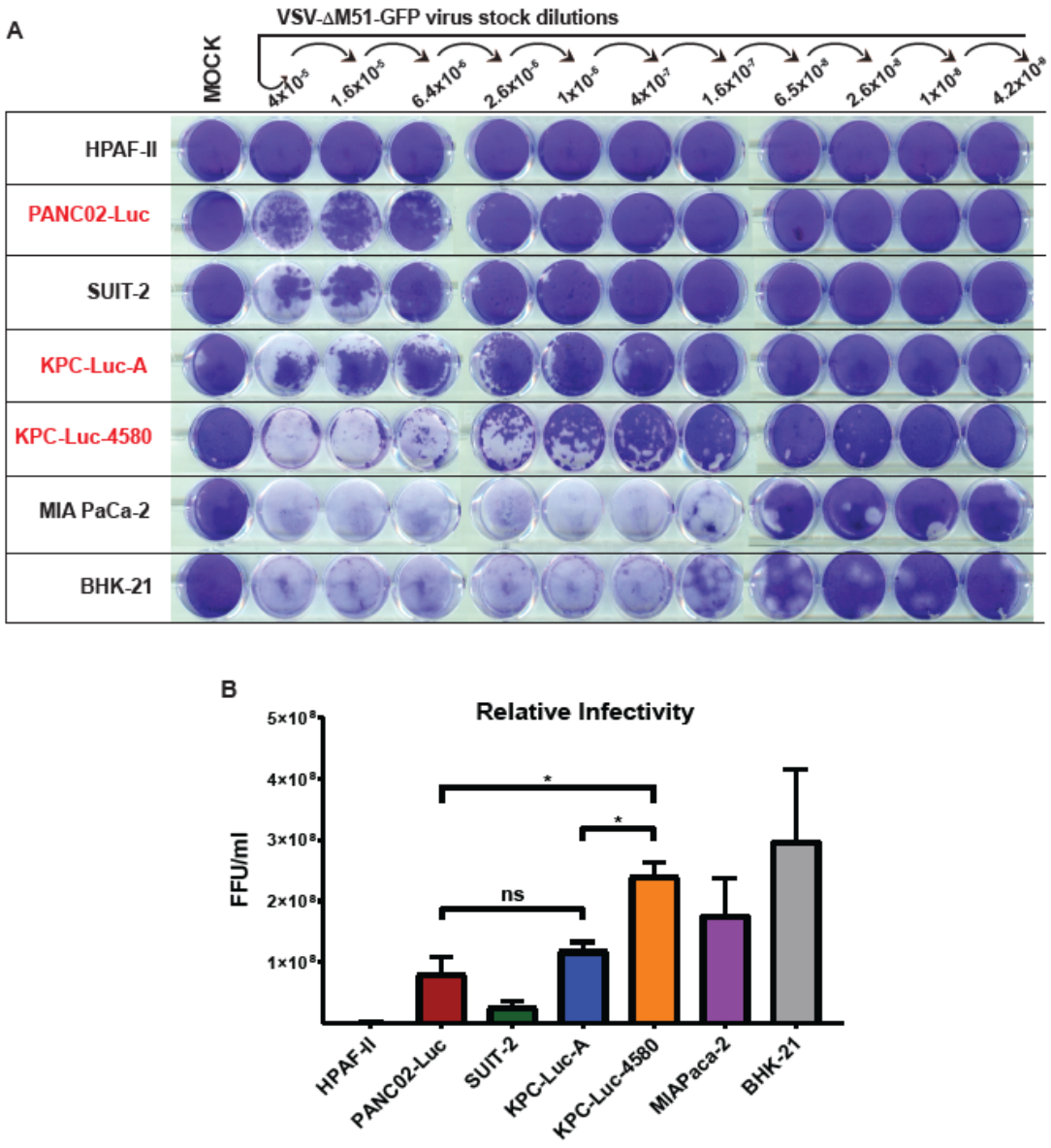

Figure 16. Relative infectivity to VSV in a panel of different cell lines. (A) Cells were either mock treated or infected with serial dilutions of VSV-ΔM51-GFP under agar from $4x10^{-5}$ to $4.2x10^{-9}$. Cells were fixed and stained at 48 h p.i. (B) In a separate experiment, cell monolayers were examined using fluorescent microscopy to count the virus-directed GFP focus forming units (FFUs) at 24 h p.i. to calculate cell line specific FFU/ml for our VSV-ΔM51-GFP stock. Results shown are representative of five independent experiments. The data points and error bars represent the means and SEM of the means, respectively. Results were analyzed to determine significance using the Student's t test. *$p<0.05$

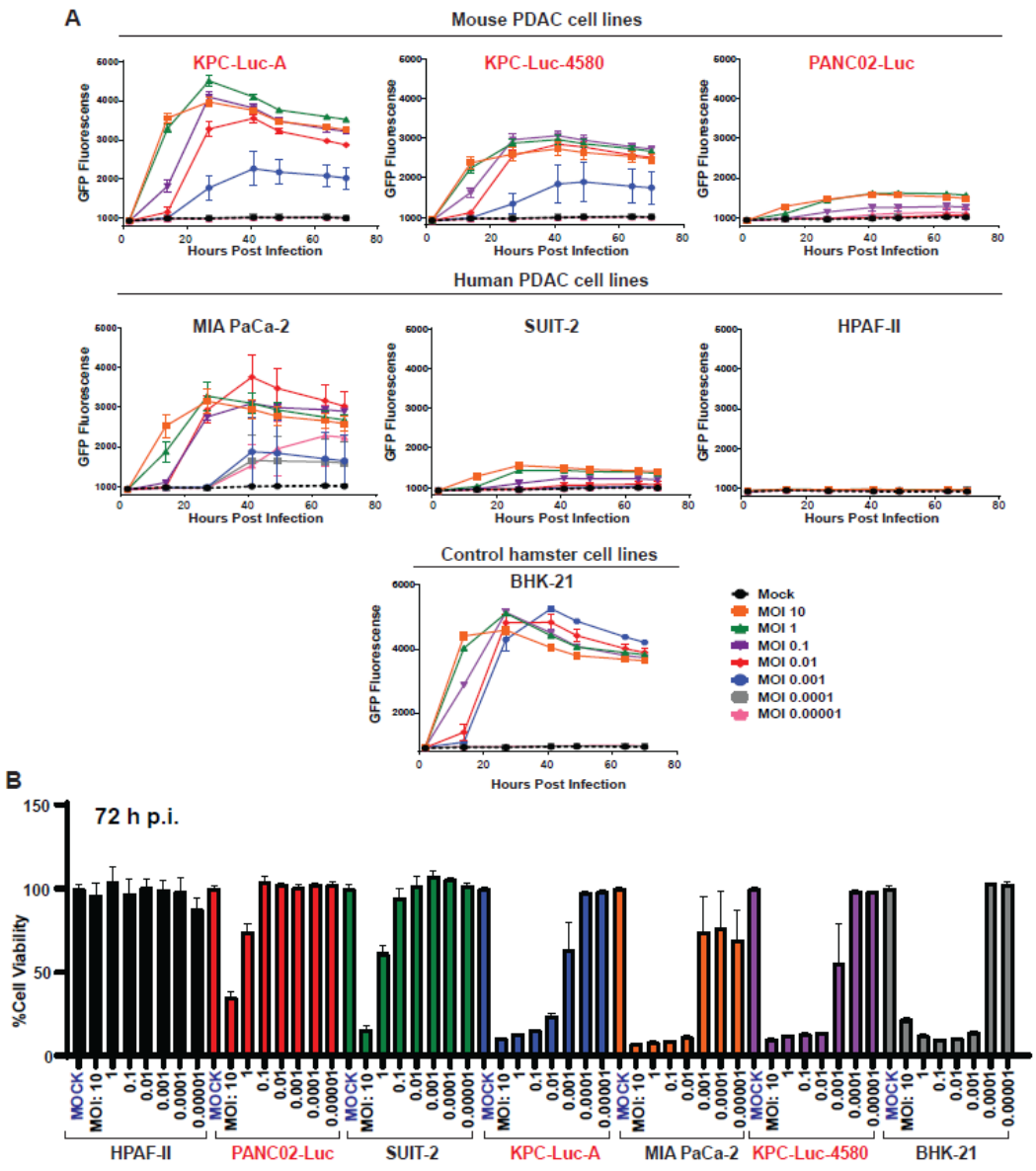

Figure 17. Viral replication kinetics and cell viability. (A) Cell lines were either mock treated or infected with VSV-ΔM51-GFP at MOIs of 10, 1, 0.1, 0.01, 0.001, 0.0001, or 0.00001. GFP fluorescence was measured over time from 1 to 72 h p.i. (B) Cell viability of cells 72 h after infection. Cell lines were either mock treated or infected with VSV-ΔM51-GFP at MOIs of 10, 1, 0.1, 0.01, 0.001, 0.0001, or 0.00001. Cell viability was measured at 72 h p.i. using a WST-8 cell viability assay. Results shown are representative of five independent experiments. All virus titers were based on BHK-21 cells. The data points and error bars shown represent the means and SEM of the means, respectively (some error bars are too small to be seen in the figures).

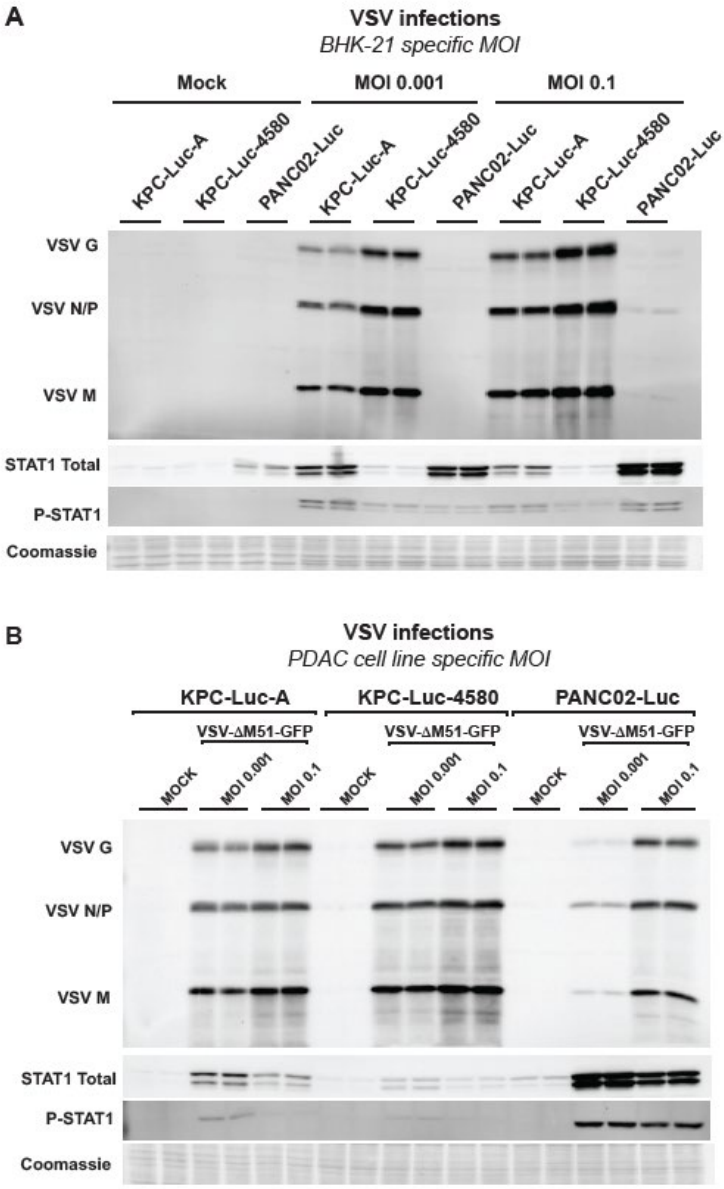

Figure 18. VSV and antiviral protein expression. Cell lines were either mock treated or infected with VSV-ΔM51-GFP at MOIs of 0.1 and 0.001 either based on virus titer on BHK-21 cells (A) or based on virus titer on each cell line (B). Protein samples were analyzed at 24 h p.i. by western blotting for expression of VSV proteins (G, N/P, and M), STAT1, and phosphor-STAT1 (P-STAT1). Cell line and treatment conditions are indicated above blots. Equal protein loading is shown by Coomassie blue.

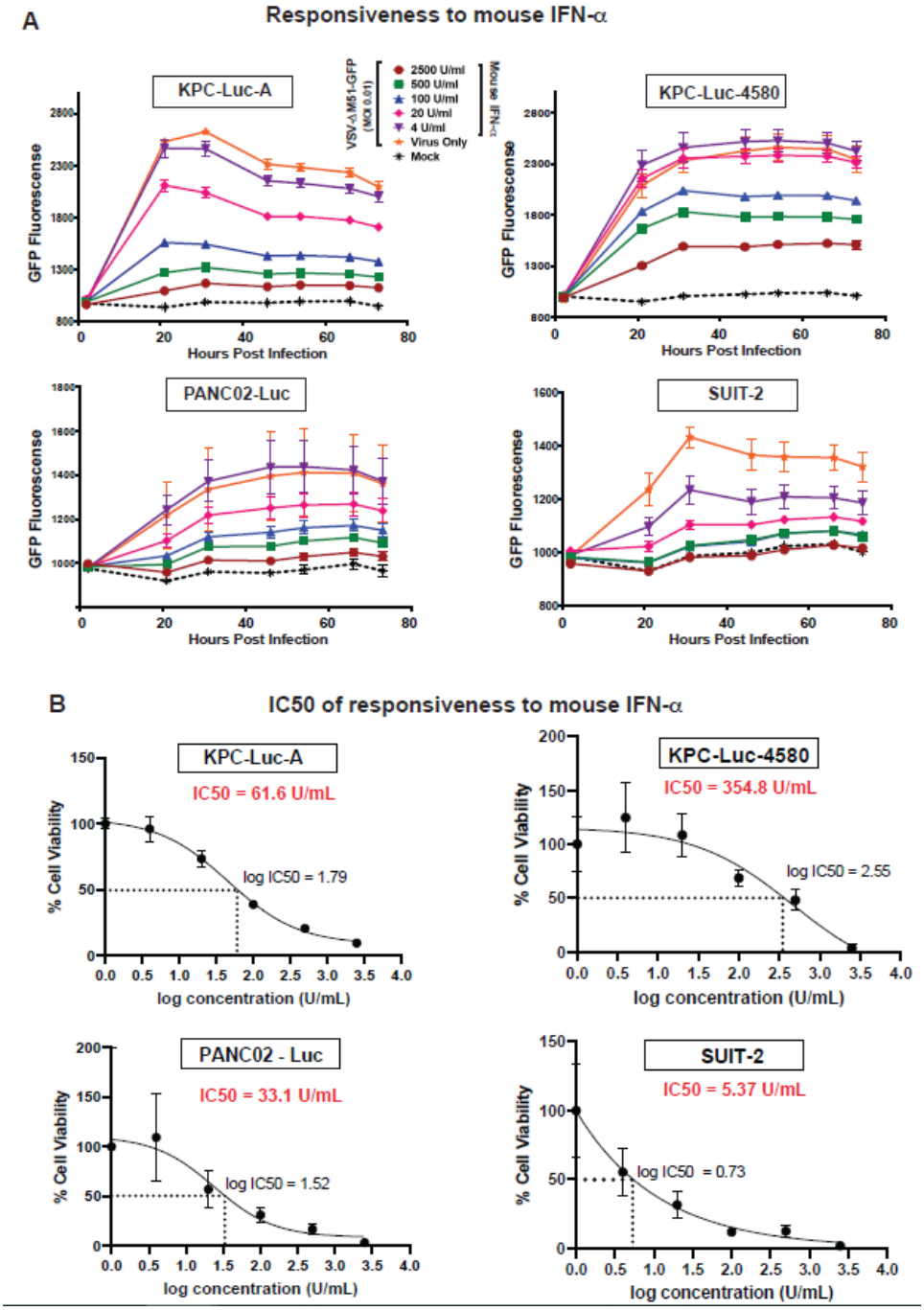

Figure 19. Responsiveness to mouse IFN-α. (A) Cells were either mock treated or infected with VSV-ΔM51-GFP at MOI 0.01 (based on BHK-21 cells). Cells were then treated with mouse IFN-α (mIFN-α) at 2500, 500, 100, 20, 4, or 0 (virus only) units/ml. GFP fluorescence was measured overtime from 1 to 73 h p.i. (B) The half maximal inhibitory concentration (IC50) of mIFN-α was determined by using GraphPad Prism 9.3.1. Results shown are representative of three independent experiments. The data points and error bars shown represent the means and SEM of the means, respectively (some error bars are too small to be seen in the figures).

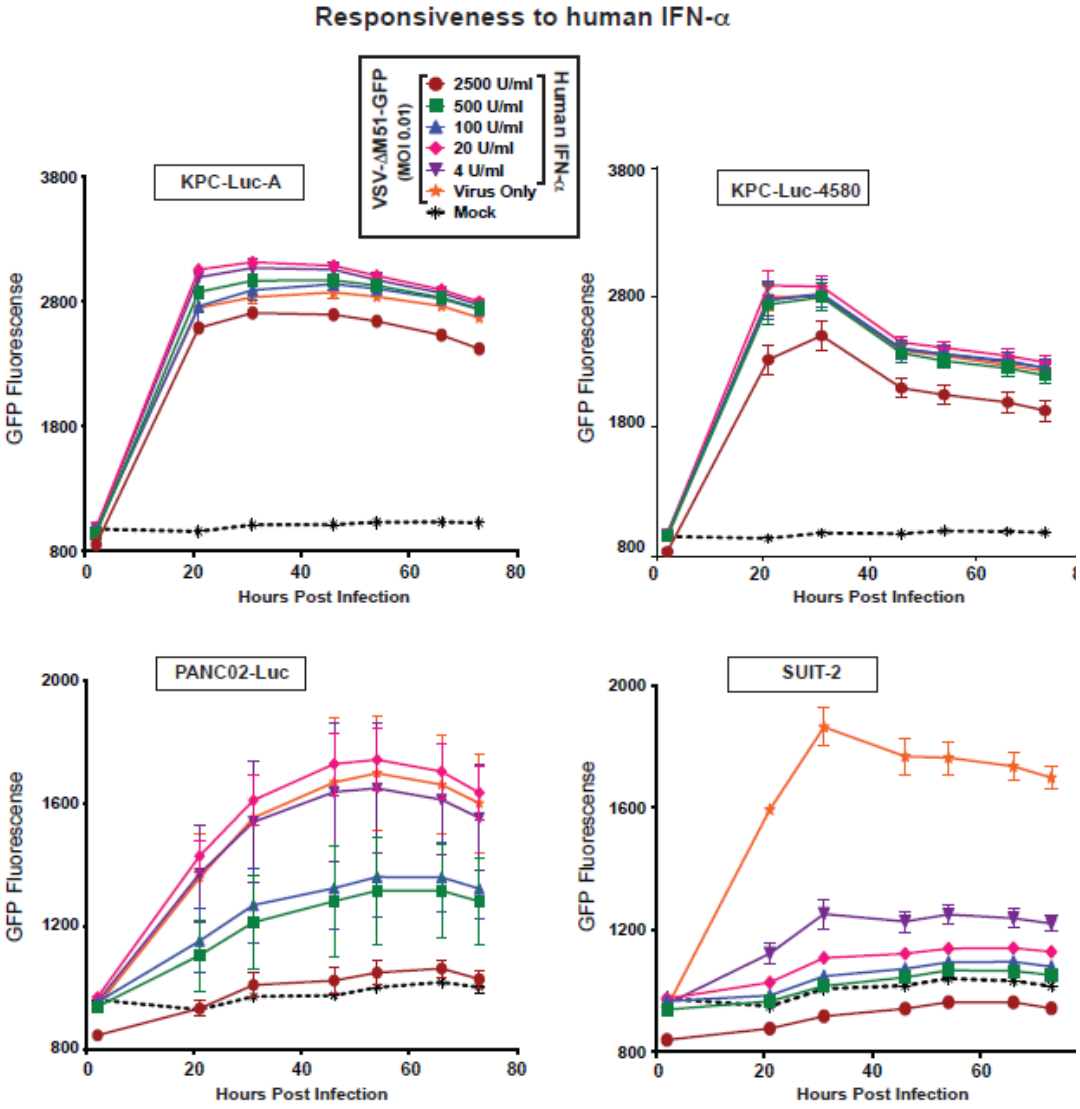

Figure 20. Responsiveness to human IFN-α. Cells were either mock treated or infected with VSV-ΔM51-GFP at MOI 0.01 (based on BHK-21 cells). Cells were then treated with human IFN-α (hIFN-α) at 2500, 500, 100, 20, 4, or 0 (virus only) units/ml. GFP fluorescence was measured over time from 1 to 73 h p.i. Results shown are representative of three independent experiments. The data points and error bars shown represent the means and SEM of the means, respectively (some error bars are too small to be seen in the figures).

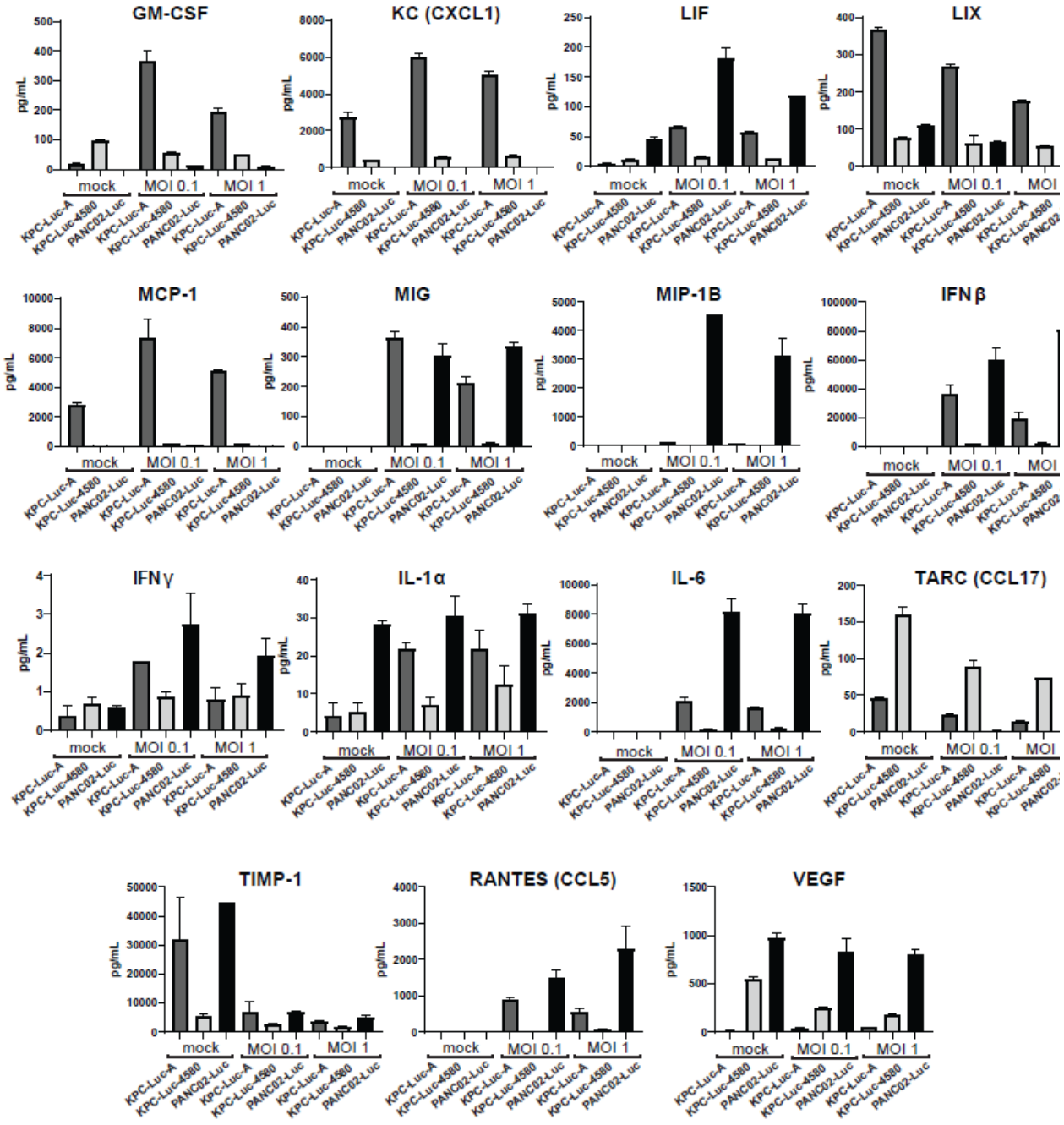

Figure 21. Cytokine array. Cells were either mock treated or infected with VSV-ΔM51-GFP at MOI 1 and 0.1 (titer was calculated based on each individual cell line). At 24 h p.i. cell supernatants were collected and sent to EVE Technologies Corp for Mouse Cytokine/Chemokine 44-Plex Discovery Assay® Array (MD44). The data points and error bars shown represent the means and SEM of the means, respectively.

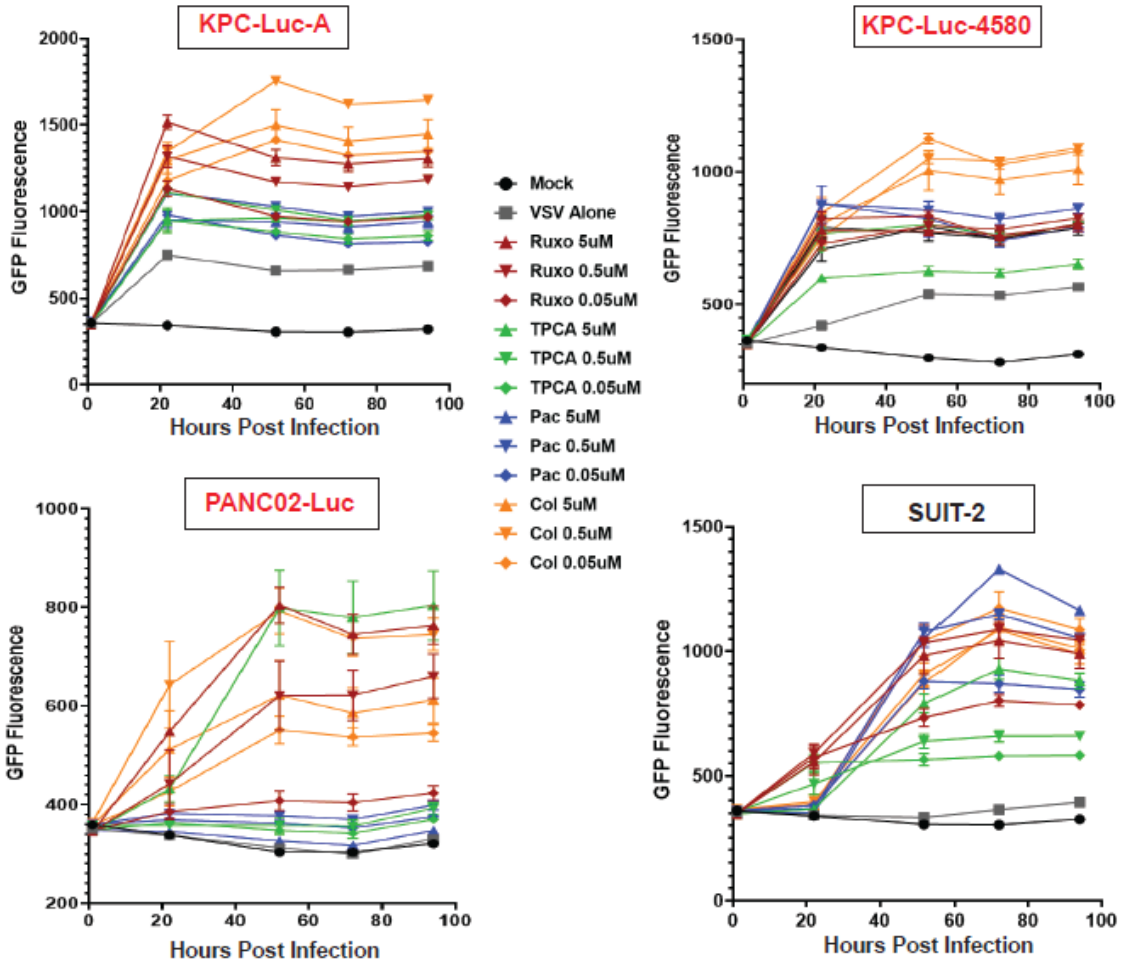

Figure 22. Combinatorial treatments of PDAC cells using VSV-ΔM51-GFP in combination with different drugs. Cells were either mock treated or infected with VSV-ΔM51-GFP at MOI 0.01 (based on BHK-21 cells). Cells were then treated with either Ruxolitinib (Ruxo), TPCA-1 (TPCA), Paclitaxel (Pac), or Colchicine (Col) at 5, 0.5, 0.05, or 0 µM (virus only). GFP fluorescence was measured over time from 1 to 94 h p.i. Results shown are representative of two independent experiments. The data points and error bars shown represent the means and SEM of the means, respectively (some error bars are too small to be seen in the figures).

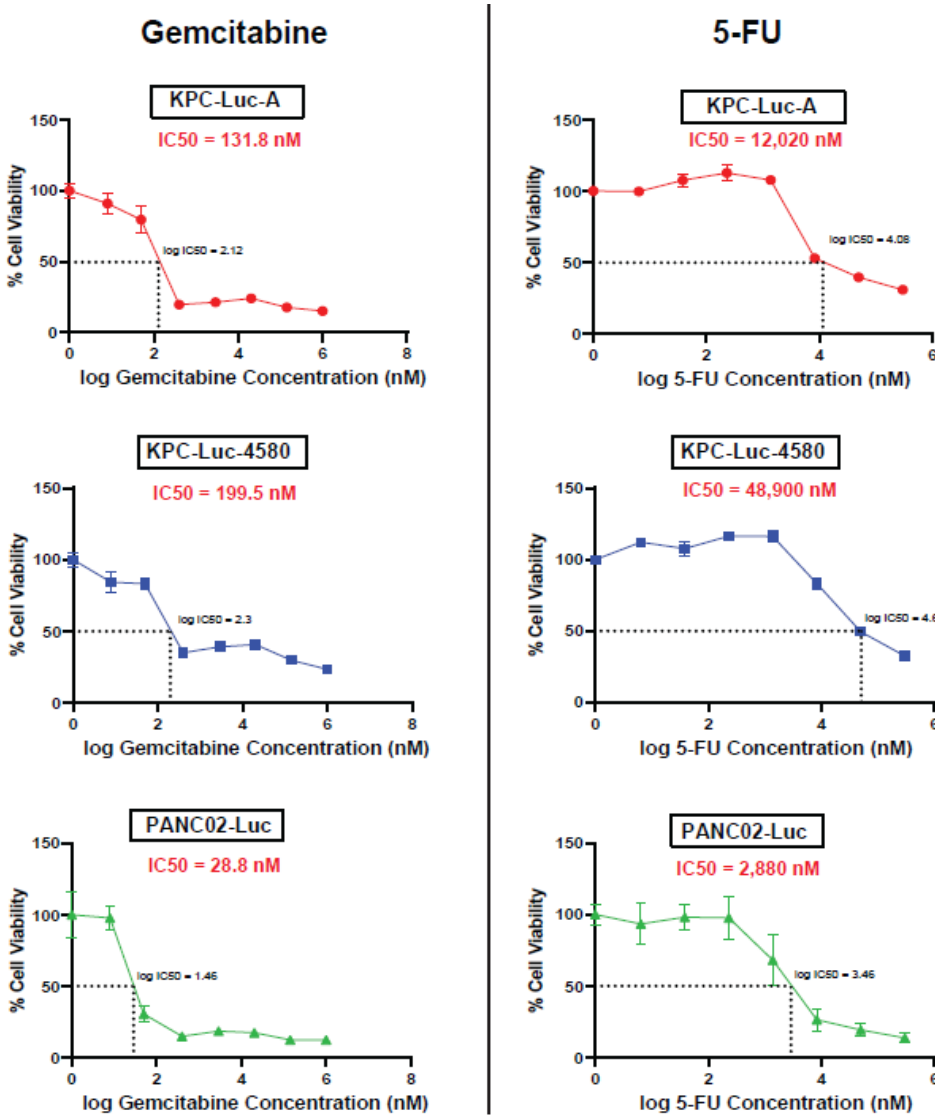

Cell line	IC50 (Gemcitabine)	IC50 (5-FU)	IC50 (VSV 72H)
KPC-Luc-4580	199.5 nM	48,900 nM	MOI 0.0013
KPC-Luc-A	131.8 nM	12,020 nM	MOI 0.0021
PANC02-Luc	28.8 nM	2,880 nM	MOI 3.89

Figure 23. Chemoresistance of mouse PDAC cell lines to gemcitabine and 5-FU. Cells were treated with serial dilutions of either gemcitabine or 5-FU, followed by a cell viability assay 72 hours after treatment. IC50 values were calculated using GraphPad Prism 9.3.1. Results shown are representative of two independent experiments. The data points and error bars shown represent the means and SEM of the means, respectively (some error bars are too small to be seen in the figures).

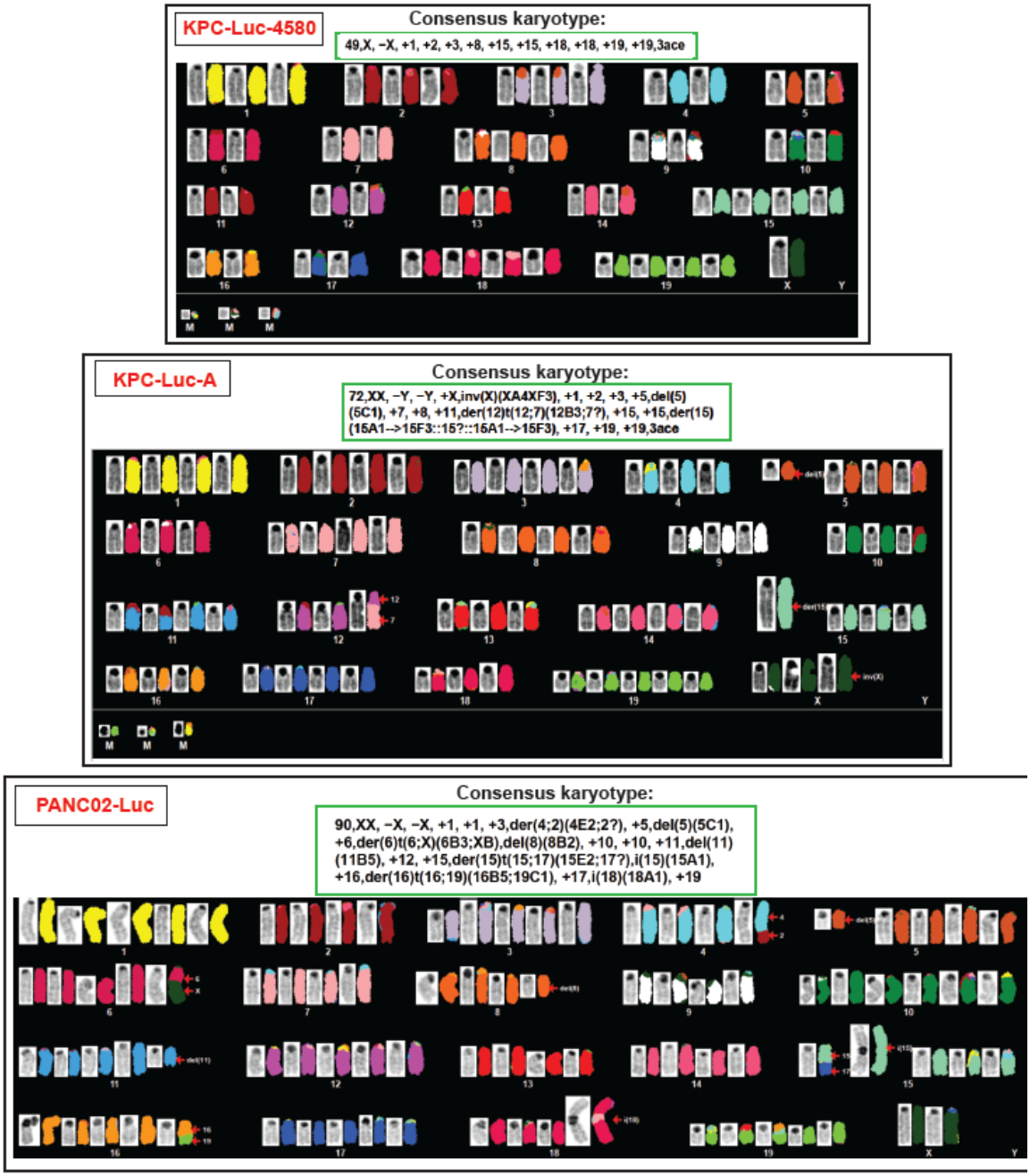

Figure 24. Spectral karyotyping (SKY) of mouse PDAC cell lines. Adherent cells were harvested with colcemid arrest, treatment with 0.75 M KCl hypotonic solution, and fixation with 3:1 methanol: acetic acid. The resulting cells were spread onto glass slides according to standard cytogenetic protocols. A Spectral Karyotyping (SKY) slide was processed according to the manufacturer's protocol (Applied Spectral Imaging). SKY uses a unique combination of five fluorescent dyes to paint all 24 chromosomes. Seven metaphase cells per sample were examined by SKY using the Olympus BX61 microscope with DAPI and SKY fluorescence filter sets. G-band and SKY metaphase cells were imaged and karyotyped using Applied Spectral Imaging (ASI) software.

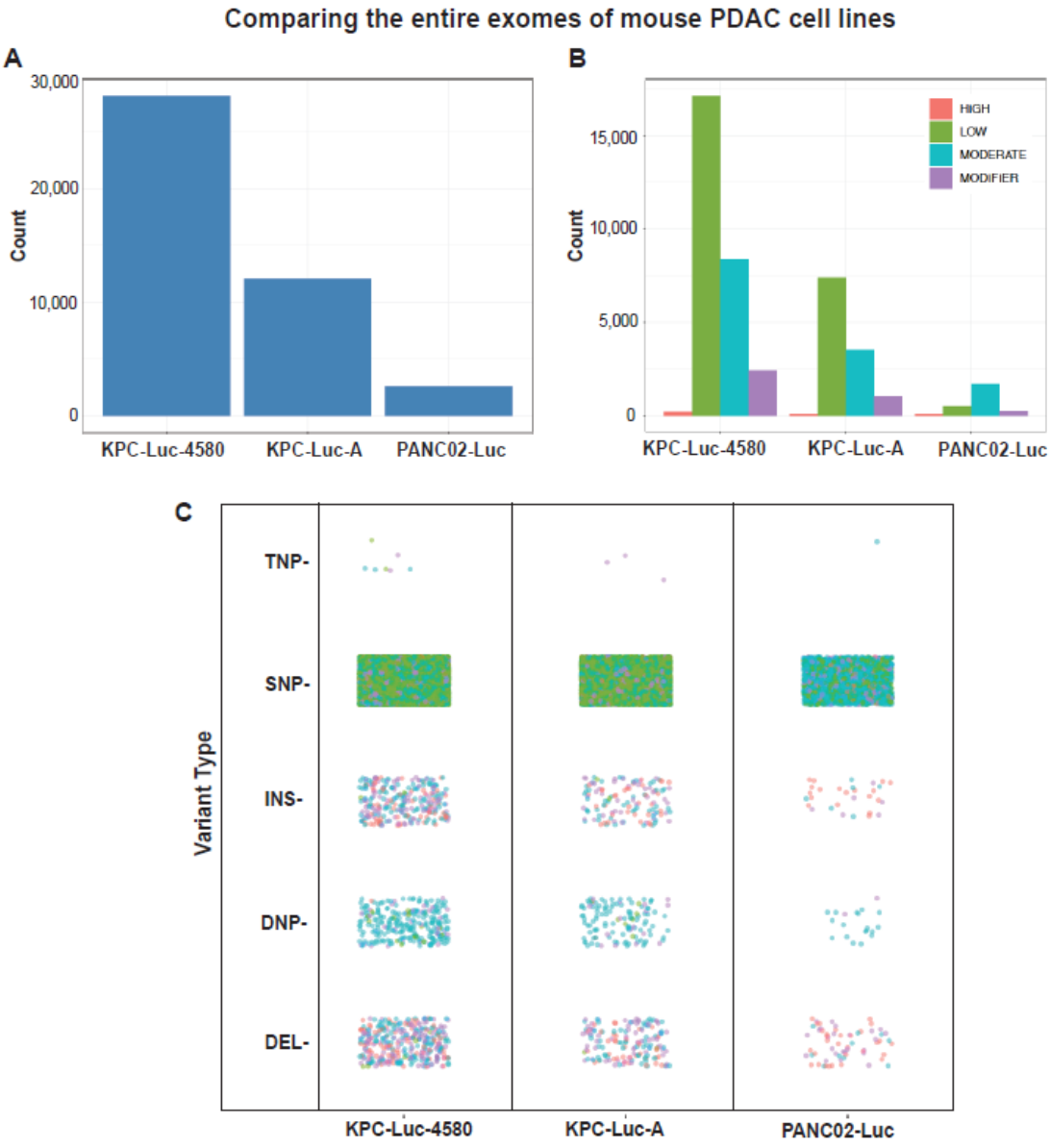

Figure 25. Exome analysis of all genes in three mouse PDAC cell lines. Abbreviations are as follows: SNP (single nucleotide polymorphisms), DNP (double nucleotide polymorphism), TNP (triple nucleotide polymorphism), INS (insertion), DEL (deletion). Mutations were annotated according to AZENTA Life Sciences Sequence Ontology pipeline, which leverages the Ensembl database of calculated variant consequences. The Impact rating uses the same qualifiers as SnpEff and SnpSift software (https://pcingola.github.io/SnpEff/se_introduction/) and can be interpreted as the following: High (disruptive, truncating, loss of function of protein), Low (harmless or unchanging to protein), Moderate (non-disruptive, but may have an effect), and Modifier (changes in non-coding regions or in regions where function and impact is unable to be assessed).

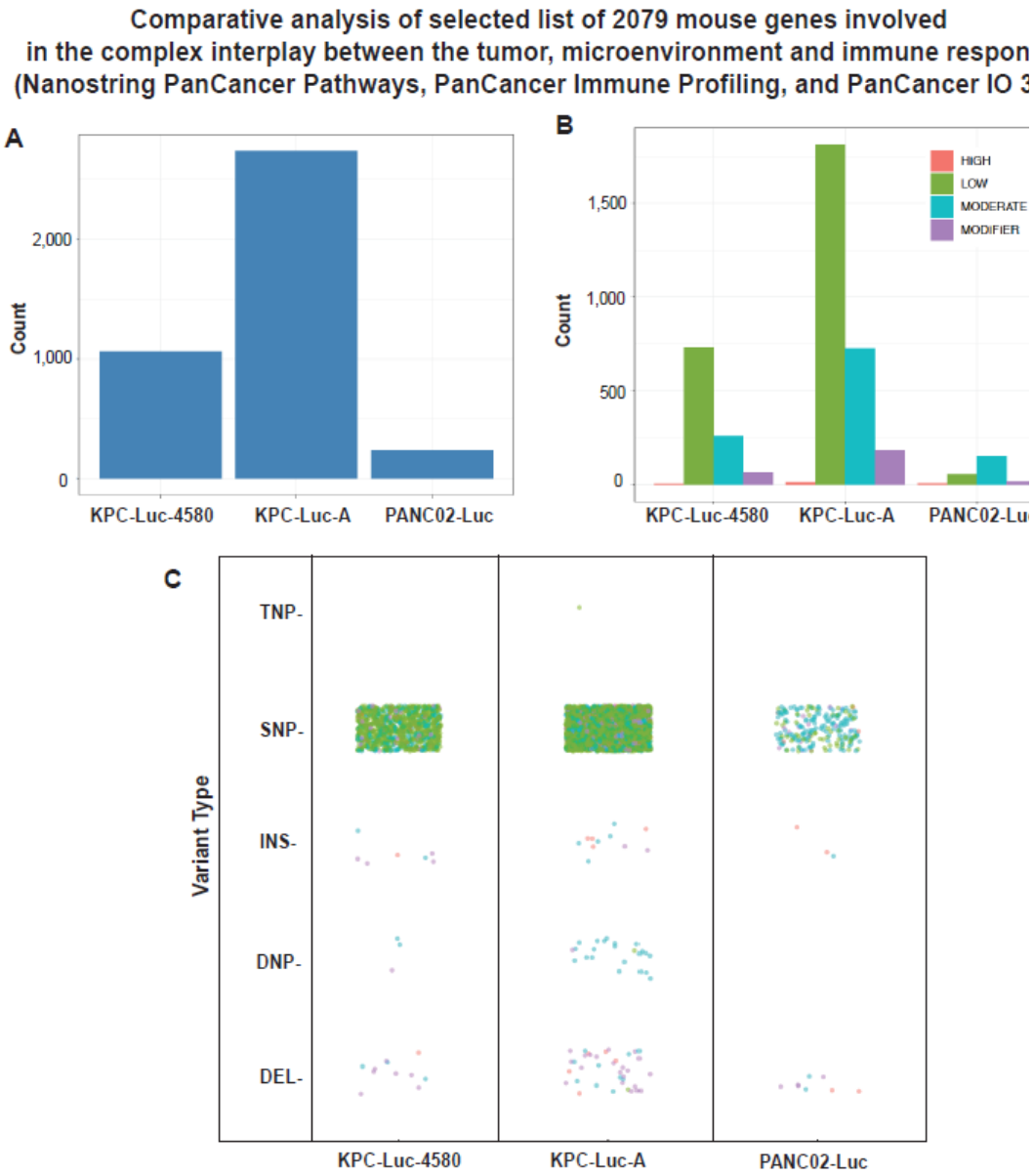

Figure 26. Exome analysis of 2079 genes involved in tumor, microenvironment and immune response. Comparative analysis of 2079 mouse genes known to be involved in the complex interplay between the tumor, microenvironment and immune response (Nanostring PanCancer Pathways, PanCancer Immune Profiling, and PanCancer IO 360), identified from Azenta Life Sciences Genewiz pipeline. Variant annotations based on Azenta Genewiz pipeline based on Ensembl Sequence Ontology. Abbreviations are as follows: SNP (single nucleotide polymorphisms), DNP (double nucleotide polymorphism), TNP (triple nucleotide polymorphism), INS (insertion), DEL (deletion). Mutations were annotated according to AZENTA Life Sciences Sequence Ontology pipeline, which leverages the Ensembl database of calculated variant consequences. The Impact rating uses the same qualifiers as SnpEff and SnpSift software (https://pcingola.github.io/SnpEff/se_introduction/).

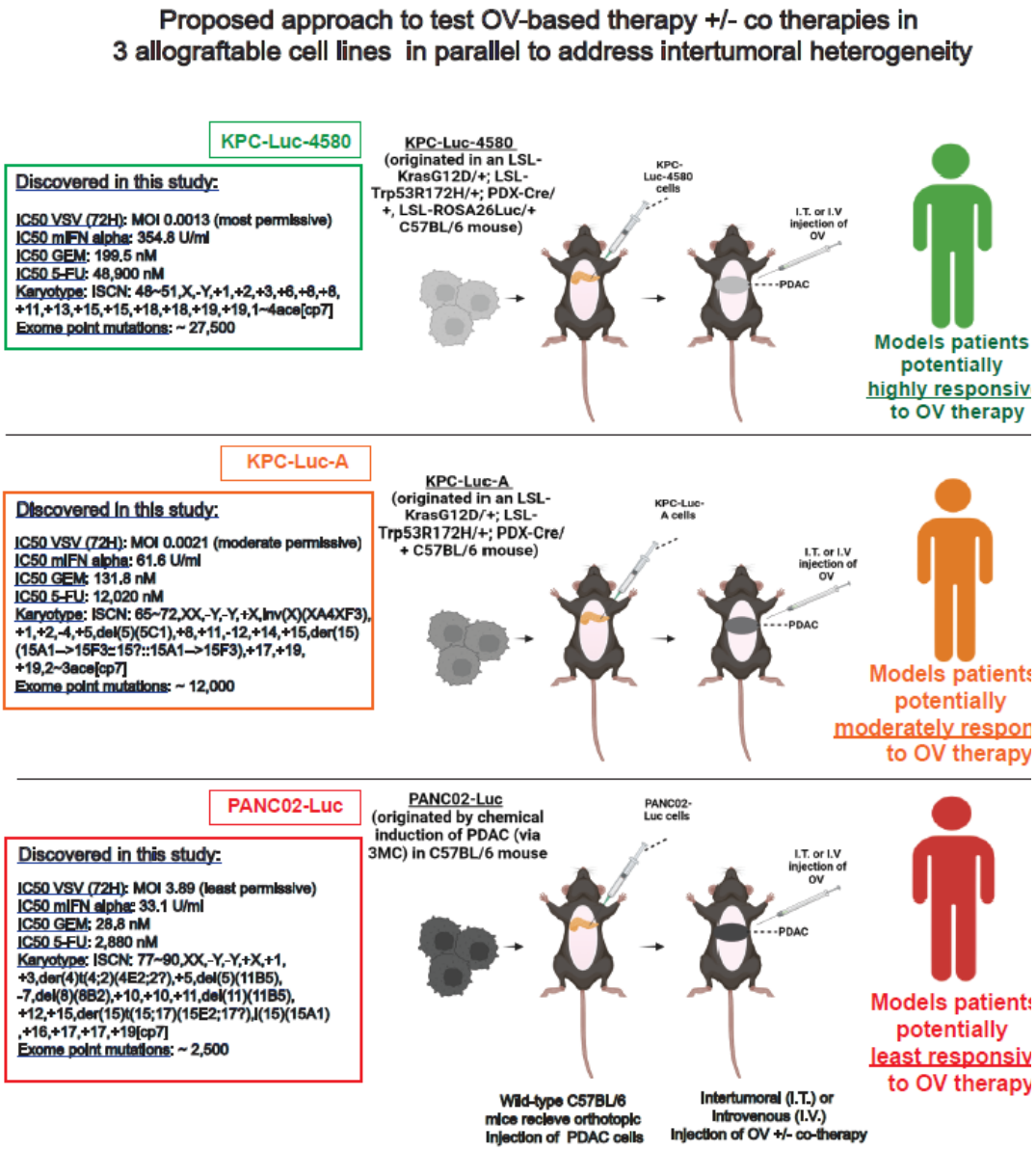

Figure 27. Proposed novel platform to study OV-based therapies against phenotypically different PDACs in immunocompetent mice. This model illustrates our proposed approach to test OV-based therapy +/- co therapies in 3 allograftable cell lines in parallel to address intertumoral heterogeneity. On the left shows data discovered in this study for each cell line. Cell lines are ordered from most permissive to VSV (top) to least permissive to VSV (bottom).

3.6 Tables

Table 4. Exome mutation in selected Type I IFN pathway genes

Gene	Cell line	Mutation type	Mutation
TYK2	KPC-Luc-4580	Missense	p.F516L
TYK2	KPC-Luc-4580	Missense	p.K382E
TYK2	KPC-Luc-4580	Missense	p.H261R
TYK2	KPC-Luc-A	Missense	p.F516L
TYK2	KPC-Luc-A	Missense	p.K382E
TYK2	KPC-Luc-A	Missense	p.H261R
STAT4	PANC02-Luc	Missense	p.S72F
OAS2	KPC-Luc-A	Missense	p.C118W
OAS2	PANC02-Luc	Missense	p.Q232R
OAS3	KPC-Luc-A	Missense	p.H897Q
OAS3	PANC02-Luc	Missense	p.L993R
IRF2	KPC-Luc-A	Missense	p.D295E
IFI203	KPC-Luc-A	Missense	p.R198Q
IFI203	KPC-Luc-A	Missense	p.I52M
IFI35	KPC-Luc-A	Missense	p.R108W
IFIH1	KPC-Luc-A	Missense	p.K647E
IFIH1	KPC-Luc-A	Missense	p.Q434H
IFIT1	PANC02-Luc	Missense	p.P51A
IFIT2	PANC02-Luc	Missense	p.R383H
TRIM21	KPC-Luc-A	Missense	p.E318K
USP18	KPC-Luc-A	Missense	p.V115L
ISG20	PANC02-Luc	Missense	p.A9P
JAK2	KPC-Luc-A	Missense	p.K575E
JAK2	KPC-Luc-4580	Missense	p.K575E
JAK3	KPC-Luc-A	Missense	p.G699C
JAK3	KPC-Luc-A	Missense	p.S1032R
JAK3	KPC-Luc-4580	Missense	p.G699C
JAK3	KPC-Luc-4580	Missense	p.S1032R
TLR9	KPC-Luc-A	Missense	p.T325N
TLR9	KPC-Luc-A	Missense	p.L378S
TLR9	KPC-Luc-A	Missense	p.T573A
TLR9	KPC-Luc-A	Missense	p.Q579H
TLR2	KPC-Luc-4580	Missense	p.M82I
TLR4	PANC02-Luc	Missense	p.Q42E
TLR4	PANC02-Luc	Missense	p.D462N
TLR5	KPC-Luc-A	Missense	p.R86Q
TLR5	KPC-Luc-A	Missense	p.G857A
TLR8	KPC-Luc-A	Missense	p.R578S

CHAPTER 4: DISSERTATION SUMMARY

Following a detailed introduction (Chapter 1), in Chapter 2, we investigated how chemoresistance in human PDAC cells impacted the efficacy of VSV-based OV-therapy. The increase in resistance to VSV correlated with upregulated levels of a subset of antiviral ISGs in each of the GR cell lines. There are several indications that the upregulation of these genes is a causative factor for resistance to viruses. First, the list of the upregulated ISGs includes many well-known antiviral genes, including MX1, MX2, IRF3, IFITM1, ISG15, RSAD2 (viperin), DHX58 (LGP2), IFIT1, IFITM3, IFI16, IFI44, and APOBEC3B. Second, GR cells not only became more resistant to VSV but also to SeV, suggesting a general virus restriction mechanism. Third, treatment of C and GR cells with a JAK1/JAK2 inhibitor ruxolitinib stimulated virus replication in GR cells but not C cells, suggesting a greater role of antiviral signaling in GR cells. These results are further supported by our previous study demonstrating specific downregulation of hundreds of ISGs by ruxolitinib in PDAC cells resistant to VSV (Hastie et al., 2016).

The role of Type I IFN signaling in cancer is multifaceted and has been comprehensively reviewed elsewhere (Arimoto et al., 2018; Chen et al., 2017; Musella et al., 2017; Zitvogel et al., 2015). The efficacy of many different therapeutic strategies against cancer, such as chemotherapy, radiotherapy, immunotherapies, and OV therapy, often depend on intact or at least partially active type I IFN signaling in cancer cells, for both direct (tumor cell inhibition) and indirect (antitumor immune response) effects (Zitvogel et al., 2015). However, despite the fact that type I IFN responses are generally considered antiproliferative, antiangiogenic, and proapoptotic, chronic inflammation and prolonged type I IFN stimulation can lead to chemoresistance, as detailed in the case of chronic viral infection (Snell et al., 2017). Intriguingly, an IFN-related DNA damage resistance signature (IRDS) was initially described by

Weichselbaum et al. across 34 different cancer cell lines, in which a subset of 36 ISGs were significantly upregulated and conferred resistance to both chemotherapy and radiotherapy (Weichselbaum, Ishwaran, Yoon, Nuyten, Baker, Khodarev, Su, Shaikh, Roach, Kreike, Roizman, Bergh, Pawitan, van de Vijver, et al., 2008). A similar expression signature consisting of 8 IRDS genes STAT1, IFI44, IFIT3, OAS1, IFIT1, ISG15, MX1, and USP18 predicted poor prognoses in glioblastoma patients' post-radiotherapy (Duarte et al., 2012). Other studies have demonstrated that the upregulation of STAT1 and other ISGs included in the IRDS signature are also upregulated in doxorubicin-resistant cells (Rickardson et al., 2005). Multiple studies implicate IRDS in the resistance to chemotherapy by the acquisition of stemness features which is understood to contribute to therapy resistance (Boelens et al., 2014; Cai et al., 2018; Prieto-Vila et al., 2017). Interestingly, our data show that many of the previously reported IRDS genes are also upregulated in GR cells. One of the ISGs identified in our study, IFITM1, has been shown previously to be not only involved in cellular defense against West Nile virus and Dengue virus (Brass et al., 2009), but is also involved in colorectal cancer progression (Andreu et al., 2006) and radioprotection (Kita et al., 2003).

Although the previous data support the notion that the IRDS is an inherent mechanism of resistance to chemotherapy and/or radiotherapy across a multitude of human cancers, it is still unclear how IRDS protects against radiotherapy and/or chemotherapy. Under normal circumstances, the type I IFN pathway sends a cytotoxic signal either in response to virus infection, DNA damage, or to IFNs. However, it has been speculated that the IRDS-positive cells demonstrate constitutive activation of the type I IFN pathway, which may reflect a history of chronic stimulation. This chronically stimulated state may select for the failure to transmit a cytotoxic signal and instead results in pro-survival signals mediated by STAT1 and other IRDS

genes (Weichselbaum, Ishwaran, Yoon, Nuyten, Baker, Khodarev, Su, Shaikh, Roach, Kreike, Roizman, Bergh, Pawitan, de Vijver, et al., 2008).

Our results clearly demonstrate an upregulation of antiviral ISGs in GR cells, and these results are consistent with the IRDS signature. However, the underlying mechanisms of this IRDS signature development in GR cells remain unclear. Here, we describe multiple possibilities that could have led to the observed IRDS signature in our GR cells.

The role of the STING pathway in promoting IFN-mediated resistance to chemotherapy has been previously demonstrated for breast cancer regrowth after chemotherapy and activation of the STING pathway in response to the chemotherapy (Gaston et al., 2016). Interestingly, many of the upregulated genes identified in that response to chemotherapy overlapped with IRDS. Moreover, STING silencing after chemotherapy re-sensitized the cancer cells to chemotherapy (Gaston et al., 2016). Therefore, the STING/IFN/STAT1 pathway may act as a cellular mechanism for cancer cell chemoresistance and survival after chemotherapy treatment. Our data are consistent with this hypothesis, as we observed increased STING expression in GR cells as early as 1 h p.i. and up to 32 h p.i.

The role of type I IFN signaling in treatment resistance may be due at least in part to the activation of signaling downstream of type I IFN, driven by unphosphorylated STAT1 and unphosphorylated ISGF3 activated upon continuing exposure, as genes upregulated by unphosphorylated STAT1 overlap with those in IRDS (Cheon & Stark, 2009). Our study shows greater unphosphorylated STAT1 expression after virus infection, and also after gemcitabine treatment.

Intriguingly, although we found a group of upregulated ISGs in uninfected GR cells, we did not observe any significant upregulation of type I, type II, or type III IFNs in these GR cells.

This suggests that the upregulation of ISGs in GR cells may occur independently of IFNs. One possible mechanism could be an IFN-independent, but STAT-dependent ISG expression in GR cells. Although we show greater STAT1 and STAT2 expression in GR cells after infection and treatment with gemcitabine, we do not observe differences in mRNA or protein expression in the absence of infection or treatment. However, as shown in Table 1, we see significant upregulation of STAT5A and STAT6 mRNA in GR cells in the absence of infection or treatment. STAT5a is activated by various cytokines and other factors including members of the IL-3 family (IL-3, IL-5 and GM-CSF), the IL-2 family (IL-2, IL-7, TSLP, IL-9, IL-15 and IL-21), growth hormone (GH), EPO (erythropoietin) and TPO (thrombopoietin) (Nan et al., 2018). Intriguingly, recent studies show that STAT5a is vital for the development of various cancers and also plays a role in chemoresistance in breast cancer (Li et al., 2021; Nan et al., 2018). STAT6 has been shown to also play a significant role in carcinogenesis and in the early development of colon cancer (Leon-Cabrera et al., 2017; Mendoza-Rodriguez et al., 2020). STAT6 function has also been related to cancer cell survival and drug resistance (Natoli et al., 2013). Moreover, it has been previously shown that STAT5a and STAT5b form a complex with CrkL, resulting in translocation to the nucleus and subsequent ISG gene transcription (Fish et al., 1999). Another previous study showed a probable role for STAT6 and ISG upregulation, as they reveal the formation of an ISGF3-like complex involving STAT6 (Gupta et al., 1999). Our future studies will examine the roles of STAT5a and STAT6 in the cross-resistance phenotype and upregulation of ISGs in GR cells.

Another possible mechanism for the IFN-independent upregulation of ISGs in GR cells could be via interferon regulatory factor 3 (IRF3), as it was shown recently for upregulation of multiple ISGs, including IFIT1, IFIT2, IFIT3, ISG15, CXCL10, MX1, and MX2, in the context of human

cytomegalovirus (HCMV) infection (Ashley et al., 2019). Indeed, another study using a tetracycline-induced expression system, demonstrated an IFN-independent, IRF3-dependent upregulation of ISGs IFIT2, IFIT3, ISG15, and RSAD2 (viperin) (Grandvaux et al., 2002). The same study demonstrated that IFIT1 upregulation can be induced directly by the expression of constitutively active IRF3. IRF3 may contribute to the upregulation of ISGs in GR cells, as our RNA-seq data reveals a significant upregulation of IRF3 in the absence of gemcitabine treatment or virus infection. However, further studies are needed to uncover the full role of IRF3.

Altogether, the cross-resistance phenotype to both chemotherapy and VSV is likely multifactorial, with no single gene or protein responsible, rather being the result of contributions from many of the aforementioned proteins. To examine this further in the future, studies need to be done by knocking out specific IRDS genes and potential upstream mediators one by one, as well as in combination, to help elucidate the importance of particular genes in this complex cross-resistant phenotype and to identify promising targets for future therapeutics. Similar studies as performed by Khodarev et al where they used shRNA to suppress STAT1, and that re-sensitized ionizing radiation (IR)-resistant squamous cell carcinoma cells to IR (Khodarev et al., 2007).

Although our study mainly focused on the potential role of the observed IRDS in GR cells, it should be noted that many additional PDAC mechanisms of resistance to gemcitabine have been described (Amrutkar & Gladhaug, 2017). Among the proteins shown to be important in resistance to gemcitabine are nucleotide transporters, deoxycytidine kinase, cytidine deaminases, ribonucleotide reductase, and thymidylate synthase. Each of these proteins act on some level to restrict gemcitabine entry and/or metabolism in the cell. Our RNA-seq analysis (Table 1) reveals

that some of these genes are differentially expressed in GR cells. It is possible that at least some of these genes are involved not only in gemcitabine resistance but also in VSV resistance.

Our study here, using an experimental evolution approach, demonstrated that the prolonged exposure to gemcitabine can lead to cross-resistance of PDAC cells to gemcitabine and oncolytic virotherapy. It is still clear if this observation can be applied to all (or most) other PDAC cell lines. To begin investigating this important question, we examined the relationship between chemoresistance and resistance to VSV-based OV therapy across a panel of ten human PDAC cell lines. Overall, we show that there is no statistically significant correlation between resistance to gemcitabine and resistance to VSV, and PDAC cell line AsPC-1, while being one of the most gemcitabine-resistant tested PDAC cell lines, was very permissive to VSV. On the other hand, 4 PDAC cell lines most resistant to VSV (HPAF-II, Hs766t, CFPAC-1, and HPAC) were also highly resistant to gemcitabine. Intriguingly, our previous studies demonstrated that HPAF-II, Hs766t, CFPAC-1, and HPAC were also the most resistant to VSV and displayed strong IRDS phenotypes (Cataldi et al., 2015; Hastie et al., 2016)·(Holbrook et al., 2021; Moerdyk-Schauwecker et al., 2013). The lack of simple correlation between resistance to gemcitabine and VSV is not surprising, as the resistance of different PDACs to chemotherapy can occur through alternative mechanisms (other than upregulation of ISGs/IRDS), and due to the different treatment histories of the patients from which the cells were initially cultured from. Overall, while most of our tested human PDAC cell lines show a correlation between resistance to chemotherapy and resistance to virus infection, there are clearly exceptions that need to be further explored. Importantly, while this study shows that chemoresistance enhances resistance to OV therapy, chemoresistance should not prevent effective OV therapy, and it should be noted that our OV treatment of GR cells was still quite effective. Rather, our study highlights a novel

interaction between two different therapies that should be considered in the future for the development of more rational and individualized treatment regimens, as well as for prescreening of patients.

In Chapter 3, we examined phenotypically and genotypically 3 commonly-used allograftable mouse PDAC cell lines: a widely used PANC02-Luc (derived from chemically induced PDAC), and two KPC cell lines originated from PDACs developed in different modified KPC mice encoding major driver mutations KrasG12D and Trp53R172H in the pancreas. We found that the three mouse PDAC cell lines were genotypically and phenotypically distinct and showed very different permissiveness to OV-based therapy, and, therefore, can serve as promising cell lines to use and address intertumoral heterogeneity *in vivo* in immunocompetent mice.

We found that each of the three mouse PDAC cell lines exhibited varying levels of permissiveness to VSV infection and VSV-mediated cell killing (Fig. 1-3). We also showed that the level of cellular permissiveness to VSV infection and VSV-mediated cell killing correlated with levels of type I IFN antiviral signaling (Fig. 4-7), including their abilities to activate STAT1 in response to VSV infection (Fig. 5). Another evidence demonstrating the differential levels of type I IFN antiviral signaling between the tested cell lines is highlighted by their sensitivity to added IFNα (Fig. 5). The mIFNα IC50 values for each cell line represent the relative ability of each cell line to respond to IFN. Consistent with data from Figure 8, between the three tested mouse cell lines, PANC02-Luc displayed the lowest mIFNα IC50 (33.1 U/mL), versus the highest IC50 in KPC-Luc-4580 cells (354.8 U/mL), and intermediate IC50 of 61.6 U/mL for KPC-Luc-A. This means that it takes almost 11 times the amount of mIFNα to bring KPC-Luc-4580 cells to the same level of type I IFN antiviral signaling as PANC02-Luc cells. We further highlight the differential levels of type I (and III) IFN antiviral signaling between these cell lines

in Figure 7, were we show the dramatic differences in secreted IFNβ and IFNγ after VSV infection. In order to investigate whether this correlation between the level of permissiveness to VSV infection with levels of type I IFN antiviral signaling was a causative one, we treated cells with two drugs known to potently inhibit major modulators of type I IFN antiviral signaling, ruxolitinib (JAK1/2 inhibitor) and TPCA-1 (JAK1 inhibitor) (Fig. 8). Our data reveal the relative level of intrinsic antiviral signaling potential in each cell line. For example, the inhibition of JAK1/2 in PANC02-Luc cells led to a greater difference of VSV replication compared to virus alone, versus the inhibition of JAK1/2 in KPC-Luc-4580 cells, which led to a relatively smaller difference in VSV replication compared to VSV alone.

Of the three tested mouse cell lines, PANC02-Luc exhibited the highest level of resistance to VSV. To speculate potential reasons why this cell line displays the highest levels of type I IFN antiviral signaling, we first look at how the cell line was generated. PANC02-Luc is a PDAC cell line isolated from a tumor generated chemically using a potent mutagen, 3-methyl-cholanthrene (3-MC) (Corbett et al., 1984). 3-MC is highly carcinogenic and has been used to induce cancer in rodents since the mid-1900s (Rhim, 1993). The use of 3-MC likely led to DNA damage and mutations in the pancreas (Stewart & Haski, 1984). In fact, a previous study showed that transformation of immortalized human uroepithelial cells by 3-methylcholanthrene increases IFN-stimulated genes (ISG) expression, including expression of well-known antiviral genes, such as 2'-5' OAS and MxA (Crosby et al., 2010). In general, there is a growing body of studies (Erdal et al., 2017; Padariya et al., 2021; Weichselbaum, Ishwaran, Yoon, Nuyten, Baker, Khodarev, Su, Shaikh, Roach, Kreike, Roizman, Bergh, Pawitan, van de Vijver, et al., 2008), including previous studies from our lab (Goad et al., 2022), suggesting that cancer cells may upregulate antiviral signaling pathways to confer protection against radiation therapy and

chemotherapy. The high degree of DNA damage caused by 3-MC in the pancreas may have led to an upregulation of antiviral signaling in PANC02-Luc cells. Consistent with this idea, we show evidence of higher DNA damage in PANC02-Luc cells in Figure 9, where the karyotype analysis reveals a highly aberrated, hyper-tetraploid genome.

Interestingly, while PANC02-Luc cells showed the greatest degree of chromosomal aberration, they exhibited the smallest number of whole exome mutations (Fig. 11 and Supplementary Fig. 1), as well as mutations in 2079 mouse genes known to be involved in the complex interplay between the tumor, microenvironment and immune response (Nanostring PanCancer Pathways, PanCancer Immune Profiling, and PanCancer IO 360) (Fig. 12, Supplementary Fig. 2, Supplementary Table 1). KPC-Luc-A contained the highest number of mutations, respectively, with both KPC cell lines harboring mutations in multiple important antiviral-associated genes, such as TYK2 and JAK2 (Table 1). These mutations in genes that encode for important antiviral signaling proteins may contribute to the higher permissiveness of KPC cells to VSV compared to PANC02-Luc cells.

Especially significant could be the lack of tumor-associated KRAS mutations in PANC02-Luc cells. Unlike PANC02-Luc cells, KPC-Luc-A and KPC-Luc-4580 cells were isolated from tumors which were formed spontaneously in GEMMs with the driver mutations KrasG12D and Trp53R172H. Higher permissiveness of KPC-Luc-A and KPC-Luc-4580 (compared to PANC02-Luc) to VSV could be also explained by the presence of KrasG12D driver mutation in these 2 KPC cell lines, while it is absent in PANC02-Luc (Wang et al., 2012). Several recent studies demonstrated that tumor-associated KRAS mutations, that result in abnormal activation of the RAS/Raf1/MEK/ERK pathway, results in multiple defects in the type I IFN signaling, thus making $KRAS^{MUT}$ cancer cells more permissive to VSV and other OVs (Battcock et al., 2006;

Christian et al., 2012; Deng et al., 2019; Noser et al., 2007; Yang & Ding, 2019). For example, Ras/MEK suppresses the basal expression levels of key components of type I IFN signaling pathway, hence leading to cellular impairment of IFN induced antiviral responses (Christian et al., 2009). Additionally, Ras/MEK regulates the activity of positive (IRF1 and Sp3) and negative (NF-κB) regulators of ISGF3 (Christian et al., 2012). Therefore, IFN-inducible genes that require up or down regulation of a co-regulator for their expression could be suppressed in cells with activated Ras/MEK. While our future studies will address this possibility experimentally, it is important to note that 90-95% of pancreatic cancers have a KRAS mutation (Waters & Der, 2018), which makes them intrinsically more permissive to VSV and other OVs via $KRAS^{MUT}$-mediated inhibition of antiviral signaling.

Interestingly, we found that KPC-Luc-A and KPC-Luc 4580 cell lines, even though isolated from PDAC tumors generated from cells that had the same driver mutations, exhibited differential responses to VSV infection. Multiple possible reasons for the differences in phenotypes and genotypes between KPC-Lu-A and KPC-Luc-4580 include: 1) different environmental factors selective pressures during tumor development in mice; 2) different selective pressures throughout cell culture adaptation, 3) random genetic changes. To our knowledge, the only difference in the original engineering design between KPC-Luc-A and KPC-Luc-4580 cells lines was the method by which each cell line was engineered to express luciferase (Fig 1A). In KPC-Luc-A mice, after PDAC cells were isolated from the tumor, the luciferase gene was incorporated into the genome via lentivirus transduction. However, the generation of KPC-Luc-4580 mice involved an additional cross with a ROSA26luc/+ mouse, leading to luciferase expression from the ROSA26 locus. A possible explanation for the differences between KPC cell lines could be that although parental mice had the same PDAC

driver mutations, subsequent alternative mutations likely developed. It is most likely that the reason for genetic differences between the KPC cell lines are in fact a combination of each of the factors mentioned above. Evidence for genomic differences between KPC cell lines is dramatically presented in Figure 10, where we show multiple different chromosomal aberrations between the KPC cell lines. Genomic differences are also highlighted at the exome level, where both KPC cell lines contain a far greater number of mutations in antiviral genes compared to PANC02-Luc cells (Fig. 11).

Whatever the reason for the phenotypic and genotypic differences between the tested KPC cell lines, these differences help contribute to their clinical translatability, as they likely better represent characteristic heterogeneity among and within PDAC patients.

As VSV-based OV therapy becomes a more commonly tested therapeutic option in clinical trials (Clinicaltrials.gov trials NCT01628640, NCT03120624, NCT04046445, NCT03865212, NCT03017820, NCT03647163), it is necessary to better understand how the effectiveness of VSV-based OV therapy is affected by the chemoresistance status of cancer cells. It has been observed in our previous studies and others (Erdal et al., 2017; Goad et al., 2022; Padariya et al., 2021; Weichselbaum, Ishwaran, Yoon, Nuyten, Baker, Khodarev, Su, Shaikh, Roach, Kreike, Roizman, Bergh, Pawitan, van de Vijver, et al., 2008) that the level of chemotherapeutic drug resistance may correlate with the level of antiviral signaling in cancer cells. This phenomenon is important to consider when determining the best therapeutic regimen for cancer patients. In this study, we hypothesized that the level of resistance to two commonly used chemotherapeutic drugs for PDAC, gemcitabine and 5-FU, would positively correlate with the level of resistance to VSV. Interestingly, we found that actually there was an inverse correlation between VSV resistance and drug resistance (Fig. 9), where the most resistant cell line to VSV (PANC02-Luc)

had the lowest IC50 for both gemcitabine and 5-FU, and the least resistant cell line to VSV (KPC-Luc-4580) had the highest IC50 for gemcitabine and 5-FU. These data suggest that even if PDAC in patients are inherently chemoresistant, VSV-based OV therapy remains a viable treatment option.

The ideal PDAC mouse model system should address both the intertumoral heterogeneity and the ability to detect and evaluate innate and adaptive immune responses against both tumor and OV. In Figure 13, we outline one such model based on our discoveries. We propose that multiple different mouse PDAC cell lines should be tested in parallel, ideally with each exhibiting varying levels of response to OV-therapy in order to better recapitulate tumor heterogeneity. KPC cell lines (as outlined in this study) are great candidates as they express luciferase (for tumor tracking), are C57BL/6 background (allowing for studies in wild-type immunocompetent mice), originated spontaneously in KPC mice via the same driver mutations as in human disease, and show different responses to OV-therapy and chemotherapeutics. While KPC cell lines contain the same driver mutations observed in ~85% of all PDAC (Luo, 2021), PANC02-Luc cells, which lack these mutations, are clinically relevant as they represent the small percent of PDACs without the classical Kras and P53 driver mutations. Figure 13 illustrates how we envision these cell lines could be used to address intertumoral heterogeneity to OVs +/- co-therapies. Each cell line represents either the most permissive to OV, moderately permissive to OV, and least permissive to OV. Importantly, novel OVs and co-therapies should be tested in parallel. The success of newly tested OVs and other co-therapies can be evaluated via a scoring system based on whether the therapy was successful in 0/3, 1/3, 2/3, or 3/3 tumor types. As illustrated in Figure 13, wild-type C57BL/6 mice should be used in order to study the role of the adaptive immune response. Additionally, although a challenging approach, tumor cells should be injected

orthotopically into the pancreas to allow investigations into the TME and metastasis. Our study provides essential data about 3 allograftable model mouse PDAC cell lines and proposes a novel platform to study OV-based therapies against phenotypically and genotypically distinct PDACs in immunocompetent mice. This study will be useful for ongoing and future studies in the field of PDAC therapeutics. Although this study focused on VSV as the oncolytic agent, alternative OVs can be tested using the model cell lines characterized in this study.

Altogether, my studies demonstrated that increased chemoresistance to gemcitabine leads to upregulation of a subset of ISGs, or IRDS, which is thought to 1) help protect cells from chemotherapy and 2) confer protection against VSV-based OV therapy. This information can be used in future studies to better understand how this upregulation of ISGs may help confer protection to cells against chemotherapy and can already be used to make better informed treatment decisions to PDAC patients. In addition, my studies have highlighted the importance of intertumoral heterogeneity in the context of a PDAC model system, and have detailed the ideal features of a PDAC mouse model system in order to best recapitulate human PDAC disease features. A clinically relevant PDAC model system is paramount to better investigate and understand this devasting disease.

REFERENCES

Agnandji, S. T., Huttner, A., Zinser, M. E., Njuguna, P., Dahlke, C., Fernandes, J. F., Yerly, S., Dayer, J. A., Kraehling, V., Kasonta, R., Adegnika, A. A., Altfeld, M., Auderset, F., Bache, E. B., Biedenkopf, N., Borregaard, S., Brosnahan, J. S., Burrow, R., Combescure, C., . . . Siegrist, C. A. (2016). Phase 1 Trials of rVSV Ebola Vaccine in Africa and Europe. *N Engl J Med*, *374*(17), 1647-1660. https://doi.org/10.1056/NEJMoa1502924

Ahmed, M., & Lyles, D. S. (1998). Effect of vesicular stomatitis virus matrix protein on transcription directed by host RNA polymerases I, II, and III. *J Virol*, *72*(10), 8413-8419. https://doi.org/10.1128/JVI.72.10.8413-8419.1998

Ahmed, M., McKenzie, M. O., Puckett, S., Hojnacki, M., Poliquin, L., & Lyles, D. S. (2003). Ability of the matrix protein of vesicular stomatitis virus to suppress beta interferon gene expression is genetically correlated with the inhibition of host RNA and protein synthesis. *Journal of Virology*, *77*(8), 4646-4657. https://doi.org/10.1128/Jvi.77.8.4646-4657.2003

Aksoy, P., Zhu, M. J., Kalari, K. R., Moon, I., Pelleymounter, L. L., Eckloff, B. W., Wieben, E. D., Yee, V. C., Weinshilboum, R. M., & Wang, L. (2009). Cytosolic 5'-nucleotidase III (NT5C3): gene sequence variation and functional genomics. *Pharmacogenet Genomics*, *19*(8), 567-576. https://doi.org/10.1097/FPC.0b013e32832c14b8

Amrutkar, M., & Gladhaug, I. P. (2017). Pancreatic Cancer Chemoresistance to Gemcitabine. *Cancers (Basel)*, *9*(11). https://doi.org/10.3390/cancers9110157

Andreu, P., Colnot, S., Godard, C., Laurent-Puig, P., Lamarque, D., Kahn, A., Perret, C., & Romagnolo, B. (2006). Identification of the IFITM family as a new molecular marker in human colorectal tumors. *Cancer Res*, *66*(4), 1949-1955. https://doi.org/10.1158/0008-5472.CAN-05-2731

Arimoto, K. I., Miyauchi, S., Stoner, S. A., Fan, J. B., & Zhang, D. E. (2018). Negative regulation of type I IFN signaling. *J Leukoc Biol*. https://doi.org/10.1002/JLB.2MIR0817-342R

Ashley, C. L., Abendroth, A., McSharry, B. P., & Slobedman, B. (2019). Interferon-Independent Upregulation of Interferon-Stimulated Genes during Human Cytomegalovirus Infection is Dependent on IRF3 Expression. *Viruses*, *11*(3). https://doi.org/10.3390/v11030246

Ball, L. A., Pringle, C. R., Flanagan, B., Perepelitsa, V. P., & Wertz, G. W. (1999). Phenotypic consequences of rearranging the P, M, and G genes of vesicular stomatitis virus. *J Virol*, *73*(6), 4705-4712. https://doi.org/10.1128/JVI.73.6.4705-4712.1999

Barr, J. N., & Wertz, G. W. (2001). Polymerase slippage at vesicular stomatitis virus gene junctions to generate poly(A) is regulated by the upstream 3 '-AUAC-5 ' tetranucleotide: Implications for the mechanism of transcription termination. *Journal of Virology*, *75*(15), 6901-6913. https://doi.org/Doi 10.1128/Jvi.75.15.6901-6913.2001

Barr, J. N., Whelan, S. P. J., & Wertz, G. W. (1997). cis-acting signals involved in termination of vesicular stomatitis virus mRNA synthesis include the conserved AUAC and the U7 signal for polyadenylation. *Journal of Virology*, *71*(11), 8718-8725. https://doi.org/Doi 10.1128/Jvi.71.11.8718-8725.1997

Battcock, S. M., Collier, T. W., Zu, D., & Hirasawa, K. (2006). Negative regulation of the alpha interferon-induced antiviral response by the Ras/Raf/MEK pathway. *J Virol*, *80*(9), 4422-4430. https://doi.org/10.1128/JVI.80.9.4422-4430.2006

Bergman, A. M., Giaccone, G., van Moorsel, C. J., Mauritz, R., Noordhuis, P., Pinedo, H. M., & Peters, G. J. (2000). Cross-resistance in the 2',2'-difluorodeoxycytidine (gemcitabine)-resistant human ovarian cancer cell line AG6000 to standard and investigational drugs. *Eur J Cancer*, *36*(15), 1974-1983. https://doi.org/10.1016/s0959-8049(00)00246-x

Bian, Z., Shi, L., Kidder, K., Zen, K., Garnett-Benson, C., & Liu, Y. (2021). Intratumoral SIRPalpha-deficient macrophages activate tumor antigen-specific cytotoxic T cells under radiotherapy. *Nat Commun*, *12*(1), 3229. https://doi.org/10.1038/s41467-021-23442-z

Black, B. L., Rhodes, R. B., McKenzie, M., & Lyles, D. S. (1993). The role of vesicular stomatitis virus matrix protein in inhibition of host-directed gene expression is genetically separable from its function in virus assembly. *J Virol*, *67*(8), 4814-4821. https://doi.org/10.1128/JVI.67.8.4814-4821.1993

Boelens, M. C., Wu, T. J., Nabet, B. Y., Xu, B., Qiu, Y., Yoon, T., Azzam, D. J., Twyman-Saint Victor, C., Wiemann, B. Z., Ishwaran, H., Ter Brugge, P. J., Jonkers, J., Slingerland, J., & Minn, A. J. (2014). Exosome transfer from stromal to breast cancer cells regulates therapy resistance pathways. *Cell*, *159*(3), 499-513. https://doi.org/10.1016/j.cell.2014.09.051

Brass, A. L., Huang, I. C., Benita, Y., John, S. P., Krishnan, M. N., Feeley, E. M., Ryan, B. J., Weyer, J. L., van der Weyden, L., Fikrig, E., Adams, D. J., Xavier, R. J., Farzan, M., & Elledge, S. J. (2009). The IFITM proteins mediate cellular resistance to influenza A H1N1 virus, West Nile virus, and dengue virus. *Cell*, *139*(7), 1243-1254. https://doi.org/10.1016/j.cell.2009.12.017

Bressy, C., Droby, G. N., Maldonado, B. D., Steuerwald, N., & Grdzelishvili, V. Z. (2019). Cell Cycle Arrest in G(2)/M Phase Enhances Replication of Interferon-Sensitive Cytoplasmic RNA Viruses via Inhibition of Antiviral Gene Expression. *Journal of Virology*, *93*(4). https://doi.org/ARTN e01885

10.1128/JVI.01885-18

Budhwani, M., Mazzieri, R., & Dolcetti, R. (2018). Plasticity of Type I Interferon-Mediated Responses in Cancer Therapy: From Anti-tumor Immunity to Resistance. *Front Oncol*, *8*, 322. https://doi.org/10.3389/fonc.2018.00322

Bulcha, J. T., Wang, Y., Ma, H., Tai, P. W. L., & Gao, G. P. (2021). Viral vector platforms within the gene therapy landscape. *Signal Transduction and Targeted Therapy*, *6*(1). https://doi.org/ARTN 53

10.1038/s41392-021-00487-6

Buscail, L., Bournet, B., & Cordelier, P. (2020). Role of oncogenic KRAS in the diagnosis, prognosis and treatment of pancreatic cancer. *Nat Rev Gastroenterol Hepatol*, *17*(3), 153-168. https://doi.org/10.1038/s41575-019-0245-4

Cai, Z., Cao, Y., Luo, Y., Hu, H., & Ling, H. (2018). Signalling mechanism(s) of epithelial-mesenchymal transition and cancer stem cells in tumour therapeutic resistance. *Clin Chim Acta*, *483*, 156-163. https://doi.org/10.1016/j.cca.2018.04.033

Carneiro, F. A., Lapido-Loureiro, P. A., Cordo, S. M., Stauffer, F., Weissmuller, G., Bianconi, M. L., Juliano, M. A., Juliano, L., Bisch, P. M., & Poian, A. T. D. (2006). Probing the interaction between vesicular stomatitis virus and phosphatidylserine. *European Biophysics Journal with Biophysics Letters*, *35*(2), 145-154. https://doi.org/10.1007/s00249-005-0012-z

Cary, Z. D., Willingham, M. C., & Lyles, D. S. (2011). Oncolytic Vesicular Stomatitis Virus Induces Apoptosis in U87 Glioblastoma Cells by a Type II Death Receptor Mechanism and Induces Cell Death and Tumor Clearance In Vivo ▿ . In *J Virol* (Vol. 85, pp. 5708-5717). https://doi.org/10.1128/jvi.02393-10

Cataldi, M., Shah, N. R., Felt, S. A., & Grdzelishvili, V. Z. (2015). Breaking resistance of pancreatic cancer cells to an attenuated vesicular stomatitis virus through a novel activity of IKK inhibitor TPCA-1. *Virology*, *485*, 340-354. https://doi.org/10.1016/j.virol.2015.08.003

Chen, K., Liu, J., & Cao, X. (2017). Regulation of type I interferon signaling in immunity and inflammation: A comprehensive review. *J Autoimmun*, *83*, 1-11. https://doi.org/10.1016/j.jaut.2017.03.008

Chen, W. H., Horoszewicz, J. S., Leong, S. S., Shimano, T., Penetrante, R., Sanders, W. H., Berjian, R., Douglass, H. O., Martin, E. W., & Chu, T. M. (1982). Human pancreatic adenocarcinoma: in vitro and in vivo morphology of a new tumor line established from ascites. *In Vitro*, *18*(1), 24-34. https://doi.org/10.1007/BF02796382

Cheon, H., & Stark, G. R. (2009). Unphosphorylated STAT1 prolongs the expression of interferon-induced immune regulatory genes. *Proc Natl Acad Sci U S A*, *106*(23), 9373-9378. https://doi.org/10.1073/pnas.0903487106

Christian Bressy, G. N. D., Bryant D. Maldonado, Nury Steuerwald, Valery Z. Grdzelishvili. (2018). Cell cycle arrest in G2/M phase enhances replication of interferon-sensitive cytoplasmic RNA viruses via inhibition of antiviral gene expression. *Journal of Virology*. https://doi.org/doi:10.1128/JVI.01885-18

Christian, S. L., Collier, T. W., Zu, D., Licursi, M., Hough, C. M., & Hirasawa, K. (2009). Activated Ras/MEK inhibits the antiviral response of alpha interferon by reducing STAT2 levels. *J Virol*, *83*(13), 6717-6726. https://doi.org/10.1128/JVI.02213-08

Christian, S. L., Zu, D., Licursi, M., Komatsu, Y., Pongnopparat, T., Codner, D. A., & Hirasawa, K. (2012). Suppression of IFN-induced transcription underlies IFN defects generated by activated Ras/MEK in human cancer cells. *PLoS One*, *7*(9), e44267. https://doi.org/10.1371/journal.pone.0044267

Connor, J. H., & Lyles, D. S. (2002). Vesicular stomatitis virus infection alters the eIF4F translation initiation complex and causes dephosphorylation of the eIF4E binding protein 4E-BP1. *J Virol*, *76*(20), 10177-10187. https://doi.org/10.1128/jvi.76.20.10177-10187.2002

Corbett, T. H., Roberts, B. J., Leopold, W. R., Peckham, J. C., Wilkoff, L. J., Griswold, D. P., Jr., & Schabel, F. M., Jr. (1984). Induction and chemotherapeutic response of two transplantable ductal adenocarcinomas of the pancreas in C57BL/6 mice. *Cancer Res*, *44*(2), 717-726. https://www.ncbi.nlm.nih.gov/pubmed/6692374

Crosby, L. M., Moore, T. M., George, M., Yoon, L. W., Easton, M. J., Ni, H., Morgan, K. T., & DeAngelo, A. B. (2010). Transformation of SV40-immortalized human uroepithelial cells by 3-methylcholanthrene increases IFN- and Large T Antigen-induced transcripts. *Cancer Cell Int*, *10*, 4. https://doi.org/10.1186/1475-2867-10-4

Cureton, D. K., Massol, R. H., Whelan, S. P., & Kirchhausen, T. (2010). The length of vesicular stomatitis virus particles dictates a need for actin assembly during clathrin-dependent endocytosis. *PLoS Pathog*, *6*(9), e1001127. https://doi.org/10.1371/journal.ppat.1001127

Dalbeth, N., Lauterio, T. J., & Wolfe, H. R. (2014). Mechanism of action of colchicine in the treatment of gout. *Clin Ther*, *36*(10), 1465-1479. https://doi.org/10.1016/j.clinthera.2014.07.017

Das, M., Shen, L., Liu, Q., Goodwin, T. J., & Huang, L. (2019). Nanoparticle Delivery of RIG-I Agonist Enables Effective and Safe Adjuvant Therapy in Pancreatic Cancer. *Mol Ther*, *27*(3), 507-517. https://doi.org/10.1016/j.ymthe.2018.11.012

Das, S. C., Nayak, D., Zhou, Y., & Pattnaik, A. K. (2006). Visualization of intracellular transport of vesicular stomatitis virus nucleocapsids in living cells. *J Virol*, *80*(13), 6368-6377. https://doi.org/10.1128/JVI.00211-06

Davis, N. L., Arnheiter, H., & Wertz, G. W. (1986). Vesicular Stomatitis Virus-N and Ns Proteins Form Multiple Complexes. *Journal of Virology*, *59*(3), 751-754. https://doi.org/Doi 10.1128/Jvi.59.3.751-754.1986

Deer, E. L., Gonzalez-Hernandez, J., Coursen, J. D., Shea, J. E., Ngatia, J., Scaife, C. L., Firpo, M. A., & Mulvihill, S. J. (2010). Phenotype and genotype of pancreatic cancer cell lines. *Pancreas*, *39*(4), 425-435. https://doi.org/10.1097/MPA.0b013e3181c15963

Deng, H., Liu, H., de Silva, T., Xue, Y., Mohamud, Y., Ng, C. S., Qu, J., Zhang, J., Jia, W. W. G., Lockwood, W. W., & Luo, H. (2019). Coxsackievirus Type B3 Is a Potent Oncolytic Virus against KRAS-Mutant Lung Adenocarcinoma. *Mol Ther Oncolytics*, *14*, 266-278. https://doi.org/10.1016/j.omto.2019.07.003

Dobrynin, Y. V. (1963). Establishment and Characteristics of Cell Strains from Some Epithelial Tumors of Human Origin. *Journal of the National Cancer Institute*, *31*(5), 1173-&. <Go to ISI>://WOS:A19635935B00001

Dock, G. (1904). The influence of complicating diseases upon leukaemia. *The American Journal of the Medical Sciences*, *127*(4).

Donina, S., Strele, I., Proboka, G., Auzins, J., Alberts, P., Jonsson, B., Venskus, D., & Muceniece, A. (2015). Adapted ECHO-7 virus Rigvir immunotherapy (oncolytic virotherapy) prolongs survival in melanoma patients after surgical excision of the tumour in a retrospective study. *Melanoma Research*, *25*(5), 421-426. https://doi.org/10.1097/Cmr.0000000000000180

Duarte, C. W., Willey, C. D., Zhi, D., Cui, X., Harris, J. J., Vaughan, L. K., Mehta, T., McCubrey, R. O., Khodarev, N. N., Weichselbaum, R. R., & Gillespie, G. Y. (2012). Expression signature of IFN/STAT1 signaling genes predicts poor survival outcome in glioblastoma multiforme in a subtype-specific manner. *PLoS One*, *7*(1), e29653. https://doi.org/10.1371/journal.pone.0029653

Emerson, S. U. (1982). Reconstitution studies detect a single polymerase entry site on the vesicular stomatitis virus genome. *Cell*, *31*(3 Pt 2), 635-642. https://doi.org/10.1016/0092-8674(82)90319-1

Engeland, C. E., & Bell, J. C. (2020). Introduction to Oncolytic Virotherapy. *Methods Mol Biol*, *2058*, 1-6. https://doi.org/10.1007/978-1-4939-9794-7_1

Erdal, E., Haider, S., Rehwinkel, J., Harris, A. L., & McHugh, P. J. (2017). A prosurvival DNA damage-induced cytoplasmic interferon response is mediated by end resection factors and is limited by Trex1. *Genes Dev*, *31*(4), 353-369. https://doi.org/10.1101/gad.289769.116

Eric Hastie, D. M. B., Nirav R. Shah, Andrea M. Murphy, Megan Moerdyk-Schauwecker, Carlos Molestina, Lopamudra Das Roy, Jennifer M. Curry, Pinku Mukherjee, Valery Z. Grdzelishvili. (2013). Oncolytic Vesicular Stomatitis Virus in an Immunocompetent Model of MUC1-Positive or MUC1-Null Pancreatic Ductal Adenocarcinoma. *Journal of Virology*, *87*(18), 10283-10294. https://doi.org/DOI: 10.1128/JVI.01412-13

Erstad, D. J., Sojoodi, M., Taylor, M. S., Ghoshal, S., Razavi, A. A., Graham-O'Regan, K. A., Bardeesy, N., Ferrone, C. R., Lanuti, M., Caravan, P., Tanabe, K. K., & Fuchs, B. C. (2018). Orthotopic and heterotopic murine models of pancreatic cancer and their different responses to FOLFIRINOX chemotherapy. *Dis Model Mech*, *11*(7). https://doi.org/10.1242/dmm.034793

Fathi, A., Dahlke, C., & Addo, M. M. (2019). Recombinant vesicular stomatitis virus vector vaccines for WHO blueprint priority pathogens. *Hum Vaccin Immunother*, *15*(10), 2269-2285. https://doi.org/10.1080/21645515.2019.1649532

Felt, S. A., Droby, G. N., & Grdzelishvili, V. Z. (2017). Ruxolitinib and Polycation Combination Treatment Overcomes Multiple Mechanisms of Resistance of Pancreatic Cancer Cells to Oncolytic Vesicular Stomatitis Virus. *J Virol*, *91*(16). https://doi.org/10.1128/JVI.00461-17

Felt, S. A., & Grdzelishvili, V. Z. (2017). Recent advances in vesicular stomatitis virus-based oncolytic virotherapy: a 5-year update. *J Gen Virol*, *98*(12), 2895-2911. https://doi.org/10.1099/jgv.0.000980

Felt, S. A., Moerdyk-Schauwecker, M. J., & Grdzelishvili, V. Z. (2015). Induction of apoptosis in pancreatic cancer cells by vesicular stomatitis virus. *Virology*, *474*, 163-173. https://doi.org/10.1016/j.virol.2014.10.026

Finkelshtein, D., Werman, A., Novick, D., Barak, S., & Rubinstein, M. (2013). LDL receptor and its family members serve as the cellular receptors for vesicular stomatitis virus. *Proceedings of the National Academy of Sciences of the United States of America*, *110*(18), 7306-7311. https://doi.org/10.1073/pnas.1214441110

Fish, E. N., Uddin, S., Korkmaz, M., Majchrzak, B., Druker, B. J., & Platanias, L. C. (1999). Activation of a CrkL-stat5 signaling complex by type I interferons. *J Biol Chem*, *274*(2), 571-573. https://doi.org/10.1074/jbc.274.2.571

Flood, E. A., McKenzie, M. O., & Lyles, D. S. (2000). Role of M protein aggregation in defective assembly of temperature-sensitive M protein mutants of vesicular stomatitis virus. *Virology*, *278*(2), 520-533. https://doi.org/10.1006/viro.2000.0675

Froeling, F. E., Marshall, J. F., & Kocher, H. M. (2010). Pancreatic cancer organotypic cultures. *J Biotechnol*, *148*(1), 16-23. https://doi.org/10.1016/j.jbiotec.2010.01.008

Gaddy, D. F., & Lyles, D. S. (2005). Vesicular Stomatitis Viruses Expressing Wild-Type or Mutant M Proteins Activate Apoptosis through Distinct Pathways. In *J Virol* (Vol. 79, pp. 4170-4179). https://doi.org/10.1128/jvi.79.7.4170-4179.2005

Gandhi, V., Legha, J., Chen, F., Hertel, L. W., & Plunkett, W. (1996). Excision of 2',2'-difluorodeoxycytidine (gemcitabine) monophosphate residues from DNA. *Cancer Res*, *56*(19), 4453-4459. https://www.ncbi.nlm.nih.gov/pubmed/8813140

Garber, K. (2006). China approves world's first oncolytic virus therapy for cancer treatment. *Journal of the National Cancer Institute*, *98*(5), 298-300. https://doi.org/10.1093/jnci/djj111

Gaston, J., Cheradame, L., Yvonnet, V., Deas, O., Poupon, M. F., Judde, J. G., Cairo, S., & Goffin, V. (2016). Intracellular STING inactivation sensitizes breast cancer cells to genotoxic agents. *Oncotarget*, *7*(47), 77205-77224. https://doi.org/10.18632/oncotarget.12858

Gilabert, M., Calvo, E., Airoldi, A., Hamidi, T., Moutardier, V., Turrini, O., & Iovanna, J. (2014). Pancreatic Cancer-Induced Cachexia Is Jak2-Dependent in Mice. *Journal of Cellular Physiology*, *229*(10), 1437-1443. https://doi.org/10.1002/jcp.24580

Gillet, J. P., Varma, S., & Gottesman, M. M. (2013). The clinical relevance of cancer cell lines. *J Natl Cancer Inst*, *105*(7), 452-458. https://doi.org/10.1093/jnci/djt007

Goad, D. W., Bressy, C., Holbrook, M. C., & Grdzelishvili, V. Z. (2022). Acquired chemoresistance can lead to increased resistance of pancreatic cancer cells to oncolytic vesicular stomatitis virus. *Mol Ther Oncolytics*, *24*, 59-76. https://doi.org/10.1016/j.omto.2021.11.019

Gower, W. R., Jr., Risch, R. M., Godellas, C. V., & Fabri, P. J. (1994). HPAC, a new human glucocorticoid-sensitive pancreatic ductal adenocarcinoma cell line. *In Vitro Cell Dev Biol Anim*, *30A*(3), 151-161. https://doi.org/10.1007/BF02631438

Grandvaux, N., Servant, M. J., tenOever, B., Sen, G. C., Balachandran, S., Barber, G. N., Lin, R., & Hiscott, J. (2002). Transcriptional profiling of interferon regulatory factor 3 target

genes: direct involvement in the regulation of interferon-stimulated genes. *J Virol*, *76*(11), 5532-5539. https://doi.org/10.1128/jvi.76.11.5532-5539.2002

Guibinga, G. H., Miyanohara, A., Esko, J. D., & Friedmann, T. (2002). Cell surface heparan sulfate is a receptor for attachment of envelope protein-free retrovirus-like particles and VSV-G pseudotyped MLV-derived retrovirus vectors to target cells. *Molecular Therapy*, *5*(5), 538-546. https://doi.org/DOI 10.1006/mthe.2002.0578

Gupta, S., Jiang, M., & Pernis, A. B. (1999). IFN-alpha activates Stat6 and leads to the formation of Stat2:Stat6 complexes in B cells. *J Immunol*, *163*(7), 3834-3841. https://www.ncbi.nlm.nih.gov/pubmed/10490982

Hamacher, R., Schmid, R. M., Saur, D., & Schneider, G. (2008). Apoptotic pathways in pancreatic ductal adenocarcinoma. In *Mol Cancer* (Vol. 7, pp. 64). https://doi.org/10.1186/1476-4598-7-64

Hastie, E., Cataldi, M., Marriott, I., & Grdzelishvili, V. Z. (2013). Understanding and altering cell tropism of vesicular stomatitis virus. *Virus Research*, *176*(1-2), 16-32. https://doi.org/10.1016/j.virusres.2013.06.003

Hastie, E., Cataldi, M., Moerdyk-Schauwecker, M. J., Felt, S. A., Steuerwald, N., & Grdzelishvili, V. Z. (2016). Novel biomarkers of resistance of pancreatic cancer cells to oncolytic vesicular stomatitis virus. *Oncotarget*, *7*(38), 61601-61618. https://doi.org/10.18632/oncotarget.11202

Hastie, E., Cataldi, M., Steuerwald, N., & Grdzelishvili, V. Z. (2015). An unexpected inhibition of antiviral signaling by virus-encoded tumor suppressor p53 in pancreatic cancer cells. *Virology*, *483*, 126-140. https://doi.org/10.1016/j.virol.2015.04.017

Hastie, E., & Grdzelishvili, V. Z. (2012). Vesicular stomatitis virus as a flexible platform for oncolytic virotherapy against cancer. *Journal of General Virology*, *93*, 2529-2545. https://doi.org/10.1099/vir.0.046672-0

He, M., Henderson, M., Muth, S., Murphy, A., & Zheng, L. (2020). Preclinical mouse models for immunotherapeutic and non-immunotherapeutic drug development for pancreatic ductal adenocarcinoma. *Ann Pancreat Cancer*, *3*. https://doi.org/10.21037/apc.2020.03.03

Henao-Restrepo, A. M., Camacho, A., Longini, I. M., Watson, C. H., Edmunds, W. J., Egger, M., Carroll, M. W., Dean, N. E., Diatta, I., Doumbia, M., Draguez, B., Duraffour, S., Enwere, G., Grais, R., Gunther, S., Gsell, P. S., Hossmann, S., Watle, S. V., Konde, M. K., . . . Kieny, M. P. (2017). Efficacy and effectiveness of an rVSV-vectored vaccine in preventing Ebola virus disease: final results from the Guinea ring vaccination, open-label, cluster-randomised trial (Ebola Ca Suffit!). *Lancet*, *389*(10068), 505-518. https://doi.org/10.1016/S0140-6736(16)32621-6

Henao-Restrepo, A. M., Longini, I. M., Egger, M., Dean, N. E., Edmunds, W. J., Camacho, A., Carroll, M. W., Doumbia, M., Draguez, B., Duraffour, S., Enwere, G., Grais, R., Gunther, S., Hossmann, S., Konde, M. K., Kone, S., Kuisma, E., Levine, M. M., Mandal, S., . . . Rottingen, J. A. (2015). Efficacy and effectiveness of an rVSV-vectored vaccine expressing Ebola surface glycoprotein: interim results from the Guinea ring vaccination cluster-randomised trial. *Lancet*, *386*(9996), 857-866. https://doi.org/10.1016/S0140-6736(15)61117-5

Her, L. S., Lund, E., & Dahlberg, J. E. (1997). Inhibition of Ran guanosine triphosphatase-dependent nuclear transport by the matrix protein of vesicular stomatitis virus. *Science*, *276*(5320), 1845-1848. https://doi.org/DOI 10.1126/science.276.5320.1845

Hingorani, S. R., Wang, L., Multani, A. S., Combs, C., Deramaudt, T. B., Hruban, R. H., Rustgi, A. K., Chang, S., & Tuveson, D. A. (2005). Trp53R172H and KrasG12D cooperate to promote chromosomal instability and widely metastatic pancreatic ductal adenocarcinoma in mice. *Cancer Cell*, *7*(5), 469-483. https://doi.org/10.1016/j.ccr.2005.04.023

Holbrook, M. C., Goad, D. W., & Grdzelishvili, V. Z. (2021). Expanding the Spectrum of Pancreatic Cancers Responsive to Vesicular Stomatitis Virus-Based Oncolytic Virotherapy: Challenges and Solutions. *Cancers (Basel)*, *13*(5). https://doi.org/10.3390/cancers13051171

Huang, P., Chubb, S., Hertel, L. W., Grindey, G. B., & Plunkett, W. (1991). Action of 2',2'-difluorodeoxycytidine on DNA synthesis. *Cancer Res*, *51*(22), 6110-6117. https://www.ncbi.nlm.nih.gov/pubmed/1718594

Iverson, L. E., & Rose, J. K. (1981). Localized Attenuation and Discontinuous Synthesis during Vesicular Stomatitis-Virus Transcription. *Cell*, *23*(2), 477-484. https://doi.org/Doi 10.1016/0092-8674(81)90143-4

Iwamura, T., Katsuki, T., & Ide, K. (1987). Establishment and Characterization of a Human Pancreatic-Cancer Cell-Line (Suit-2) Producing Carcinoembryonic Antigen and Carbohydrate Antigen-19-9. *Japanese Journal of Cancer Research*, *78*(1), 54-62. <Go to ISI>://WOS:A1987G320700009

Jayakar, H. R., Murti, K. G., & Whitt, M. A. (2000). Mutations in the PPPY motif of vesicular stomatitis virus matrix protein reduce virus budding by inhibiting a late step in virion release. *J Virol*, *74*(21), 9818-9827. https://doi.org/10.1128/jvi.74.21.9818-9827.2000

Jazowiecka-Rakus, J., Sochanik, A., Hadrys, A., Fidyk, W., Chmielik, E., Rahman, M. M., & McFadden, G. (2022). Combination of LIGHT (TNFSF14)-Armed Myxoma Virus Pre-Loaded into ADSCs and Gemcitabine in the Treatment of Experimental Orthotopic

Murine Pancreatic Adenocarcinoma. *Cancers (Basel)*, *14*(8). https://doi.org/10.3390/cancers14082022

Jones, S. M., Feldmann, H., Stroher, U., Geisbert, J. B., Fernando, L., Grolla, A., Klenk, H. D., Sullivan, N. J., Volchkov, V. E., Fritz, E. A., Daddario, K. M., Hensley, L. E., Jahrling, P. B., & Geisbert, T. W. (2005). Live attenuated recombinant vaccine protects nonhuman primates against Ebola and Marburg viruses. *Nature Medicine*, *11*(7), 786-790. https://doi.org/10.1038/nm1258

Jordan, M. A., & Wilson, L. (2004). Microtubules as a target for anticancer drugs. *Nature Reviews Cancer*, *4*(4), 253-265. https://doi.org/10.1038/nrc1317

Katz, J. B., Eernisse, K. A., Landgraf, J. G., & Schmitt, B. J. (1997). Comparative performance of four serodiagnostic procedures for detecting bovine and equine vesicular stomatitis virus antibodies. *J Vet Diagn Invest*, *9*(3), 329-331. https://doi.org/10.1177/104063879700900321

Khodarev, N. N., Minn, A. J., Efimova, E. V., Darga, T. E., Labay, E., Beckett, M., Mauceri, H. J., Roizman, B., & Weichselbaum, R. R. (2007). Signal transducer and activator of transcription 1 regulates both cytotoxic and prosurvival functions in tumor cells. *Cancer Res*, *67*(19), 9214-9220. https://doi.org/10.1158/0008-5472.CAN-07-1019

Kita, K., Sugaya, S., Zhai, L., Wu, Y. P., Wano, C., Chigira, S., Nomura, J., Takahashi, S., Ichinose, M., & Suzuki, N. (2003). Involvement of LEU13 in interferon-induced refractoriness of human RSa cells to cell killing by X rays. *Radiat Res*, *160*(3), 302-308. https://doi.org/10.1667/rr3039

Knipe, D. M., Baltimore, D., & Lodish, H. F. (1977). Separate Pathways of Maturation of Major Structural Proteins of Vesicular Stomatitis-Virus. *Journal of Virology*, *21*(3), 1128-1139. https://doi.org/Doi 10.1128/Jvi.21.3.1128-1139.1977

Kong, K. W., Guo, M., Liu, Y. F., & Zheng, J. M. (2020). Progress in Animal Models of Pancreatic Ductal Adenocarcinoma. *Journal of Cancer*, *11*(6), 1555-1567. https://doi.org/10.7150/jca.37529

Kyriazis, A. A., Kyriazis, A. P., Sternberg, C. N., Sloane, N. H., & Loveless, J. D. (1986). Morphological, biological, biochemical, and karyotypic characteristics of human pancreatic ductal adenocarcinoma Capan-2 in tissue culture and the nude mouse. *Cancer Res*, *46*(11), 5810-5815. https://www.ncbi.nlm.nih.gov/pubmed/3019537

Kyriazis, A. P., Kyriazis, A. A., Scarpelli, D. G., Fogh, J., Rao, M. S., & Lepera, R. (1982). Human pancreatic adenocarcinoma line Capan-1 in tissue culture and the nude mouse: morphologic, biologic, and biochemical characteristics. *Am J Pathol*, *106*(2), 250-260. https://www.ncbi.nlm.nih.gov/pubmed/6278935

Lee, J. W., Komar, C. A., Bengsch, F., Graham, K., & Beatty, G. L. (2016). Genetically Engineered Mouse Models of Pancreatic Cancer: The KPC Model (LSL-Kras(G12D/+) ;LSL-Trp53(R172H/+) ;Pdx-1-Cre), Its Variants, and Their Application in Immuno-oncology Drug Discovery. *Curr Protoc Pharmacol*, *73*, 14 39 11-14 39 20. https://doi.org/10.1002/cpph.2

Leon-Cabrera, S. A., Molina-Guzman, E., Delgado-Ramirez, Y. G., Vazquez-Sandoval, A., Ledesma-Soto, Y., Perez-Plasencia, C. G., Chirino, Y. I., Delgado-Buenrostro, N. L., Rodriguez-Sosa, M., Vaca-Paniagua, F., Avila-Moreno, F., Gutierrez-Cirlos, E. B., Arias-Romero, L. E., & Terrazas, L. I. (2017). Lack of STAT6 Attenuates Inflammation and Drives Protection against Early Steps of Colitis-Associated Colon Cancer. *Cancer Immunology Research*, *5*(5), 385-396. https://doi.org/10.1158/2326-6066.Cir-16-0168

Li, Z., Chen, C., Chen, L., Hu, D., Yang, X., Zhuo, W., Chen, Y., Yang, J., Zhou, Y., Mao, M., Zhang, X., Xu, L., Ju, S., Shen, J., Wang, Q., Dong, M., Xie, S., Wei, Q., Jia, Y., . . . Wang, L. (2021). STAT5a Confers Doxorubicin Resistance to Breast Cancer by Regulating ABCB1. *Front Oncol*, *11*, 697950. https://doi.org/10.3389/fonc.2021.697950

Lichty, B. D., Power, A. T., Stojdl, D. F., & Bell, J. C. (2004). Vesicular stomatitis virus: re-inventing the bullet. *Trends Mol Med*, *10*(5), 210-216. https://doi.org/10.1016/j.molmed.2004.03.003

Little, E. C., Wang, C., Watson, P. M., Watson, D. K., Cole, D. J., & Camp, E. R. (2012). Novel immunocompetent murine models representing advanced local and metastatic pancreatic cancer. *J Surg Res*, *176*(2), 359-366. https://doi.org/10.1016/j.jss.2011.10.025

Liu, G., Cao, W., Salawudeen, A., Zhu, W., Emeterio, K., Safronetz, D., & Banadyga, L. (2021). Vesicular Stomatitis Virus: From Agricultural Pathogen to Vaccine Vector. *Pathogens*, *10*(9). https://doi.org/10.3390/pathogens10091092

Longley, D. B., Harkin, D. P., & Johnston, P. G. (2003). 5-fluorouracil: mechanisms of action and clinical strategies. *Nat Rev Cancer*, *3*(5), 330-338. https://doi.org/10.1038/nrc1074

Lowery, M. A., & O'Reilly, E. M. (2015). Novel Therapeutics for Pancreatic Adenocarcinoma. *Hematol Oncol Clin North Am*, *29*(4), 777-787. https://doi.org/10.1016/j.hoc.2015.04.006

Luo, J. (2021). KRAS mutation in pancreatic cancer. *Semin Oncol*, *48*(1), 10-18. https://doi.org/10.1053/j.seminoncol.2021.02.003

Lyles, D. S. (2000). Cytopathogenesis and inhibition of host gene expression by RNA viruses. *Microbiol Mol Biol Rev*, *64*(4), 709-724. https://doi.org/10.1128/MMBR.64.4.709-724.2000

Lyles DS, R., CE. (2007). Rhabdoviridae. In *Fields Virology* (5th ed., pp. 1363-1408). Lippincott Williams & Wilkins.

Mackey, J. R., Mani, R. S., Selner, M., Mowles, D., Young, J. D., Belt, J. A., Crawford, C. R., & Cass, C. E. (1998). Functional nucleoside transporters are required for gemcitabine influx and manifestation of toxicity in cancer cell lines. *Cancer Res*, *58*(19), 4349-4357. https://www.ncbi.nlm.nih.gov/pubmed/9766663

Manuel, E. R., Chen, J., D'Apuzzo, M., Lampa, M. G., Kaltcheva, T. I., Thompson, C. B., Ludwig, T., Chung, V., & Diamond, D. J. (2015). Salmonella-Based Therapy Targeting Indoleamine 2,3-Dioxygenase Coupled with Enzymatic Depletion of Tumor Hyaluronan Induces Complete Regression of Aggressive Pancreatic Tumors. *Cancer Immunol Res*, *3*(9), 1096-1107. https://doi.org/10.1158/2326-6066.CIR-14-0214

Masters, P. S., & Banerjee, A. K. (1988). Resolution of Multiple Complexes of Phosphoprotein Ns with Nucleocapsid Protein-N of Vesicular Stomatitis-Virus. *Journal of Virology*, *62*(8), 2651-2657. https://doi.org/Doi 10.1128/Jvi.62.8.2651-2657.1988

Mavrakis, M., Iseni, F., Mazza, C., Schoehn, G., Ebel, C., Gentzel, M., Franz, T., & Ruigrok, R. W. H. (2003). Isolation and characterisation of the rabies virus N degrees-P complex produced in insect cells. *Virology*, *305*(2), 406-414. https://doi.org/10.1006/viro.2002.1748

Mazewski, C., Perez, R. E., Fish, E. N., & Platanias, L. C. (2020). Type I Interferon (IFN)-Regulated Activation of Canonical and Non-Canonical Signaling Pathways. *Front Immunol*, *11*, 606456. https://doi.org/10.3389/fimmu.2020.606456

Mendoza-Rodriguez, M. G., Sanchez-Barrera, C. A., Callejas, B. E., Garcia-Castillo, V., Beristain-Terrazas, D. L., Delgado-Buenrostro, N. L., Chirino, Y. I., Leon-Cabrera, S. A., Rodriguez-Sosa, M., Gutierrez-Cirlos, E. B., Perez-Plasencia, C., Vaca-Paniagua, F., Meraz-Rios, M. A., & Terrazas, L. I. (2020). Use of STAT6 Phosphorylation Inhibitor and Trimethylglycine as New Adjuvant Therapies for 5-Fluorouracil in Colitis-Associated Tumorigenesis. *International Journal of Molecular Sciences*, *21*(6). https://doi.org/ARTN 2130

10.3390/ijms21062130

Mesa, R. A. (2010). Ruxolitinib, a selective JAK1 and JAK2 inhibitor for the treatment of myeloproliferative neoplasms and psoriasis. *IDrugs*, *13*(6), 394-403. https://www.ncbi.nlm.nih.gov/pubmed/20506062

Metzgar, R. S., Gaillard, M. T., Levine, S. J., Tuck, F. L., Bossen, E. H., & Borowitz, M. J. (1982). Antigens of human pancreatic adenocarcinoma cells defined by murine monoclonal antibodies. *Cancer Res*, *42*(2), 601-608. https://www.ncbi.nlm.nih.gov/pubmed/7034925

Mire, C. E., & Whitt, M. A. (2011). The protease-sensitive loop of the vesicular stomatitis virus matrix protein is involved in virus assembly and protein translation. *Virology*, *416*(1-2), 16-25. https://doi.org/10.1016/j.virol.2011.04.013

Mizrahi, J. D., Surana, R., Valle, J. W., & Shroff, R. T. (2020). Pancreatic cancer. *Lancet*, *395*(10242), 2008-2020. <Go to ISI>://WOS:000547825600018

Moerdyk-Schauwecker, M., Shah, N. R., Murphy, A. M., Hastie, E., Mukherjee, P., & Grdzelishvili, V. Z. (2013). Resistance of pancreatic cancer cells to oncolytic vesicular stomatitis virus: Role of type I interferon signaling. *Virology*, *436*(1), 221-234. https://doi.org/10.1016/j.virol.2012.11.014

Munis, A. M., Bentley, E. M., & Takeuchi, Y. (2020). A tool with many applications: vesicular stomatitis virus in research and medicine. *Expert Opin Biol Ther*, *20*(10), 1187-1201. https://doi.org/10.1080/14712598.2020.1787981

Murphy, A. M., Besmer, D. M., Moerdyk-Schauwecker, M., Moestl, N., Ornelles, D. A., Mukherjee, P., & Grdzelishvili, V. Z. (2012). Vesicular Stomatitis Virus as an Oncolytic Agent against Pancreatic Ductal Adenocarcinoma. *Journal of Virology*, *86*(6), 3073-3087. https://doi.org/10.1128/Jvi.05640-11

Musella, M., Manic, G., De Maria, R., Vitale, I., & Sistigu, A. (2017). Type-I-interferons in infection and cancer: Unanticipated dynamics with therapeutic implications. *OncoImmunology*, *6*(5), e1314424. https://doi.org/10.1080/2162402X.2017.1314424

Nan, Y., Wu, C., & Zhang, Y. J. (2018). Interferon Independent Non-Canonical STAT Activation and Virus Induced Inflammation. *Viruses*, *10*(4). https://doi.org/10.3390/v10040196

Naqvi, I., Gunaratne, R., McDade, J. E., Moreno, A., Rempel, R. E., Rouse, D. C., Herrera, S. G., Pisetsky, D. S., Lee, J., White, R. R., & Sullenger, B. A. (2018). Polymer-Mediated Inhibition of Pro-invasive Nucleic Acid DAMPs and Microvesicles Limits Pancreatic Cancer Metastasis. *Mol Ther*, *26*(4), 1020-1031. https://doi.org/10.1016/j.ymthe.2018.02.018

Narayanan, J. S. S., Ray, P., Hayashi, T., Whisenant, T. C., Vicente, D., Carson, D. A., Miller, A. M., Schoenberger, S. P., & White, R. R. (2019). Irreversible Electroporation Combined with Checkpoint Blockade and TLR7 Stimulation Induces Antitumor Immunity in a Murine Pancreatic Cancer Model. *Cancer Immunol Res*, *7*(10), 1714-1726. https://doi.org/10.1158/2326-6066.CIR-19-0101

Natoli, A., Lupertz, R., Merz, C., Muller, W. W., Kohler, R., Krammer, P. H., & Li-Weber, M. (2013). Targeting the IL-4/IL-13 signaling pathway sensitizes Hodgkin lymphoma cells

to chemotherapeutic drugs. *Int J Cancer*, *133*(8), 1945-1954. https://doi.org/10.1002/ijc.28189

Noser, J. A., Mael, A. A., Sakuma, R., Ohmine, S., Marcato, P., Lee, P. W., & Ikeda, Y. (2007). The RAS/Raf1/MEK/ERK signaling pathway facilitates VSV-mediated oncolysis: implication for the defective interferon response in cancer cells. *Mol Ther*, *15*(8), 1531-1536. https://doi.org/10.1038/sj.mt.6300193

Ohhashi, S., Ohuchida, K., Mizumoto, K., Fujita, H., Egami, T., Yu, J., Toma, H., Sadatomi, S., Nagai, E., & Tanaka, M. (2008). Down-regulation of deoxycytidine kinase enhances acquired resistance to gemcitabine in pancreatic cancer. *Anticancer Res*, *28*(4B), 2205-2212. https://www.ncbi.nlm.nih.gov/pubmed/18751396

Okabe, T., Yamaguchi, N., & Ohsawa, N. (1983). Establishment and characterization of a carcinoembryonic antigen (CEA)-producing cell line from a human carcinoma of the exocrine pancreas. *Cancer*, *51*(4), 662-668. https://doi.org/10.1002/1097-0142(19830215)51:4<662::aid-cncr2820510419>3.0.co;2-x

Orloff, M. (2016). Spotlight on talimogene laherparepvec for the treatment of melanoma lesions in the skin and lymph nodes. *Oncolytic Virotherapy*, *5*, 91-98. https://doi.org/10.2147/Ov.S99532

Orth, M., Metzger, P., Gerum, S., Mayerle, J., Schneider, G., Belka, C., Schnurr, M., & Lauber, K. (2019). Pancreatic ductal adenocarcinoma: biological hallmarks, current status, and future perspectives of combined modality treatment approaches. *Radiat Oncol*, *14*(1), 141. https://doi.org/10.1186/s13014-019-1345-6

Owens, R. B., Smith, H. S., Nelson-Rees, W. A., & Springer, E. L. (1976). Epithelial cell cultures from normal and cancerous human tissues. *J Natl Cancer Inst*, *56*(4), 843-849. https://doi.org/10.1093/jnci/56.4.843

Padariya, M., Sznarkowska, A., Kote, S., Gomez-Herranz, M., Mikac, S., Pilch, M., Alfaro, J., Fahraeus, R., Hupp, T., & Kalathiya, U. (2021). Functional Interfaces, Biological Pathways, and Regulations of Interferon-Related DNA Damage Resistance Signature (IRDS) Genes. *Biomolecules*, *11*(5). https://doi.org/10.3390/biom11050622

Patton, J. T., Davis, N. L., & Wertz, G. W. (1984). N protein alone satisfies the requirement for protein synthesis during RNA replication of vesicular stomatitis virus. *J Virol*, *49*(2), 303-309. https://doi.org/10.1128/JVI.49.2.303-309.1984

Pelner, L. (1958). Effects of concurrent infections and their toxins on the course of leukemia. *Acta Medica Scandinavica*, *338*, 1-47.

Peluso, R. W., & Moyer, S. A. (1988). Viral proteins required for the in vitro replication of vesicular stomatitis virus defective interfering particle genome RNA. *Virology*, *162*(2), 369-376. https://doi.org/10.1016/0042-6822(88)90477-1

Piszczatoski, C. R., & Gums, J. G. (2020). Ervebo (Ebola Zaire Vaccine, Live/rVSV Delta G-ZEBOV-GP): The First Licensed Vaccine for the Prevention of Ebola Virus Disease. *Journal of Pharmacy Technology*, *36*(6), 243-250. https://doi.org/Artn 8755122520950692

10.1177/8755122520950692

Prieto-Vila, M., Takahashi, R. U., Usuba, W., Kohama, I., & Ochiya, T. (2017). Drug Resistance Driven by Cancer Stem Cells and Their Niche. *Int J Mol Sci*, *18*(12). https://doi.org/10.3390/ijms18122574

Quillien, L., Top, S., Kappler-Gratias, S., Redoute, A., Dusetti, N., Quentin-Froignant, C., Lulka, H., Camus-Bouclainville, C., Buscail, L., Gallardo, F., Bertagnoli, S., & Cordelier, P. (2021). A Novel Imaging Approach for Single-Cell Real-Time Analysis of Oncolytic Virus Replication and Efficacy in Cancer Cells. *Hum Gene Ther*, *32*(3-4), 166-177. https://doi.org/10.1089/hum.2020.294

Quint, K., Tonigold, M., Di Fazio, P., Montalbano, R., Lingelbach, S., Ruckert, F., Alinger, B., Ocker, M., & Neureiter, D. (2012). Pancreatic cancer cells surviving gemcitabine treatment express markers of stem cell differentiation and epithelial-mesenchymal transition. *Int J Oncol*, *41*(6), 2093-2102. https://doi.org/10.3892/ijo.2012.1648

Ramakrishnan, M. A. (2016). Determination of 50% endpoint titer using a simple formula. *World J Virol*, *5*(2), 85-86. https://doi.org/10.5501/wjv.v5.i2.85

Rhim, J. S. (1993). Neoplastic transformation of human cells in vitro. *Crit Rev Oncog*, *4*(3), 313-335. https://www.ncbi.nlm.nih.gov/pubmed/8485202

Rickardson, L., Fryknas, M., Dhar, S., Lovborg, H., Gullbo, J., Rydaker, M., Nygren, P., Gustafsson, M. G., Larsson, R., & Isaksson, A. (2005). Identification of molecular mechanisms for cellular drug resistance by combining drug activity and gene expression profiles. *Br J Cancer*, *93*(4), 483-492. https://doi.org/10.1038/sj.bjc.6602699

Rose, J. K. (1980). Complete intergenic and flanking gene sequences from the genome of vesicular stomatitis virus. *Cell*, *19*(2), 415-421. https://doi.org/10.1016/0092-8674(80)90515-2

Russell, S. J., Peng, K. W., & Bell, J. C. (2012). Oncolytic virotherapy. *Nat Biotechnol*, *30*(7), 658-670. https://doi.org/10.1038/nbt.2287

Salo-Mullen, E. E., O'Reilly, E. M., Kelsen, D. P., Ashraf, A. M., Lowery, M. A., Yu, K. H., Reidy, D. L., Epstein, A. S., Lincoln, A., Saldia, A., Jacobs, L. M., Rau-Murthy, R., Zhang, L. Y., Kurtz, R. C., Saltz, L., Offit, K., Robson, M. E., & Stadler, Z. K. (2015). Identification of Germline Genetic Mutations in Patients With Pancreatic Cancer. *Cancer*, *121*(24), 4382-4388. https://doi.org/10.1002/cncr.29664

Samulitis, B. K., Pond, K. W., Pond, E., Cress, A. E., Patel, H., Wisner, L., Patel, C., Dorr, R. T., & Landowski, T. H. (2015). Gemcitabine resistant pancreatic cancer cell lines acquire an invasive phenotype with collateral hypersensitivity to histone deacetylase inhibitors. *Cancer Biol Ther*, *16*(1), 43-51. https://doi.org/10.4161/15384047.2014.986967

Schlegel, R., Tralka, T. S., Willingham, M. C., & Pastan, I. (1983). Inhibition of Vsv Binding and Infectivity by Phosphatidylserine - Is Phosphatidylserine a Vsv-Binding Site. *Cell*, *32*(2), 639-646. https://doi.org/Doi 10.1016/0092-8674(83)90483-X

Schloemer, R. H., & Wagner, R. R. (1975). Cellular adsorption function of the sialoglycoprotein of vesicular stomatitis virus and its neuraminic acid. *J Virol*, *15*(4), 882-893. https://doi.org/10.1128/JVI.15.4.882-893.1975

Schoumacher, R. A., Ram, J., Iannuzzi, M. C., Bradbury, N. A., Wallace, R. W., Hon, C. T., Kelly, D. R., Schmid, S. M., Gelder, F. B., Rado, T. A., & et al. (1990). A cystic fibrosis pancreatic adenocarcinoma cell line. *Proc Natl Acad Sci U S A*, *87*(10), 4012-4016. https://doi.org/10.1073/pnas.87.10.4012

Shalhout, S. Z., Miller, D. M., Emerick, K. S., & Kaufman, H. L. (2023). Therapy with oncolytic viruses: progress and challenges. *Nat Rev Clin Oncol*, *20*(3), 160-177. https://doi.org/10.1038/s41571-022-00719-w

Shi, W., Yao, X., Fu, Y., & Wang, Y. (2022). Interferon-alpha and its effects on cancer cell apoptosis. *Oncol Lett*, *24*(1), 235. https://doi.org/10.3892/ol.2022.13355

Siegel, R. L., Miller, K. D., & Jemal, A. (2020). Cancer statistics, 2020. *CA Cancer J Clin*, *70*(1), 7-30. https://doi.org/10.3322/caac.21590

Siegel, R. L., Miller, K. D., Wagle, N. S., & Jemal, A. (2023). Cancer statistics, 2023. *CA Cancer J Clin*, *73*(1), 17-48. https://doi.org/10.3322/caac.21763

Snell, L. M., McGaha, T. L., & Brooks, D. G. (2017). Type I Interferon in Chronic Virus Infection and Cancer. *Trends Immunol*, *38*(8), 542-557. https://doi.org/10.1016/j.it.2017.05.005

Soria, M., Little, S. P., & Huang, A. S. (1974). Characterization of Vesicular Stomatitis-Virus Nucleocapsids .1. Complementary 40 S Rna Molecules in Nucleocapsids. *Virology*, *61*(1), 270-280. https://doi.org/Doi 10.1016/0042-6822(74)90261-X

Springfeld, C., Jager, D., Buchler, M. W., Strobel, O., Hackert, T., Palmer, D. H., & Neoptolemos, J. P. (2019). Chemotherapy for pancreatic cancer. *Presse Medicale*, *48*(3), E159-E174. https://doi.org/UNSP e159-e174

10.1016/j.lpm.2019.02.025

Stanifer, M. L., Cureton, D. K., & Whelan, S. P. J. (2011). A Recombinant Vesicular Stomatitis Virus Bearing a Lethal Mutation in the Glycoprotein Gene Uncovers a Second Site Suppressor That Restores Fusion. *Journal of Virology*, *85*(16), 8105-8115. https://doi.org/10.1128/Jvi.00735-11

Stewart, B. W., & Haski, R. (1984). Relationships between carcinogen metabolism, adduct binding and DNA damage in 3-methylcholanthrene-exposed lung. *Chem Biol Interact*, *52*(1), 111-128. https://doi.org/10.1016/0009-2797(84)90087-5

Stojdl, D. F., Lichty, B., Knowles, S., Marius, R., Atkins, H., Sonenberg, N., & Bell, J. C. (2000). Exploiting tumor-specific defects in the interferon pathway with a previously unknown oncolytic virus. *Nature Medicine*, *6*(7), 821-825. https://doi.org/10.1038/77558

Stojdl, D. F., Lichty, B. D., tenOever, B. R., Paterson, J. M., Power, A. T., Knowles, S., Marius, R., Reynard, J., Poliquin, L., Atkins, H., Brown, E. G., Durbin, R. K., Durbin, J. E., Hiscott, J., & Bell, J. C. (2003). VSV strains with defects in their ability to shutdown innate immunity are potent systemic anti-cancer agents. *Cancer Cell*, *4*(4), 263-275. https://doi.org/Doi 10.1016/S1535-6108(03)00241-1

Stopczynski, R. E., Normolle, D. P., Hartman, D. J., Ying, H., DeBerry, J. J., Bielefeldt, K., Rhim, A. D., DePinho, R. A., Albers, K. M., & Davis, B. M. (2014). Neuroplastic changes occur early in the development of pancreatic ductal adenocarcinoma. *Cancer Res*, *74*(6), 1718-1727. https://doi.org/10.1158/0008-5472.CAN-13-2050

Suder, E., Furuyama, W., Feldmann, H., Marzi, A., & de Wit, E. (2018). The vesicular stomatitis virus-based Ebola virus vaccine: From concept to clinical trials. *Hum Vaccin Immunother*, *14*(9), 2107-2113. https://doi.org/10.1080/21645515.2018.1473698

Tian, Y., Xie, D., & Yang, L. (2022). Engineering strategies to enhance oncolytic viruses in cancer immunotherapy. *Signal Transduct Target Ther*, *7*(1), 117. https://doi.org/10.1038/s41392-022-00951-x

Torres, M. P., Rachagani, S., Souchek, J. J., Mallya, K., Johansson, S. L., & Batra, S. K. (2013). Novel pancreatic cancer cell lines derived from genetically engineered mouse models of

spontaneous pancreatic adenocarcinoma: applications in diagnosis and therapy. *PLoS One*, *8*(11), e80580. https://doi.org/10.1371/journal.pone.0080580

Travieso, T., Li, J., Mahesh, S., Mello, J., & Blasi, M. (2022). The use of viral vectors in vaccine development. *NPJ Vaccines*, *7*(1), 75. https://doi.org/10.1038/s41541-022-00503-y

van Pesch, V., Lanaya, H., Renauld, J. C., & Michiels, T. (2004). Characterization of the murine alpha interferon gene family. *J Virol*, *78*(15), 8219-8228. https://doi.org/10.1128/JVI.78.15.8219-8228.2004

Van Rompay, A. R., Johansson, M., & Karlsson, A. (1999). Phosphorylation of deoxycytidine analog monophosphates by UMP-CMP kinase: molecular characterization of the human enzyme. *Mol Pharmacol*, *56*(3), 562-569. https://doi.org/10.1124/mol.56.3.562

Villarreal, L. P., Breindl, M., & Holland, J. J. (1976). Determination of molar ratios of vesicular stomatitis virus induced RNA species in BHK21 cells. *Biochemistry*, *15*(8), 1663-1667. https://doi.org/10.1021/bi00653a012

Walters, D. M., Stokes, J. B., Adair, S. J., Stelow, E. B., Borgman, C. A., Lowrey, B. T., Xin, W. J., Blais, E. M., Lee, J. K., Papin, J. A., Parsons, J. T., & Bauer, T. W. (2013). Clinical, Molecular and Genetic Validation of a Murine Orthotopic Xenograft Model of Pancreatic Adenocarcinoma Using Fresh Human Specimens. *PLoS One*, *8*(10). https://doi.org/ARTN e77065

10.1371/journal.pone.0077065

Wang, B. X., Rahbar, R., & Fish, E. N. (2011). Interferon: current status and future prospects in cancer therapy. *J Interferon Cytokine Res*, *31*(7), 545-552. https://doi.org/10.1089/jir.2010.0158

Wang, Y., Zhang, Y., Yang, J., Ni, X., Liu, S., Li, Z., Hodges, S. E., Fisher, W. E., Brunicardi, F. C., Gibbs, R. A., Gingras, M. C., & Li, M. (2012). Genomic sequencing of key genes in mouse pancreatic cancer cells. *Curr Mol Med*, *12*(3), 331-341. https://doi.org/10.2174/156652412799218868

Waters, A. M., & Der, C. J. (2018). KRAS: The Critical Driver and Therapeutic Target for Pancreatic Cancer. *Cold Spring Harb Perspect Med*, *8*(9). https://doi.org/10.1101/cshperspect.a031435

Weber, H., Valenzuela, D., Lujber, G., Gubler, M., & Weissmann, C. (1987). Single Amino-Acid Changes That Render Human Ifn-Alpha-2 Biologically-Active on Mouse Cells. *Embo Journal*, *6*(3), 591-598. https://doi.org/DOI 10.1002/j.1460-2075.1987.tb04795.x

Weichselbaum, R. R., Ishwaran, H., Yoon, T., Nuyten, D. S., Baker, S. W., Khodarev, N., Su, A. W., Shaikh, A. Y., Roach, P., Kreike, B., Roizman, B., Bergh, J., Pawitan, Y., van de Vijver, M. J., & Minn, A. J. (2008). An interferon-related gene signature for DNA damage resistance is a predictive marker for chemotherapy and radiation for breast cancer. *Proc Natl Acad Sci U S A*, *105*(47), 18490-18495. https://doi.org/10.1073/pnas.0809242105

Weichselbaum, R. R., Ishwaran, H., Yoon, T., Nuyten, D. S. A., Baker, S. W., Khodarev, N., Su, A. W., Shaikh, A. Y., Roach, P., Kreike, B., Roizman, B., Bergh, J., Pawitan, Y., de Vijver, M. J. V., & Minn, A. J. (2008). An interferon-related gene signature for DNA damage resistance is a predictive marker for chemotherapy and radiation for breast cancer. *Proceedings of the National Academy of Sciences of the United States of America*, *105*(47), 18490-18495. https://doi.org/10.1073/pnas.0809242105

Wennier, S. T., Liu, J., Li, S., Rahman, M. M., Mona, M., & McFadden, G. (2012). Myxoma virus sensitizes cancer cells to gemcitabine and is an effective oncolytic virotherapeutic in models of disseminated pancreatic cancer. *Mol Ther*, *20*(4), 759-768. https://doi.org/10.1038/mt.2011.293

Wertz, G. W., Perepelitsa, V. P., & Ball, L. A. (1998). Gene rearrangement attenuates expression and lethality of a nonsegmented negative strand RNA virus. *Proc Natl Acad Sci U S A*, *95*(7), 3501-3506. https://doi.org/10.1073/pnas.95.7.3501

Whitlow, Z. W., Connor, J. H., & Lyles, D. S. (2006). Preferential translation of vesicular stomatitis virus mRNAs is conferred by transcription from the viral genome. *Journal of Virology*, *80*(23), 11733-11742. https://doi.org/10.1128/Jvi.00971-06

Wiegand, M. A., Bossow, S., Schlecht, S., & Neubert, W. J. (2007). De novo synthesis of N and P proteins as a key step in Sendai virus gene expression. *Journal of Virology*, *81*(24), 13835-13844. https://doi.org/10.1128/Jvi.00914-07

Wolf, Y. I., Kazlauskas, D., Iranzo, J., Lucia-Sanz, A., Kuhn, J. H., Krupovic, M., Dolja, V. V., & Koonin, E. V. (2018). Origins and Evolution of the Global RNA Virome. *mBio*, *9*(6). https://doi.org/10.1128/mBio.02329-18

Wollmann, G., Rogulin, V., Simon, I., Rose, J. K., & van den Pol, A. N. (2010). Some Attenuated Variants of Vesicular Stomatitis Virus Show Enhanced Oncolytic Activity against Human Glioblastoma Cells relative to Normal Brain Cells. *Journal of Virology*, *84*(3), 1563-1573. https://doi.org/10.1128/Jvi.02040-09

Wong, A., Soo, R. A., Yong, W. P., & Innocenti, F. (2009). Clinical pharmacology and pharmacogenetics of gemcitabine. *Drug Metab Rev*, *41*(2), 77-88. https://doi.org/10.1080/03602530902741828

Xu, H., Faber, C., Uchiki, T., Racca, J., & Dealwis, C. (2006). Structures of eukaryotic ribonucleotide reductase I define gemcitabine diphosphate binding and subunit assembly. *Proc Natl Acad Sci U S A*, *103*(11), 4028-4033. https://doi.org/10.1073/pnas.0600440103

Xu, Y. Z., & Plunkett, W. (1992). Modulation of deoxycytidylate deaminase in intact human leukemia cells. Action of 2',2'-difluorodeoxycytidine. *Biochem Pharmacol*, *44*(9), 1819-1827. https://doi.org/10.1016/0006-2952(92)90077-v

Yang, L., & Ding, J. L. (2019). MEK1/2 Inhibitors Unlock the Constrained Interferon Response in Macrophages Through IRF1 Signaling. *Front Immunol*, *10*, 2020. https://doi.org/10.3389/fimmu.2019.02020

Yunis, A. A., Arimura, G. K., & Russin, D. J. (1977). Human pancreatic carcinoma (MIA PaCa-2) in continuous culture: sensitivity to asparaginase. *Int J Cancer*, *19*(1), 128-135. https://doi.org/10.1002/ijc.2910190118

Zeng, S., Pottler, M., Lan, B., Grutzmann, R., Pilarsky, C., & Yang, H. (2019). Chemoresistance in Pancreatic Cancer. *Int J Mol Sci*, *20*(18). https://doi.org/10.3390/ijms20184504

Zhang, K. X., Matsui, Y., Hadaschik, B. A., Lee, C., Jia, W., Bell, J. C., Fazli, L., So, A. I., & Rennie, P. S. (2010). Down-regulation of type I interferon receptor sensitizes bladder cancer cells to vesicular stomatitis virus-induced cell death. *International journal of cancer*, *127*(4), 830-838. https://doi.org/10.1002/ijc.25088

Zitvogel, L., Galluzzi, L., Kepp, O., Smyth, M. J., & Kroemer, G. (2015). Type I interferons in anticancer immunity. *Nat Rev Immunol*, *15*(7), 405-414. https://doi.org/10.1038/nri3845